# Modeling Human And Machine-In-The-Loop In Car-Following Theory

Karim Fadhloun

Dissertation submitted to the faculty of the Virginia Polytechnic Institute and State University in partial fulfillment of the requirements for the degree of

Doctor of Philosophy
In
Civil Engineering

Hesham A. Rakha, Chair
Amara Loulizi
Ihab E. El-Shawarby
Kathleen L. Hancock

September 25th, 2019
Blacksburg, Virginia

Keywords: Human Behavior, Car Following Theory, Platooning, Driving Pattern, Human-In-The-Loop.

# Modeling Human And Machine-In-The-Loop In Car-Following Theory

Karim Fadhloun

## ABSTRACT

Most phenomena in engineering fields involve physical variables that can potentially be predicted using simple or complex mathematical models. However, traffic engineers and researchers are faced with a complex challenge since they have to deal with the human element. For instance, it can be stated that the biggest challenge facing researchers in the area of car-following theory relates to accounting for the human-in-the-loop while modeling the longitudinal motion of the vehicles. In fact, a major drawback of existing car-following models is that the human-in-the-loop is not modeled explicitly. This is specifically important since the output from car-following models directly impacts several other factors and measures of effectiveness, such as vehicle emissions and fuel consumption levels.

The main contribution of this research relates to modeling and incorporating, in an explicit and independent manner, the human-in-the-loop component in car-following theory in such a way that it can be either activated or deactivated depending on if a human driver is in control of the vehicle. That would ensure that a car-following model is able to reflect the different control and autonomy levels that a vehicle could be operated under. Besides that, this thesis offers a better understanding of how humans behave and differ from each other. In fact, through the implementation of explicit parameters representing the human-in-the-loop element, the heterogeneity of human behavior, in terms of driving patterns and styles, is captured.

To achieve its contributions, the study starts by modifying the maximum acceleration vehicle-dynamics model by explicitly incorporating parameters that aim to model driver behavior in its expression making it suitable for the representation of typical acceleration behavior. The modified variant of the model is demonstrated to have a flexible shape that allows it to model different types of variations that drivers can generate, and to be superior to other similar models in that it predicts more accurate acceleration levels in all domains. The

resulting model is then integrated in the Rakha-Pasumarthy-Adjerid car-following model, which uses a steady-state formulation along with acceleration and collision avoidance constraints to model the longitudinal motion of vehicles. The validation of the model using a naturalistic dataset found that the modified formulation successfully integrated the human behavior component in the model and that the new formulation decreases the modeling error.

Thereafter, this dissertation proposes a new car-following model, which we term the Fadhloun-Rakha model. Even though structurally different, the developed model incorporates the key components of the Rakha-Pasumarthy-Adjerid model in that it uses the same steady state formulation, respects vehicle dynamics, and uses very similar collision-avoidance strategies to ensure safe following distances between vehicles. Besides offering a better fit to empirical data, the Fadhloun-Rakha model is inclusive of the following characteristics: (1) it models the driver throttle and brake pedal input; (2) it captures driver variability; (3) it allows for shorter than steady-state following distances when following faster leading vehicles; (4) it offers a much smoother acceleration profile; and (5) it explicitly captures driver perception and control inaccuracies and errors. Through a quantitative and qualitative evaluation using naturalistic data, the new model is demonstrated to outperform other state-of-the-practice car-following models. In fact, the model is proved to result in a significant decrease in the modeling error, and to generate trajectories that are highly consistent with the observed car-following behavior.

The final part of this study investigates a case in which the driver is excluded and the vehicles are operating in a connected environment. This section aims to showcase a scenario in which the human-in-the-loop is deactivated through the development of a platooning strategy that governs the motion of connected cooperative multi-vehicle platoons.

# Modeling Human And Machine-In-The-Loop In Car-Following Theory

Karim Fadhloun

## GENERAL AUDIENCE ABSTRACT

Even though the study of the longitudinal motion of vehicles spanned over several decades leading to the development of more precise and complex car-following models, an important aspect was constantly overlooked in those models. In fact, due to the complexity of modeling the human-in-the-loop, the vehicle and the driver were almost always assumed to represent a single entity. More specifically, ignoring driver behavior and integrating it to the vehicle allowed avoiding to deal with the challenges related to modeling human behavior.

The difficulty of mathematically modeling the vehicle and the driver as two independent components rather than one unique system is due to two main reasons. First, there are numerous car models and types that make it difficult to determine the different parameters impacting the performance of the vehicle as they differ from vehicle to vehicle. Second, different driving patterns exist and the fact that they are mostly dependent on human behavior and psychology makes them very difficult to replicate mathematically.

The research presented in this thesis provides a comprehensive investigation of the human-in-the-loop component in car-following theory leading to a better understanding of the human-vehicle interaction. This study was initiated due to the noticeable overlooking of driver behavior in the existing literature which, as a result, fails to capture the effect of human control and perception errors.

# DEDICATION

*"Strange feelings come when you leave a particular place of great meaning; a feeling you get from knowing you will miss all the wonderful people you have been touched by but most importantly the person that you have become at that moment and feeling you will never feel this wonderful ever again. Change is good, remembering is wonderful and never forgetting where you came from is magnificent but the most spectacular trait is to never stop moving forward or growing."*

***TO MY BELOVED FATHER HFAIEDH, MY GRANDMOTHER MAYSSA, AND MY GREAT-UNCLE EL-BEY: YOU WILL ALWAYS HAVE A SPECIAL PLACE IN MY HEART AND BE REMEMBERED.***

***TO MY MOTHER AMAL***

***TO MY WIFE ASMA***

# ACKNOWLEDGEMENTS

First of all, All Praise is due to Allah the most Merciful for this achievement, I thank him and seek his guidance and forgiveness. I would also like to express my deepest gratitude to my advisor Dr. Hesham Rakha for his continuous guidance, help and support. Professor Rakha is a great and outstanding advisor who was always available to discuss and guide my research. He gave me the opportunity to work on several research projects and collaborate with notable institutions allowing me to acquire and develop my knowledge about traffic engineering and academic research. With his advice and assistance, I was able to write several journal articles and attend famous conferences. I would also like to thank Dr. Amara Loulizi, Dr. Ihab El-Shawarby and Dr. Kathleen Hancock for serving on my committee and for their guidance and contributions to this work. I would also like to thank all the staff of the Charles Edward Via, Jr. Department of Civil and Environmental Engineering and of the Virginia Tech Transportation Institute for their availability and help and for providing me with an excellent work environment.

My deepest thanks and recognition go to my parents Hfaiedh and Amal who are the main source of any success I achieved and will achieve in my life. Special thanks go to my wife Asma Khouildi for being there for me unconditionally. Her love, support, encouragement, and prayers contributed significantly to finishing my PhD. I would also like to thank my brother Zied, my father-in-law Bechir, my mother-in-law Raja, my great-aunt Fatma, my aunt Fatiha and her husband Nabil Ben Hadj Khalifa, my cousins Kais, Safa and Youssef, my brother-in-law Ahmed, and my sisters-in-law Oumaima and Imen. Special thanks go to my great-uncle Heshmi Khalifa and his wife Anne: thank you for your encouragement, support and sincere kindness.

A very big and special thank you goes to Dr. Saher Lahouar and his wife Afek Jaballah for your kindness and support. I will never forget the good moments I spent in your house and I wish you all the best for your family. Special thanks to all my friends I knew in Blacksburg, namely (in alphabetical order) Abdessattar Abdelkefi and his wife Samah Ben Ayed, Bilel Aydi and his wife Hana Dammak, Faycal Beji and his wife Autumn Taylor, Mohamed Jrad and his wife Maha Elouni, Nejib Masghouni and his wife Marwa Assali, Said Mseddi and his wife

Bochra Bouchhima, Yassine Mahjoubi and his wife Imen Tenniche, and Youssef Bichiou and his wife Amira Haouel. I and Asma will never forget all the good moments and memories we spend together. I am also very grateful to Dr. Amara Loulizi for having recommended me to my advisor and for all the good times we shared during his summer visits to Blacksburg.

# TABLE OF CONTENTS

# LIST OF FIGURES

# LIST OF TABLES

# Chapter 1 Introduction

## 1.1 INTRODUCTION

Most phenomena in engineering fields involve physical variables that can potentially be predicted using simple or complex mathematical models. However, traffic engineers and researchers are faced with a complex challenge since they have to deal with the human element, which is difficult to model. Understandably, the biggest challenge facing traffic engineering researchers is how to account for human behavior, a non-physical parameter, in transportation modeling. In fact, a major drawback of existing car-following models is that the human-in-the-loop is not modeled explicitly. This is specifically important since the output from car-following models directly impacts several other factors and measures of effectiveness (MOE), such as vehicle emissions and fuel consumption levels.

The difficulty of mathematically modeling the vehicle and the driver as two independent components rather than one unique system is due to two main reasons. First, there are numerous car models and types that make it difficult to determine the different parameters impacting the performance of the vehicle as they differ from vehicle to vehicle. Second, different driving patterns exist and the fact that they are mostly dependent on human behavior and psychology makes them very difficult to replicate mathematically.

A major issue that can be easily perceived in the literature is that the driver and the vehicle are tied to each other. This is due to the fact that traffic engineers mostly rely on simulated data in their research due to the practicality and the simplicity of its acquisition. In other words, the success in modeling the driver/vehicle interaction aspect is related to the accuracy and the precision of the mathematical models implemented in the traffic simulation software producing these data. A main component of these types of software which has been a subject of several studies over the last fifty years is the car-following model. Car-following models [1-13] predict the temporal and spatial behavior of a following vehicle when the time-space profile of the leading vehicle is known. It is noteworthy that the output from car-following models directly impacts several other factors and measures of effectiveness (MOE), such as vehicle emissions and fuel consumption levels. The main objective of these models is

to generate vehicle trajectories that mimic empirical driving behavior as realistically as possible. While existing car-following models are numerous and have evolved gradually in terms of accuracy and complexity of their mathematical expression, significant research is still needed to improve their mathematical representations.

Car-following models can be categorized into collision avoidance models [7, 8], psycho-physical models [9-11], and Gazis-Herman-Rothery (GHR) family models [3]. Alternatively, they can also be categorized based on whether they include vehicle dynamics in their expression. Kinematics-based models attempt to replicate the car-following behavior of vehicles as it occurs in the field, but ignore the mechanical characteristics of the vehicle, which represents one of their major weaknesses. Notable state-of-the-art kinematic models include the Gipps model [7] and the Intelligent Driver Model (IDM) [8]. On the other hand, car-following models [12, 13] that consider vehicle dynamics explicitly in their expressions account for both the tractive and resistive forces that act on the vehicle. These models are more complicated in terms of mathematical representation and development. A state-of-the-practice vehicle dynamics model is the Rakha-Pasumarthy-Adjerid (RPA) model [12], which controls the car-following behavior used in the INTEGRATION software [14, 15].

The success of a car-following model to capture observed traffic behavior as realistically as possible is not the sole criterion of its performance. In fact, as with any other prediction model, the validity and the suitability of a certain car-following model for traffic simulation depends on achieving that goal with the smallest number of calibration parameters while, at the same time, not ignoring most of the parameters significantly influencing traffic. In that regard, finding the optimal balance between complexity and simplicity is the key starting point in achieving an “ideal” car-following model. Such a model would be one with the most straightforward and simple mathematical expression without any compromise in its ability to replicate reality.

## 1.2 RESEARCH CONTRIBUTIONS AND OBJECTIVES

Even though the development of car-following theory spanned over several decades leading to more precise and complex models, it can be conservatively stated that an important aspect of traffic was constantly overlooked in the existing car-following models. In fact, due to the complexity of modeling the human-in-the-loop, the vehicle component and the driver component were assumed to represent one single entity. To put it more precisely, integrating the driver to the vehicle allowed avoiding to deal with the challenges related to modeling

human behavior. That surprisingly resulted in the existing car-following models being more adequate to describe the motion of the newly emerging technologies of connected and autonomous vehicles rather than regular driver-operated vehicles.

The idea behind this research effort stems from the necessity that car-following theory be able to reflect the transition from human driven vehicles to connected and self-driving vehicles. In that regard, the main contribution of the research presented herein relates to modeling and incorporating, in an explicit and independent manner, the human-in-the-loop in car-following theory in such a way that it can be either activated or deactivated depending on if a human driver is in control of the vehicle. That would ensure that a car-following model is able to reflect the different control and autonomy levels that a vehicle could be operated under. Besides that, an additional contribution of this thesis to traffic flow theory is that it offers a better understanding of how humans behave and differ from each other. In fact, through the implementation of explicit parameters representing the human-in-the-loop element, the heterogeneity of human behavior, in terms of driving patterns and styles, is captured.

This dissertation achieves its stated contributions and objectives through addressing each of the following points:

- Incorporate driver behavior variability in a vehicle dynamics model to make it capable of estimating typical accelerations behavior. Besides taking into account the mechanical characteristics of vehicles, the resulting model needs to consider parameters that are reflective of different driving patterns. The proposed model can be cast as an extension to the work of Rakha et al. [16, 17]. In relation to the validation of the resulting model, its performance is compared to that of other existing models in terms of goodness of fit.
- Integrate the above vehicle dynamics model accounting for human behavior component in the RPA car-following model and evaluate its performance using naturalistic car-following data.
- Develop a new dynamics-based car-following model (the Fadhloun-Rakha model) [18] that, besides offering a better fit to empirical data, is inclusive of the following characteristics: (1) it models the driver throttle and brake pedal input; (2) it captures driver variability; (3) it allows for shorter than steady-state following distances when following faster leading vehicles; (4) it offers a much smoother acceleration profile; and (5) it explicitly captures driver perception and control inaccuracies and errors.

- Validate the newly developed car-following model and compare its performance to state-of-the-practice car-following models.
- Unlike the previous points in which the human element is present, the final task of the thesis looks to investigate a case in which the human-in-the-loop component is deactivated, thus excluding the driver effect. That is achieved through the development of a car-following strategy that governs the motion of connected cooperative vehicles. The strategy consists of a platooning controller that regulates the longitudinal motion of vehicles in multi-vehicle platoons.

## 1.3 THESIS LAYOUT

This dissertation is organized into 9 chapters. Chapter 1 briefly exposes the problem overview along with the study objectives and contributions. That is followed, in Chapter 2, by a review of the literature that is relevant to the topics covered in the dissertation. In fact, the literature is reviewed in two main areas: (1) Overview of car-following theory with a special focus on how the human factor is modeled, and (2) Overview of cooperative adaptive cruise control systems which relate to modeling the longitudinal motion of a platoon when cooperation and connectivity exist between the vehicles.

The resulting six papers from this work constitute the next chapters of this thesis. In Chapter 3, the maximum acceleration vehicle-dynamics model is modified by explicitly incorporating parameters that aim to model driver behavior in its expression making it suitable for the representation of typical acceleration behavior. In fact, the proposed model has a flexible shape that allows it to incorporate different types of variations that drivers can generate. Furthermore, the model is proved to be superior to other similar models in that it predicts more accurate acceleration levels in all domains.

The resulting model is incorporated, in Chapter 4, in the Rakha-Pasumarthy-Adjerid (RPA) car-following model, which uses a steady-state formulation along with acceleration and collision avoidance constraints to model the longitudinal motion of vehicles. The model is calibrated and validated using a dataset that is extracted from the naturalistic data of the 100-Car study that was gathered by the Virginia Tech Transportation Institute. An analysis of the proposed modified variant of the RPA model using the aforementioned naturalistic driving dataset found that the modified formulation successfully integrated the human behavior component in the RPA model and that the new formulation decreases the modeling error.

Next, in order to overcome certain issues in the RPA model, a new car-following model, which we term the Fadhloun-Rakha (FR) model, is proposed in Chapter 5. Even though structurally different, the developed FR model incorporates the key components of the Rakha-Pasumarthy-Adjerid (RPA) model in that it uses the same steady state formulation, respects vehicle dynamics, and uses very similar collision-avoidance strategies to ensure safe following distances between vehicles. Through a quantitative and qualitative evaluation, the proposed FR model demonstrated a significant decrease in the modeling error when compared to the original RPA model and generated trajectories that are highly consistent with empirically observed car-following behavior. The performance of the FR model is further validated in Chapter 6 and Chapter 7. The first validation effort, subject of Chapter 6, consists of a statistical study in which the performance of the FR model is compared to that of state-of-the-practice car-following models. The second validation methodology is presented in Chapter 7 and consisted on estimating the effect of the predicted trajectory from the FR model and different car-following models on the estimated consumed fuel of different gasoline cars. Using both methodologies, the FR model is demonstrated to outperform the other models.

Thereafter, Chapter 8 investigates a case in which the driver is excluded and the vehicles are operating in a connected environment. Under those conditions; the role of the driver in the longitudinal motion of the vehicles is mostly eliminated and meaningless. In order to showcase a scenario in which the human-in-the-loop is deactivated, Chapter 8 describes the development of a platooning controller that governs the motion of connected cooperative multi-vehicle platoons. Finally, Chapter 9 provides a summary of the findings of this study.

# Chapter 2 Literature Review

In this chapter, the research topics pertaining to this dissertation are identified and presented. The review of the literature is organized in two sections that cover two independent research areas. The first section presents a comprehensive overview of car-following theory in which the most relevant state-of-practice models are described. Furthermore, a special focus is dedicated to how the human factor is modeled in car-following theory. The second section relates to cooperative adaptive cruise control systems which involve modeling the longitudinal motion of a multi-vehicle platoon in a cooperative and connected environment.

## 2.1 OVERVIEW OF CAR-FOLLOWING THEORY

The analysis of car-following behavior constitutes a pillar of traffic flow theory. In fact, several models aiming to emulate the way with which vehicles follow each other have been developed over the last fifty years. Over the time, those models have evolved gradually in terms of accuracy; and subsequently, complexity of their mathematical expression. It should be noted that car-following models are as important to traffic analysts as they are for roadway geometric designers. As a matter of fact, a significant part of traffic analysis is based on data that are generated by microscopic simulation software. The obtained data and results from the latter programs are highly dependent on the car-following model that is incorporated in their algorithms. Subsequently, not only an accurate estimation of vehicles trajectories, velocities and accelerations is necessary to get correct estimation of travel times and delays; but also it directly impacts the precision of predicting other measures of effectiveness parameters such as fuel consumption and emissions.

From a technical point of view, car-following models can be divided into two categories. The first category encloses all the models that were developed based on kinematics. While those models imitate to a certain level the car-following behavior of vehicles as it occurs in the field, they totally ignore the mechanical characteristics of the vehicle which represents one of their major weaknesses. The second category is composed of models that incorporate vehicle dynamics. Car-following models that consider vehicle dynamics explicitly in their

expressions account for both tractive and resistive forces that act on the vehicle. These models are more complicated in terms of mathematical representation and development.

Another way of categorizing car-following models is with regards to their order. This method of categorization depends on if the car-following model has a unique expression that is valid for all data domains or if it has several expressions (usually one for the uncongested regime and one for the congested regime). While higher order models offer a better representation of traffic which is understandable, they are usually more complicated and harder to implement.

In what follows, we present some of the most known car-following models that were developed during the last six decades with an emphasis on their strengths and weaknesses. First, a set of models that are based on kinematics is presented. After that, some dynamics-based car-following models are described.

### 2.1.1 Kinematics Based Models

Kinematics based car-following models describe the motion of vehicles considering the mathematical relationships between the acceleration, the speed, and the distance that is traveled by the vehicle without consideration of the causes of the motion. In other words, in these models, the mathematical representations of the acceleration totally ignore the vehicle characteristics, the driving pattern, and the roadway effects. Generally, these models are the direct result of an analysis of fictive or field vehicle trajectories. The most famous of these models is the very simple constant acceleration model [19]. As its name implies, the model assumes a constant acceleration level for the entire length of the trip. From that point, the speed and the distance traveled are determined by successive integrations leading to a linear expression of speed and a quadratic expression of distance as a function of time. Whilst this model is easy to apply, it is far from reality since everybody knows that vehicle acceleration is never constant. This model is justified for use in geometric design since it produces conservative values for the design parameters (length of acceleration lanes for example), but cannot be used in traffic simulation software.

Subsequently, in a later effort, noticing that vehicles' ability to accelerate is higher at low speeds, Bham and Benekohal [20] developed a dual regime model that only differs from the constant acceleration model by the fact that it considers two acceleration rates: one for low speeds which is the higher one, and the other is for the second regime enclosing higher speeds.

Other well-known acceleration models that are based on kinematics include Drew's linear decay model [19] developed in 1968, and shown by Equation II.1. For Drew's model, Long [21] has provided a complete analysis of the values that can be adopted by the two parameters $\alpha$ and $\beta$.

$$a(u) = \alpha - \beta u \tag{II.1}$$

Where α is the maximum acceleration rate and α /β is the maximum attainable speed.

A similar but a slightly different model was proposed by Lee [22] in 1977. The only difference between Lee's model and Drew's model resides in the fact that it is sensitive to the time rather than to the speed as presented in Equation II.1.

Other notable models include the gamma model, proposed by Bham and Benekohal [20], the three acceleration models that were developed by Akcelik [23] as well as the three kinematics models, namely the haversine model, the triangular model and the sinusoidal model, that were proposed by Varat and Husher [24].

The previously cited models are some of the most simplistic car-following models. One main drawback of the latter models is that they produce unrealistic results that do not describe what is actually happening on the field. Next, some famous car-following models that are used in different microscopic simulation software are described in more detail. In fact, microscopic simulation software use a variety of car-following models such as Gipps' Model [7] which is used in AIMSUN [25], SISTM, and DRACULA; Wiedemann's model [10, 11] used in VISSIM [26], Pitt's model in CORSIM, and Fritzsche's model [9] in PARAMICS [27]. Understandably, those models have better capabilities of emulating the behavior of vehicles in real life conditions. However, that characteristic comes at the price of a more complex and complicated mathematical expression that requires a substantial effort to be calibrated.

#### *2.1.1.1 Intelligent Driver Model (IDM)*

The first model that will be presented is the IDM car-following model (Intelligent Driver Model) [8], which expression is presented in Equation II.2.

$$a\ (u_\alpha, s_\alpha, \Delta u_\alpha) = a\left(1 - \left(\frac{u_\alpha}{u_0}\right)^\delta - \left(\frac{s^*(u_\alpha, \Delta u_\alpha)}{s_\alpha}\right)^2\right) \tag{II.2.1}$$

With

$$s^*(u_\alpha, \Delta u_\alpha) = s_0 + u_\alpha T + \frac{u_\alpha \Delta u_\alpha}{2\sqrt{ab}} \quad \text{(II.2.2)}$$

Where $u_\alpha$ is the velocity of vehicle α, $a$ is the maximum acceleration, $u_0$ is the desired velocity, $\Delta u_\alpha$ is the velocity difference between vehicle $\alpha$ and the leading vehicle, $s_\alpha$ is the spacing between the vehicle and its leader, $s_0$ is the minimum spacing, $T$ is the desired time headway, and $b$ is the comfortable braking deceleration. Finally, δ is an exponent that is usually equal to 4.

The IDM model, proposed by Treiber et al. [8], is widely used for the simulation of freeway traffic. The big fame of this model is mainly due to its mathematical stability resulting in stable vehicle trajectories.

The IDM model [8] was developed in the aim of reproducing traffic as realistically as possible and with the smallest number of parameters. The main strength of the IDM model is that it is able to simulate instabilities as well as hysteresis effects.

The IDM model [8] formulation is innovative in that it combines both acceleration and deceleration strategies. The acceleration strategy is sensitive to the ratio of the instantaneous speed and desired speed, and raises this value by the acceleration exponent. The deceleration strategy, on the other hand, examines the desired spacing that ensures that no collisions would occur.

#### *2.1.1.2 Gazis-Herman-Rothery (GHR) Model*

The GHR model [3] can be perceived as a series of different models that were developed experimentally from the late fifties until the mid-sixties. The experiments were conducted by General Motors, which is the reason why the GHR is usually referred to as the GM model. Over the period of the experiments, five variants of the GM model were developed. However, the family of the different variants is englobed by the fifth and final formulation of the model, sometimes referred to as the GM-5 model. The formulation of the GM-5 model is given in Equation II.3.

$$\ddot{x}_{n+1}(t) = \left\{ \frac{\alpha[\dot{x}_{n+1}(t)]^z}{[\Delta x_{n \to n+1}(t-\tau)]^l} \right\} \cdot [\Delta \dot{x}_{n \to n+1}(t-\tau)] \quad \text{(II.3)}$$

Where α, z and l are the parameters that need to be calibrated.

The GM model is a very special model that has been the subject of a lot of research. In fact, it can be cast as a pillar to the subject of car-following analysis. The reason behind that is that there are many other microscopic and macroscopic models that can be represented as special cases of the generalized formulation of the GM model. In fact, the Greenshields single-regime traffic stream model is one such case [28, 29]. It can be expressed as a GM model by setting the z and l parameters to be equal to 0 and 2. Furthermore, the Pipes car-following model [30] is another special case. In fact, the formulation of the Pipes model is obtainable from the generalized GM model when the z and l parameters are set equal to zero.

However, a main drawback of the GM model is that it is very sensitive and, if not handled appropriately, would become easily instable and results in growing oscillations in the estimated time-space trajectories.

#### *2.1.1.3 Gipps Model*

This model [7] was developed by Gipps as a result to the proliferation and success of GM type models [3] in the late-1970s and implemented in the traffic simulation software *AIMSUN* [25]. Mathematically speaking, Gipps model is formulated as a system of differential difference equations. Using a time step $\Delta t$ that aims to model the reaction time of drivers, the model computes the following vehicle speed $u_n$ at time $t+\Delta t$ as a function of its speed and the leading vehicle speed $u_{n-1}$ at the preceding time step $t$.

As shown in Equation II.4, the speed of the following vehicle is estimated by determining the minimum of two arguments. The first term governs the cases characterized by uncongested traffic and relatively large headways. Under such conditions, the following vehicle speed increases until the free-flow speed of the facility $u_f$ is reached. The model formulation is also inclusive of a condition that ensures that $u_f$ is never exceeded once achieved. The second argument of the model is attained when congestion prevails and speeds are constrained by the behavior of the vehicles ahead of them. Due to the collision avoidance mechanism it implements, the congested regime branch is the one responsible for making the Gipps model collision-free.

$$u_n(t+\Delta t) = min\left[\begin{array}{c} u_n(t) + 2.5A_{max}^{des}.\Delta t\left(1-\frac{u_n(t)}{u_f}\right)\sqrt{0.025+\frac{u_n(t)}{u_f}} \\ D_{max}^{des}.\Delta t + \sqrt{\left(D_{max}^{des}.\Delta t\right)^2 - D_{max}^{des}\left(2\left(\Delta x_{n-1\to n}(t)-L_{n-1}\right)-\Delta t.u_n(t)-\frac{u_{n-1}^2(t)}{\hat{D}_{n-1}}\right)} \end{array}\right] \quad \text{II.(4)}$$

Where $A_{max}^{des}$ and $D_{max}^{des}$ are the respective desired maximum acceleration and deceleration of vehicle $n$ in $\left(m/s^2\right)$, and $\hat{D}_{n-1}$ denote the maximum deceleration rate of vehicle $n-1$ in $\left(m/s^2\right)$. Those three parameters are the ones requiring calibration for Gipps model.

In a later separate effort, Rakha et al. [31, 32] derived the macroscopic fundamental diagram from the steady state portion of the model. It was found that the speed-flow relationship can be computed using Equation II.5.

$$q = \frac{1{,}000 * \dot{x}_{n+1}}{\Delta x_j + \frac{1}{2.4} * \tau * \dot{x}_{n+1} + \frac{1}{25.92 * \ddot{x}_{d-min}} * \left(1 - \frac{\ddot{x}_{d-min}}{\ddot{x}_{d-min,n}}\right) * \dot{x}_{n+1}^{\,2}} \tag{II.5}$$

### 2.1.1.4 *Wiedemann Model*

Wiedemann model [10] is a psycho-physical car-following model that is widely known in the traffic engineering community due to its integration in the microscopic multi-modal traffic simulation software *VISSIM* [26]. The initial formulation of the model [10], proposed in 1974, was calibrated mostly based on conceptual ideas rather than real traffic data. As a result, a much-needed recalibration of the model [11] was performed in the early-1990s using an instrumented vehicle.

The Wiedemann model framework, as implemented in *VISSIM*, uses five bounding functions in the $\Delta v - \Delta x$ domain —*AX*, *ABX*, *SDX*, *SDV* and *OPDV*— to define the thresholds between four traffic regimes — free driving, closing-in, following and emergency — as presented in Figure 1.a. The figure illustrates the Wiedemann model logic graphically by showing how a following vehicle would behave as it is approaching a lead vehicle. Depending on the traffic regime in which the following vehicle is located, the acceleration is set equal to a predefined specific rate as illustrated in Figure 1.a. The mathematical expressions of the five regime thresholds are given in Equations (II.6- II.10).

$$AX = L_{n-1} + \left[AX_{add} + AX_{mult} \times RND1\right] \tag{II.6}$$

$$ABX = AX + \left[BX_{add} + BX_{mult} \times RND1\right].\sqrt{min\left(u_{n-1}, u_n\right)} \tag{II.7}$$

$$SDX = AX + \left[EX_{add} + EX_{mult} \times \left(NRND - RND2\right)\right] \times \left[BX_{add} + BX_{mult} \times RND1\right]\sqrt{min\left(u_{n-1}, u_n\right)} \tag{II.8}$$

$$SDV = \left( \frac{\Delta x - L_{n-1} - AX}{CX} \right)^2 \quad \text{(II.9)}$$

$$OPDV = SDV \times \left[ -OPDV_{add} - OPDV_{mult} \times NRND \right] \quad \text{(II.10)}$$

Where *RND1*, *RND2*, *RND3*, *RND4* and *NRND* are normally distributed parameters that aim to model the randomness associated with different driving patterns and behaviors, $L_{n-1}$ is the length of the leading vehicle in meters, $u_{n-1}$ is the leading vehicle speed in (*m/s)*, and *CX* is a model parameter that is assumed to be equal to 40. Finally, the remaining variables, named using the standard format $PARAMETER_{add}$ or $PARAMETER_{mult}$, are the model parameters requiring calibration.

### *2.1.1.5 Frietzsche Model*

Frietzsche model [9] is a car-following model that shares the same structure as Wiedemann model. In this model, six threshold parameters are used to define five driving regimes. The thresholds are defined for four gap ($\Delta x$) values and two differences in speed ($\Delta v$) values between the leader and the follower vehicles. The four gap threshold parameters, *AR*, *AS*, *AD*, and *AB* are presented by Equation II.11 through II.14, respectively; while the two differences in speed thresholds, *PTP* and *PTN*, are given by Equation II.15 and II.16.

The five different driving regimes are shown by Figure 1.b along with the acceleration rates assigned for each regime. We note that the expression of the acceleration rate $a_n$ associated with the "closing in" regime is given by Equation II.17.

$$AR = s_{n-1} + T_r \times u_{n-1} \quad \text{(II.11)}$$

$$AS = s_{n-1} + T_s \times u_n \quad \text{(II.12)}$$

$$AD = s_{n-1} + T_D \times u_n \quad \text{(II.13)}$$

$$AB = AR + \frac{\Delta u^2}{\Delta b_m} \quad \text{(II.14)}$$

$$PTP = K_{PTP} \times (\Delta x - s_{n-1})^2 + f_x \quad \text{(II.15)}$$

$$PTN = -K_{PTN} \times (\Delta x - s_{n-1})^2 - f_x \quad \text{(II.16)}$$

$$a_n = \frac{u_{n-1}^2 - u_n^2}{2 \times d_c} \tag{II.17}$$

$$d_c = \Delta x - AR + u_{n-1} \times \Delta t \tag{II.18}$$

Where $T_r$, $T_s$, $T_D$ and $\Delta b_m$ are calibration parameters expressed in seconds.

**(a)**

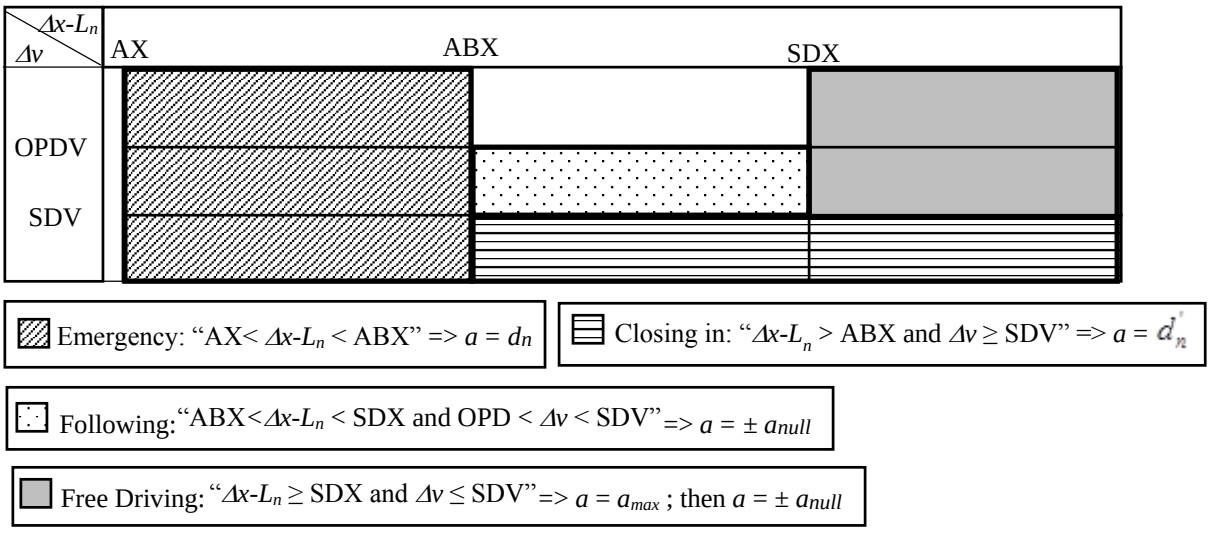


**(b)**

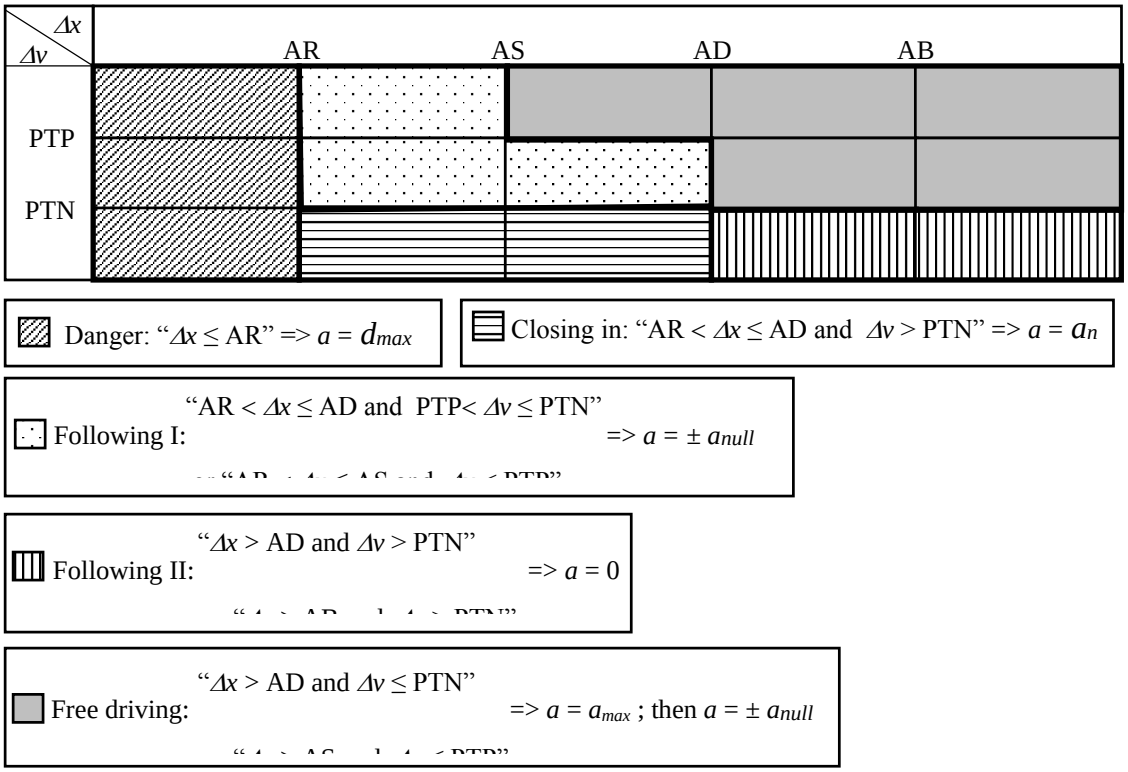


**Figure 1: Model structure of: a. Wiedemann model; b. Frietzsche model**

Finally, it should be noted that the main drawback of kinematics models including the ones cited above remains the complete ignorance of the dynamics of the vehicle and the resisting forces acting on it. In the next section, car-following models that consider the last two critical factors are presented and briefly discussed.

### 2.1.2 Vehicle Dynamics Based Models

#### *2.1.2.1 Searle Model*

With regards to vehicle dynamics models, Searle [13] was among the pioneers who developed a model for the determination of speeds and traveled distances. However, his proposed model does not account for resistive forces. Furthermore, the model, shown by Equation II.19 and Equation II.20, is only useful for computations that involve maximum acceleration of the vehicle which is not representative of the way with which vehicles accelerate typically in the field.

$$u^2(t) = u_0^2 + \frac{15.8\eta P_{\max}}{M} t \tag{II.19}$$

$$u^3(x) = u_0^3 + \frac{23.7\eta P_{\max}}{M} x \tag{II.20}$$

Where $u_0$ is the initial speed, $\eta$ is the acceleration efficiency, $P_{max}$ is the maximum engine power, $M$ is the mass of the vehicle, $t$ is the time, $x$ is the position.

#### *2.1.2.2 The RPA Car Following Model*

The RPA model [12] is a car-following model that controls the longitudinal motion of the vehicles in the INTEGRATION traffic simulation software [14, 15]. The model is composed of three main components: the steady-state, the collision avoidance and the vehicle dynamics models. Having the values of its three components, the RPA model computes the speed of the following vehicle as shown in Equation II.21.

$$u_{n+1}(t) = \min\left(u_{n+1}^{VA}(t), u_{n+1}^{CA}(t), u_{n+1}^{DYN}(t)\right) \tag{II.21}$$

Here $u_{n+1}^{VA}(t)$, $u_{n+1}^{CA}(t)$ and $u_{n+1}^{DYN}(t)$ are the speeds calculated using the three modules described previously and which expressions are given in what follows.

#### *2.1.2.2.1 First-order Steady-state Car-following Model*

The RPA model utilizes the Van Aerde nonlinear functional form to control the steady-state behavior of traffic. The latter model was proposed by Van Aerde and Rakha [33] and is formulated as presented in Equation II.22.

$$s_{n+1}^{VA}(t) = c_1 + \frac{c_2}{u_f - u_{n+1}(t)} + c_3 u_{n+1}(t) \tag{II.22}$$

Here $s_{n+1}^{VA}(t)$ is the steady state spacing (in meters) between the leading vehicle *n* and vehicle *n+1* at time *t*, $u_{n+1}(t)$ is the speed of vehicle $n + 1$, in (m/s), $u_f$ is the free-flow speed expressed in m/s, and $c_1$ (m), $c_2$ (m$^2$/s) and $c_3$ (s) are constants used for the Van Aerde steady-state model that have been shown to be directly related to the macroscopic parameters defining the fundamental diagram of the roadway.

Finally, it should be noted that from the perspective of car-following modeling, the main objective is to determine how the following vehicle responds to changes in the behavior of the leading vehicle. Subsequently, a speed formulation is adopted from the Van Aerde model, as demonstrated in Equation II.23, which is easily derived from Equation II.22 using basic mathematics.

$$u_{n+1}^{VA}(t) = \frac{-c_1 + c_3 u_f + \Delta x_{n \to n+1}(t) - \sqrt{\left(c_1 - c_3 u_f - s_{n+1}(t)\right)^2 - 4c_3\left(s_{n+1}(t) u_f - c_1 u_f - c_2\right)}}{2c_3} \tag{II.23}$$

#### *2.1.2.2.2 Collision Avoidance Model*

The expression of the collision avoidance term is shown in Equation II.24 and is directly related to a simple derivation of the maximum distance that a vehicle can travel to decelerate from its initial speed to the speed of the vehicle ahead of it while ensuring that, in the case of a complete stop, the jam density spacing between the two vehicles is respected.

$$u_{n+1}^{CA}(t) = \sqrt{\left(u_n(t)\right)^2 + 2b\left(\Delta x_{n \to n+1}(t) - \Delta x_j\right)} \tag{II.24}$$

Here *b* is the maximum deceleration at which the vehicles are allowed to decelerate.

#### *2.1.2.2.3 Vehicle Dynamics Model*

The final component of the RPA model is the vehicle dynamics model [16, 34] that ensures that the vehicle's mechanical capabilities do not limit it from attaining the speeds that are

dictated by the steady-state component. This model computes the typical acceleration of the following vehicle as the ratio of the resultant force to the vehicle mass *M* (Equation II.25). The resultant force is computed as the difference between the tractive force acting on the following vehicle $F_{n+1}$ (Equation II.26) and the sum of the resistive forces acting on the vehicle which include the aerodynamics, rolling and grade resistances.

$$a_{n+1}^{DYN}(t) = \frac{F_{n+1}(t) - \left(R_{a\,n+1}(t) + R_{r\,n+1}(t) + R_{g\,n+1}(t)\right)}{M_{n+1}} \tag{II.25}$$

With

$$F_{n+1}(t) = \min\left(3600\eta\ \frac{\gamma P}{u_{n+1}(t)}, 9.8066\ \mu\ M_{ta}\right) \tag{II.26}$$

Here *P* is the engine power, $\mu$ is the coefficient of friction between the tires and the pavement, $\gamma$ is the vehicle throttle level (taken as the percentage of the maximum observed throttle level that a certain driver uses), $\eta$ is the power transmission efficiency, $M_{ta}$ is the vehicle mass on the tractive axle.

The acceleration computed using the dynamics model is then used to calculate the maximum feasible speed $u_{n+1}^{DYN}$ using a first Euler approximation.

### 2.1.3 Human Behavior Modeling in Car-Following Theory

Modeling the impact of human behavior in traffic flow theory has been always overlooked. The ignorance of such an important element in traffic is not random. In fact, traffic engineers and researchers have always had a complex challenge with modeling the complex behavior of the human driving the vehicle. The difficulty of mathematically modeling the vehicle and the driver as a one unique component is due to the fact that traffic engineers mostly rely on simulated data in their research due to the practicality and the simplicity of its acquisition.

In other words, the success in modeling the driver/vehicle interaction aspect is related to the accuracy and the precision of the mathematical models implemented in the traffic simulation software producing these data. When focusing on the human element in car-following theory, the existing models could be categorized in two major categories. The first category encloses all the models that were developed from an engineering standpoint. While those models imitate to a certain level the car-following behavior of vehicles as it occurs in the field, they are mostly exclusive of any parameters that aim to relate to how humans behave and differ from each other and usually try to represent human behavior in the most simplistic

manner by just introducing a lag and a delay in the response of the drivers (a perception-reaction time). The second category is composed of models that were developed considering human factors. The latter models are usually more complicated in terms of mathematical representation and development.

With regards to the first category, it includes the majority of the existing car-following models which will usually fall within one of these families: GHR models and their extensions, linear models, optimal velocity models and collision avoidance models. It is noteworthy to mention that extensions that aim to account for human behavior were developed for some of these models. For example, Van Wissum [35] modified Helly's linear model [36] from a human behavior standpoint. The study of Van Wissum is pretty straightforward and easy to understand. It aims to more effectively incorporate human behavioral considerations into some engineering car-following models. The proposed modification consists on capturing human behavior through the estimation of a desired time headway. Subsequently, any differences between drivers in responses to driving conditions and mental efforts would be mainly represented by the differences in the time headway. In other words, an aggressive driver who is used to the road taken and familiar with his vehicle will be using a shorter time headway than a passive driver who will be taking less risk to avoid collisions.

The second category of car-following models includes those that were developed from a human perspective and aim to provide a psychological plausible characterization of how humans approach and think about the driving task. Looking at driving from a human perspective makes the modeling offered by the car-following model more logical and realistic since it does not look at finding an optimal solution that optimizes all the resources, but rather it looks at approximating trajectories that are feasible and prone to error (such as the possibility of a crash occurring which surprisingly is something impossible to happen in engineering car-following models). Over the years, researchers have identified different human factors that influence driving. The list includes socio-economic characteristics such as age and gender, reaction time, estimation errors as a human can only estimate spacing and speeds with limited accuracy, perception threshold, imperfect driving, aggressiveness, passivity, risk taking, distraction, driving skills, etc.

Among the first models that considered human factors, one can mention the model proposed by Wiedemann that uses perceptual thresholds (the minimum value of the stimulus that a driver can perceive and subsequently responds to). Another noteworthy theory is the one that considers that humans respond to the change in the visual angle that they perceive. In fact,

researchers have shown that humans are not well suited to estimate longitudinal distances and speeds, but rather respond to the perceived changes in the size of the leading vehicle which gets bigger as they get closer to it. There exists also models which explicitly consider driver error and distraction. Such models include the one proposed by Van Wissum that was discussed earlier.

## 2.2 OVERVIEW OF COOPERATIVE ADAPTIVE CRUISE CONTROL SYSTEMS

The second section of the literature review related to this thesis provides a brief overview of the most significant research conducted in relation to cooperative adaptive cruise control systems. Over the last decade, the interest in vehicle cooperation as a means of mitigating congestion and increasing traffic flow has grown exponentially among traffic engineers and researchers. While the fundamental concepts and the theories behind vehicle platooning were investigated as early as the 1960s, it is only quite recently that the vehicle cooperation concept was explored from an implementation and experimentation perspective. The main factor that contributed to the transition of vehicle platooning from a theoretical concept to a feasible functional system is the advancement in wireless communication technology. It is noteworthy to mention that the affordability and reliability of wireless communication technology is complemented by the diverse and advanced driver assistance systems and navigation systems.

To illustrate how this traffic concept is rapidly converging towards becoming a reality, there is no better argument than noticing the number of recent studies funded by the legislator preparing the technical and legal ground to vehicle cooperation and other intelligent transportation systems (ITS). Two projects of the Federal Highway Administration (FHWA) can serve as examples for the latter statement. The first study [37] relates, among others, to investigating the human factors involved in the cooperative adaptive cruise control (CACC) concept, identifying the necessary equipment and resources, and assisting researchers in the design process of test scenarios. The main contribution of the study is the development of a framework that can be used to evaluate the human-factors, safety, and implementation issues associated with CACC. The second must be answered FHWA project [38] is oriented towards the case in which the CACC concept is applied to heavy trucks. Aiming to evaluate the commercial feasibility of Driver Assistive Truck Platooning (DATP), the study performed the necessary technical work, evaluation, and industry engagement to identify the key questions that prior to market introduction of heavy truck platooning.

Technically speaking, intelligent vehicle cooperation can be cast as an extension or an upgrade to the commercially available adaptive cruise control systems (ACC). Through transmitting information about the speeds and positions of the vehicles in the platoon using centralized and/or decentralized wireless communication, a controller automatically adjusts the speeds of the vehicles in the platoon resulting in a higher traffic flow as vehicles operate at a much closer spacing. A successful cooperative adaptive cruise control system would be one that is implementable in a fast and cost-effective manner without resulting in any disruptions and instabilities to the flow of vehicles or giving rise to any safety concerns and accidents.

In what follows, some of the most recent literature that involved developing and investigating cooperative vehicle platooning strategies in an experimental setting is outlined. For instance, one can mention the research conducted by Naus et. al [39] in which a CACC system was designed and tested using two vehicles for scenarios involving both constant and speed-dependent inter-vehicle spacing. The objective of the study was oriented towards investigating the feasibility and the stability of the proposed control system. It was demonstrated that a speed-dependent gap between vehicles is necessary in order to ensure the overall string stability. Another practical CACC system was proposed in [40]. The underlying controller was examined by implementing it in four production passenger vehicles and testing it in several experimental settings. Among the experimental trials that were carried out, we distinguish situations that aim to emulate cut-in and cut-out maneuvers as well as the case in which the time gap setting is changed by the driver. The system performance was then evaluated by comparing its resulting traffic behavior against that generated by the original ACC system of the vehicles.

In relation to heavy duty vehicles (HDV), platooning and cooperative systems have been extensively investigated. The intense interest in developing and designing control strategies that specifically target HDVs is due to the significant reduction in fuel consumption and emissions they result in. In fact, through minimizing the inter-vehicle gap, fuel efficiency and emission reduction are achieved through lowering the aerodynamic resistance to which the truck is exposed. Aside from the environmental impact and financial benefit to transportation companies, it is worth mentioning that truck platooning is conceptually different than when passenger vehicles are involved. The latter is explained by the huge impact that the heavy mass, the air drag and the road grade has on the system dynamics.

Motivated by the significant savings in fuel costs resulting from truck platooning, Alam [41] developed a framework for the design, implementation, and evaluation of energy efficient

HDV platooning. Using game theory, HDV platooning was investigated as an optimization problem that aims to minimize the inter-vehicular gap between trucks while ensuring that the platoon is string-stable and collision-free. In that regard, a decentralized feedback controller was developed. In a first stage, the control system adjusted the behavior of the following truck as a function of just its immediate predecessor. However, the controller was modified later on to account for several preceding vehicles. The main contribution of this research resides in the fact that it proceeded to validate the developed control strategy both through computer simulation and experimental testing using real HDVs. The experiments demonstrate that fuel savings of at least 4% and up to 20% could be achieved depending on the tested scenario.

All of the aforementioned studies share in common the fact that a prototype was created and implemented in real vehicles allowing for experimental testing of the system ensuring both its functionality and safety to a certain degree. In other words, it was verified that they were incorporative of the different transmission and response delays along with any non-linear dynamics involved. The latter is not the case for several studies about vehicle platooning which are usually based on simplified theoretical models and assumptions. Research that fall under the latter category include the study of Stanger and Del Re [42]. Noticing the achievability of a lower fuel consumption using CACC, the study developed a linear model predictive control approach that aims to directly optimize the fuel efficiency of the vehicles in the platoon rather than trying to minimize the acceleration variability or the inter-vehicular gap. For that purpose, the authors assumed a simplified linear car-following model along with a piecewise quadratic approximation of the non-linear static fuel consumption map of the internal combustion engine. Using numerical simulation, the proposed control approach was validated by observing that the CACC scenario results in around 20% fuel efficiency when compared to the standard non-cooperative case. With a similar stated objective of attaining an optimal fuel efficiency, Deng and Ma [43] derived a speed planning algorithm that is based on the Pontryagin Minimum Principle (PMP) for the case of HDVs. First, the study investigated the case of a single vehicle before extending it, in a second stage, to a platoon of two trucks. The Oguchi fuel consumption model was used in order to evaluate the potential energy savings due to the control strategy. Through numerical investigation, the developed controller was demonstrated to result in a 30% reduction in fuel consumption when decelerating and a 3.5% reduction when accelerating.

Another control approach that aims to achieve both fuel and emissions efficiency in a CACC environment was proposed by Schmied et al. [44]. The paper opted for a Nonlinear Model Predictive Control (NMPC) approach to develop a CACC system that ensures efficiency

at the level of fuel consumption and emissions. It is noteworthy here to mention that the use of a NMPC has many advantages when compared to a basic linear model predictive control. For instance, NMPCs would allow to achieve several goals and objectives even if they contradict each other while ensuring the respect of several constraints. Despite the latter, linear model predictive controls remain the ones implemented in vehicles due to the fact that NMPCs are computationally burdensome compared to linear controls. That could possibly explain why the proposed NMPC for cooperative adaptive cruise control [44] was tested in a Hardware In the Loop (HIL) configuration on a dynamic engine test bench rather than implemented directly in a real vehicle. A scenario involving two consecutive vehicles with infrastructure-to-vehicle (I2V) communication was tested using the HIL configuration. The outcome of the conducted experiments demonstrates the potential for a 13% reduction in the fuel consumption level and a decrease of NOx and PM emissions by 24% and 28% respectively. The quantification of the previous rates of change was made possible through the use of a flow meter, a Horiba 7100 device and an AVL Opacimeter to respectively measure the fuel injected in the engine, NOx and PM emissions. A very similar experimental setting was used in another research effort [45] in which a controller was integrated to a HIL configuration. Three key differences exist between [45] and [44]. First, a heuristic controller was developed and used for vehicle cooperation rather than a NMPC. Second, the objective of the study was just limited to achieving fuel efficiency. Third, fuel consumption was measured using a static dynamometer. Similarly to the NMPC of [44], the heavy computational load due to the heuristic algorithm might be the justifying factor behind the choice of a HIL configuration on a real engine for validation purposes. In terms of the heuristic controller efficiency, the conducted experiments show a decrease in fuel consumption that ranges between 15% and 20%. In a different study, Diaby and Sorkati [46] selected a very specific traffic phenomenon that combines most of the elements that results in a huge increase of fuel consumption and tried to investigate the effect of platooning on it. Put simply, the study investigated the case in which a platoon of heavy trucks is traveling in a hilly region and presented a method that results in a minimal fuel consumption with respect to both the topography of the area and the air drag. The proposed algorithm consists on formulating the problem as a convex quadratic programming problem that optimizes the speeds of the different trucks in the platoon.

Further, it is worth mentioning the innovative research effort presented in [47] which targets the vehicle cooperation problem for the specific case of electric vehicles. Assuming that the power is 100% related to energy consumption of EVs and that the longitudinal behavior of

the vehicles is governed by the modified Gipps car-following model, the study developed an EV-Eco-CACC that aims to increase energy efficiency and tested it through computer simulation.

# Chapter 3 A Vehicle Dynamics Model for Estimating Typical Vehicle Accelerations

**Authors:**

Karim Fadhloun

Hesham Rakha, Ph.D, P.Eng.

Amara Loulizi, Ph.D, P.E.

Abdessattar Abdelkefi, Ph.D.

*Presented at the 2015 TRB Annual Meeting and Published in the Transportation Research Record: Journal of the Transportation Research Board, 2015.*

## 3.1 ABSTRACT

Developing mathematical modeling for accurate estimation of the longitudinal acceleration behavior of vehicles is one of the important challenges in traffic engineering. The complexity of modeling vehicle acceleration is due to its dependence on the vehicle's type and human driving behavior, which are the most important factors to deal with for roadway designers and traffic analysts. Existing acceleration dynamics models have tied typical accelerations to maximum acceleration models. While doing so results in a better fitting of field data which is understandable and predictable, the proposed models do not take into account different driving behaviors. The research presented in this paper develops a model that overcomes this limitation by explicitly incorporating driver behavior in the mathematical expression of a dynamics-based acceleration model. The proposed model has a flexible shape that allows it to incorporate different types of variations that drivers can generate. Furthermore, the model is proved to be superior to other similar models in that it predicts more accurate acceleration rates in all domains.

## 3.2 INTRODUCTION

The analysis of car-following behavior constitutes a pillar of traffic flow theory. In fact, several models aiming to emulate the way with which vehicles follow each other have been developed over the last fifty years. While it is true that, over the time, car-following models have evolved gradually in terms of accuracy; and subsequently, complexity of their mathematical expression;

an important component of these models had been surprisingly overlooked. In fact, few studies treated the effects of the vehicle characteristics and driver behavior on the acceleration function without which no car-following model would make sense. It is quite surprising that such an important element has not been thoroughly studied as it is mainly dealing with the key component composing traffic, namely the system of the vehicle and its driver. Furthermore, it should be noted that vehicle acceleration directly impacts several other factors and aspects of traffic engineering besides car-following models which are used in microscopic simulation traffic software. As an example, one can mention the state-of the-art emissions and fuel consumption models for which accurate models of typical acceleration behavior is necessary for precise predictions of these measures of effectiveness (MOE). However, coming up with accurate and precise typical acceleration models is easier said than done. The difficulty in completing such a task is mainly due to the existence of countless vehicle types and to the different driving behaviors that can be adopted by different drivers. This paper describes research performed to develop a vehicle dynamics acceleration model that is sensitive to the characteristics of the vehicle as well as human driving behavior.

Besides providing a brief comprehensive overview of the literature, the objectives and contributions of this paper are two-fold:

- Develop a vehicle dynamics model that is capable of estimating typical accelerations behavior. Besides taking into account the mechanical characteristics of vehicles, the model explicitly considers parameters that are reflective of different driving patterns. The proposed model can be cast as an extension to the work of Rakha et al. [16, 17].
- Validate the developed model by comparing its performance to that of other existing models in terms of goodness of fit.

Concerning the layout, this paper is organized as follows. First, a brief comprehensive overview of the literature is provided. After that, the field experiments that generated the data used in this study are described and the analysis related to the calibration procedure as well as the validation process of the proposed model is presented. Finally, the conclusions of the paper are drawn and insights for future work are provided.

## 3.3 BACKGROUND

Developing mathematical modeling for accurate estimation of the longitudinal acceleration behavior of vehicles is one of the important challenges in traffic engineering. The complexity

of modeling vehicle longitudinal acceleration is due to its dependence to the vehicle's type and human driving behavior, which are the most important factors to deal with for roadway design.

Acceleration rates are also as important to traffic analysts as they are for roadway geometric designers. As a matter of fact, a significant part of traffic analysis is based on data that are generated by microscopic simulation software. The obtained data and results from the latter programs are highly dependent on the car-following model that is incorporated in their algorithms. Subsequently, not only an accurate acceleration function is primordial to get correct estimation of travel times and delays; but also it directly impacts the precision of predicting other MOE parameters such as fuel consumption and emissions.

As a natural result to its noticeable importance and the diversity of its applications, researchers have thoroughly investigated the acceleration behavior of vehicles over the last fifty years and have developed several models that aim to predict maximum as well as typical acceleration levels [13, 16, 17, 20-22, 34, 48]. While the existing acceleration models are numerous and have evolved over the time in terms of exactitude and complexity of their mathematical expressions, one cannot deny the fact that the topic is still kind of overlooked and that there is still a lot of research studies to be performed to improve these mathematical representations. The overlooking of this sensitive research topic is due to several reasons. For example, one can state the fact that there are so many parameters that intervene and have an effect on the acceleration produced by a vehicle, such as its mechanical characteristics, type of the roadway on which it is traveling, and randomness in human driving behavior.

From a technical point of view, acceleration models can be divided into two categories. The first category encloses all the models that were developed based on kinematics. While those models imitate to a certain level the car-following behavior of vehicles as it occurs in the field, they totally ignore the mechanical characteristics of the vehicle which represents one of their major weaknesses. The second category is composed of models that incorporate vehicle dynamics. Acceleration models that consider vehicle dynamics explicitly in their expressions account for both tractive and resistive forces that act on the vehicle. These models are more accurate; however, they are more complicated in terms of mathematical representation and development.

### 3.3.1 Kinematics Based Models

Kinematics models describe the motion of vehicles considering the mathematical relationships between the acceleration, the speed, and the distance that is traveled by the vehicle without

consideration of the causes of the motion. In other words, in these models, the mathematical representations of the acceleration totally ignore the vehicle characteristics, the driving pattern, and the roadway effects. Generally, these models are the direct result of an analysis of fictive or field vehicle trajectories. The most famous of these models is the very simple constant acceleration model [19]. As its name implies, the model assumes a constant acceleration level for the entire length of the trip. From that point, the speed and the distance traveled are determined by successive integrations leading to a linear expression of speed and a quadratic expression of distance as a function of time. Whilst this model is easy to apply, it is far from reality since everybody knows that vehicle acceleration is never constant. This model is justified for use in geometric design since it produces conservative values for the design parameters (length of acceleration lanes for example), but cannot be used in traffic simulation software.

Subsequently, in a later effort, noticing that vehicles' ability to accelerate is higher at low speeds, Bham and Benekohal [20] developed a dual regime model that only differs from the constant acceleration model by the fact that it considers two acceleration rates: one for low speeds which is the higher one, and the other is for the second regime enclosing higher speeds.

Without going into much details, other well-known acceleration models that are based on kinematics include Drew's linear decay model [19] developed in 1968, and shown by Equation III.1. For Drew's model, Long [21] has provided a complete analysis of the values that can be adopted by the two parameters $\alpha$ and $\beta$.

$$a(v) = \alpha - \beta v \tag{III.1}$$

Where α is the maximum acceleration rate and α /β is the maximum attainable speed.

A similar but a slightly different model was proposed by Lee [22] in 1977. The only difference between Lee's model and Drew's model resides in the fact that it is sensitive to the time rather than to the speed as presented in Equation 1. However, Bham and Benekohal [20], based on the obtained results of their study, did not recommend the use of the modified version of the linear decay model.

Other notable models include the gamma model, proposed by Bham and Benekohal [20], the three acceleration models that were developed by Akcelik [23] as well as the three kinematics models, namely the haversine model, the triangular model and the sinusoidal model, that were proposed by Varat and Husher [24].

The last model that will be mentioned is the acceleration function of the IDM car-following model (Intelligent Driver Model) [8], which expression is presented in Equation III.2.

$$\dot{v_\alpha}(v_\alpha, s_\alpha, \Delta v_\alpha) = a\left(1 - \left(\frac{v_\alpha}{v_0}\right)^\delta - \left(\frac{s^*(v_\alpha, \Delta v_\alpha)}{s_\alpha}\right)^2\right) \quad \text{(III.2.1)}$$

With

$$s^*(v_\alpha, \Delta v_\alpha) = s_0 + v_\alpha T + \frac{v_\alpha \Delta v_\alpha}{2\sqrt{ab}} \quad \text{(III.2.2)}$$

Where $v_\alpha$ is the velocity of vehicle α, $a$ is the maximum acceleration, $v_0$ is the desired velocity, $\Delta v_\alpha$ is the velocity difference between vehicle $\alpha$ and the leading vehicle, $s_\alpha$ is the spacing between the vehicle and its leader, $s_0$ is the minimum spacing, $T$ is the desired time headway, and $b$ is the comfortable braking deceleration. Finally, δ is an exponent that is usually equal to 4.

The IDM model, proposed by Treiber et al. [8], is widely used for the simulation of freeway traffic. The big fame of this model is mainly due to its mathematical stability resulting in stable vehicle trajectories. It should be noted that when only one vehicle is on the road, the distance to the leading vehicle $s_\alpha$ can be assumed to be very large, and therefore one can neglect the second term presented in Equation III.2.1 to produce Equation III.3.

$$a(v_\alpha) = a\left(1 - \left(\frac{v_\alpha}{v_0}\right)^\delta\right) \quad \text{(III.3)}$$

This equation was used by the research team, as presented later on, to validate their acceleration model developed under free road behavior.

Finally, it should be noted that the main drawback of all the previously cited models remain the complete ignorance of the dynamics of the vehicle and the resisting forces acting on it. Next, a set of the most famous models that consider the last two critical factors are presented and briefly discussed.

### 3.3.2 Vehicle Dynamics Based Models

Searle [13] was among the pioneers who developed a model for the determination of speeds and traveled distances. However, his proposed model does not account for resistive forces. Furthermore, the model, shown by Equation III.4 and Equation III.5, is only useful for

computations that involve maximum acceleration of the vehicle which is not representative of the way with which vehicles accelerate typically in the field.

$$v^2(t) = v_0^2 + \frac{15.8\eta P_{max}}{M} t \tag{III.4}$$

$$v^3(t) = v_0^3 + \frac{23.7\eta P_{max}}{M} x \tag{III.5}$$

Where $v_0$ is the initial speed, $\eta$ is the acceleration efficiency, $P_{max}$ is the maximum engine power, $M$ is the mass of the vehicle, $t$ is the time, and $x$ is the position.

Similar to Searle's model, in that it is only valid for the estimation of maximum acceleration, Rakha et al. developed a constant power model [34] and a variable power model [48] that allow predicting the maximum acceleration of trucks. The variable power model can be cast as an extension to the constant power model in that it accounts for the power loss due to the effect of successive gear shifting at low speeds.

The constant power model, which is presented by equation III.6, was proved in a later study by Rakha et al. [16] to be also adequate for the prediction of the maximum acceleration of light duty vehicles. This model computes the maximum acceleration of the vehicle as the ratio of the resultant force to the vehicle mass $M$ (Equation III.6.1). The resultant force is computed as the difference between the traction force acting on the vehicle $F$ (Equation III.6.2) and the sum of the resistive forces; namely the aerodynamics resistance $R_a$ (Equation III.6.3), the rolling resistance $R_r$ (Equation III.6.4) and the grade resistance $R_g$ (Equation III.6.5).

$$a = \frac{F - \left(R_a + R_r + R_g\right)}{M} \tag{III.6.1}$$

$$F = \min\left(3600\eta \frac{P}{u}, 9.8066\mu . M_{ta}\right) \tag{III.6.2}$$

$$R_a = c_1 C_d C_h A u^2 \tag{III.6.3}$$

$$R_r = 9.8066 . C_r(c_2 u + c_3) \frac{M}{1000} \tag{III.6.4}$$

$$R_g = 9.8066.M.i \quad \text{(III.6.5)}$$

Where $P$ is the engine power, $\mu$ is the coefficient of friction between the tires and the pavement, $u$ is the vehicle speed, $\eta$ is the power transmission efficiency, $M_{ta}$ is the vehicle mass on the tractive axle, $c_1$ is a constant equal to 0.047285, $C_d$ is the air drag coefficient, $C_h$ is an altitude coefficient, $A$ is the frontal area of the vehicle, $C_r$, $c_2$ and $c_3$ are rolling resistance coefficients, $i$ is the pavement grade.

Although the previous vehicle dynamics models directly tie the estimated acceleration rates to the characteristics of the vehicle, their usefulness is limited to the prediction of the maximum acceleration levels. In fact, regardless of the driving pattern considered, drivers almost never use the full acceleration capabilities of their vehicle. Subsequently, the developed maximum acceleration models can only serve as an envelope curve to the functions that model typical accelerations which are more important than maximum accelerations in terms of application.

It should be noted at this level that modeling typical accelerations is much harder than modeling maximum acceleration. The reason beyond that is that drivers rarely use the full capabilities of their vehicles. Furthermore, under normal driving conditions, drivers do control vehicle acceleration by how they step on the gas pedal. Subsequently, it is not systematic that the variation and the shape of the typical acceleration function would follow that of the function characterizing maximum acceleration.

In that context, Searle [13] acquired field data from six subject vehicles from which he concluded that the shape and the behavior of the maximum acceleration is similar to that observed under normal driving conditions. Rakha et al. [17] also investigated typical driver behavior. Based on the results of a controlled experiment, the authors modeled typical acceleration behavior using a reduction factor that is specific to each driver and that is applied to the constant power model described earlier. The set of experiments that was performed is briefly detailed in the next section as the resulting dataset constitutes the pillar for this study.

## 3.4 ANALYSIS

As was presented in the “Background” section, existing acceleration dynamics models have tied typical accelerations to maximum acceleration models. While doing so results in a better

fitting of field data which is understandable and predictable, the proposed models do not take into account different driving behaviors. This means that, regardless of the aggressiveness and the personal characteristics of the driver, the acceleration function will always have the shape of the maximum acceleration model.

The research described in this paper attempts to develop a model that overcomes this limitation by explicitly incorporating driver behavior in the mathematical expression of a dynamics-based acceleration model. Therefore, the proposed model should be flexible to incorporate different types of variations that drivers can generate.

This section is organized as follows. First, the set of experiments used to derive the proposed model are briefly described. After that, the analysis related to the calibration procedure of the model is presented including the justification of the choice of the functional form as well as the exponential smoothing of the resulting model to make it more consistent with physical observations. Finally, the performance of the proposed model is compared to other state-of-the-art models for validation purposes and the results are discussed.

### 3.4.1 Field Experiments

Field experiments that were conducted in 2002 at the VA Smart Road controlled test facility were found to be useful for fulfilling the objective of this research. The generated data was used then to study the effect of the driver characteristics on typical acceleration behavior [17]. During those field experiments, a group of 20 drivers that is representative of the driving population (gender, age, etc…) was asked to accelerate a test vehicle from a complete stop over a distance of approximately 335m (1100 ft) at their normal acceleration rate. The road segment on which the testing was performed was relatively straight and flat to neglect any effects that grades and curves might have. The same testing vehicle, a 1999 Ford Crown Victoria, was used by all the drivers. Characteristics of the testing vehicle and the roadway, which are needed for the dynamic based Rakha et al. model (Equation III.6), are shown in Table 1. Twenty five runs were performed by each driver to ensure that only differences between drivers are captured and the variability for each driver is taken into account.

**Table 1: Characteristics of the test vehicle and the roadway**

| | | | |
|---|---|---|---|
| **Mass, *M* (kg)** | 2300 | $C_d$ | 0.34 |
| **Power, *P* (kW)** | 149.2 | $C_h$ | 0.95 |
| $M_{ta}$ | 1357 | $c_1$ | 0.047284 |
| $i$ | 0 | $c_2$ | 0.0328 |
| $\eta$ | 0.7 | $c_3$ | 4.575 |
| $\mu$ | 0.6 | $C_r$ | 1.25 |
| **Altitude (m)** | 599 | $A$ ($m^2$) | 2.44 |

### 3.4.2 Calibration of the Proposed Model

The idea behind this research resides in the fact that the power delivered by the engine during driving cannot be assumed to be equal to the maximum power that the engine is able to produce nor to a constant percentage of that maximum power as modeled by Rakha et al.[17]. It is well-known that delivered engine power is directly sensitive to the percentage of the throttle opening, which itself is related to the speed of the vehicle and the way with which drivers press on the gas pedal. Subsequently, this study is based on a very basic idea which consists on incorporating a throttle function in the already developed Rakha et al. [16] constant power model.

However, the way with which the throttle varies as a function of speed made coming up with a functional form that is descriptive of its behavior a difficult task. The challenges that were encountered are mainly related to the fact that once a driver reaches his/her maximum comfortable throttle level (first portion of the throttle variation with speed), the decrease rate from that point to the level needed to maintain the driver's target speed will be usually significantly higher than the increase rate of the first portion. This phenomenon is in accordance with traffic flow theory and with 'typical' driver behavior. In fact, starting from a complete stop, drivers would push gradually on the gas pedal in order to accelerate until they reach a speed level that is generally close to their target speed. From that point, they will release the throttle, decreasing it to only the percentage needed to maintain their desired speed.

The research team first investigated a quadratic polynomial function for the modeling of the throttle, which was considered for the relative simplicity of its expression. However, a quadratic model was found to not result in such a good representation of the throttle data on hand. In fact, the symmetry characterizing parabolas around their extreme point results in similar variation rates for both the increasing and the decreasing portions, which contradicts

field observed driver behavior. Subsequently, more complicated functions were investigated. The challenge resides in the fact that the most adequate function should be able to behave freely around its maximum. This means that the variation of the first and the second segments of the function should be as independent as possible to allow for accurate modeling of different types of drivers (aggressiveness, passiveness, etc…).

After thorough investigation, the function presented by Equation III.7 was found to constitute the best fit to the data produced from 15 drivers that participated in the experiments. The proposed hyperbolic model requires the calibration of three parameters $t_1$, $t_2$, and $t_3$ for each driver.

$$t\left(u/u_d\right) = \frac{u/u_d}{t_1 + \frac{t_2}{1 - u/u_d} + t_3\, u/u_d} \tag{III.7}$$

Where $t(u/u_d)$ is the throttle value, $u$ is the speed and $u_d$ is the target speed of the driver.

Figure 2 illustrates the variation of the throttle as a function of the speed for several drivers. The data presented in the figure were chosen to reflect the different driving patterns observed among all the participants of the experiments. Figure 2.a to Figure 2.d illustrate aggressive drivers that keep pushing hard on the gas pedal until they reach more than 90% percent of their target speed. At that point, they will stop their pushing maneuver and therefore the throttle rapidly decreases to the level needed to maintain their desired speed. The two remaining subfigures (Figure 2.e and Figure 2.f) shows the behavior that is adopted by less aggressive participants. This category of drivers starts releasing the throttle at about 60% of their target speed; thus experiencing smaller acceleration rates in their convergence to $u_d$.

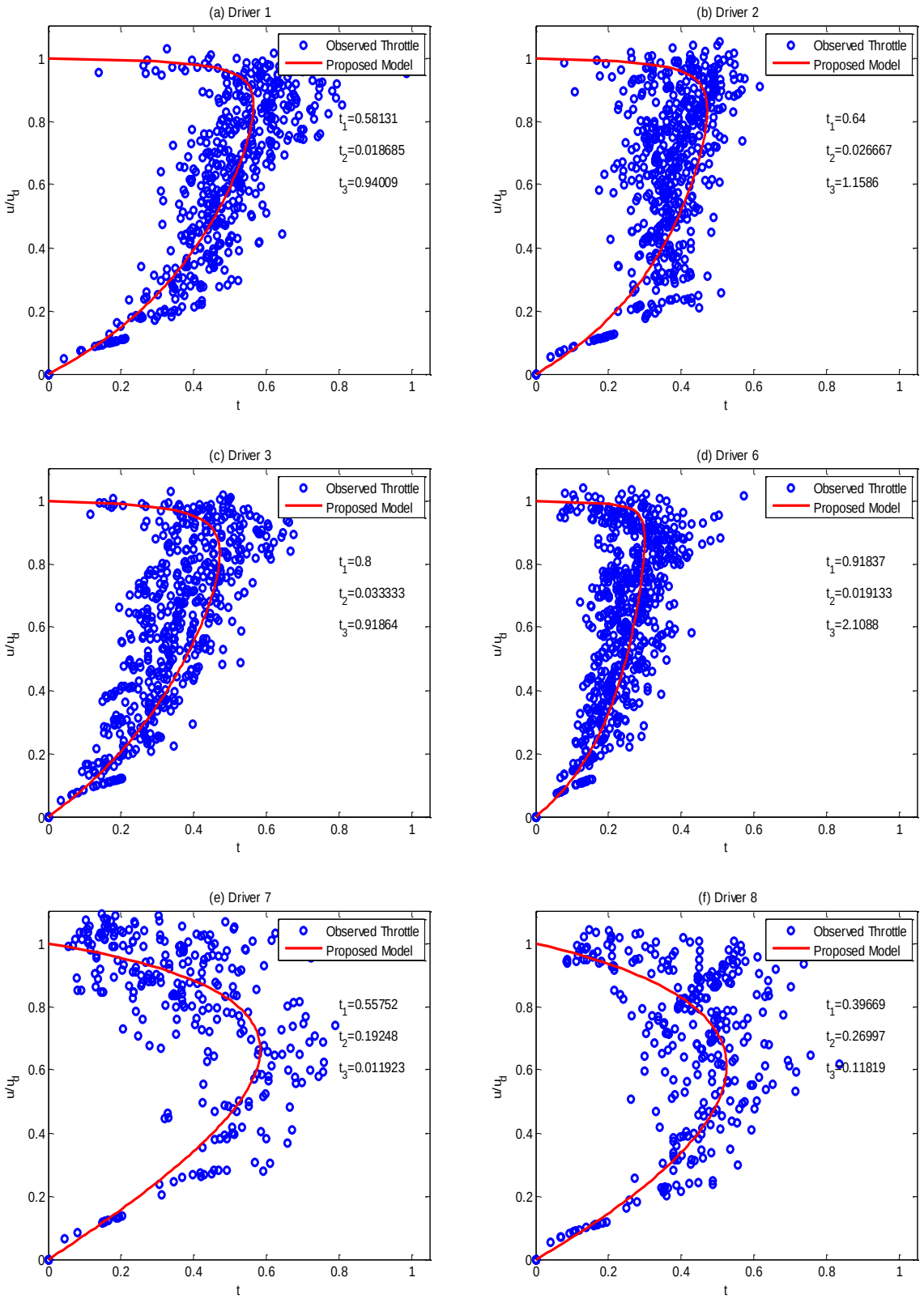


**Figure 2: Variation of the throttle as a function of the speed for different drivers**

One more important thing that should be noted is that the full capabilities of the vehicle were found to never be used; thus confirming the need for a reductive function for the computation of typical accelerations from the constant power model.

A significant shortcoming of the so-far proposed function is the fact that the throttle would be equal to zero when the target speed of the driver is reached. A zero throttle physically means a decrease in the vehicle's speed until it completely comes to a stop, which is not the case. In reality, there is a throttle value, $t^*$, for which the vehicle remains at its desired speed. This value could be easily found by solving Equation III.8 for $t^*$. This equation is nothing but the constant power model in which u is equal to $u_d$ and the acceleration is equal to zero.

$$\frac{\min\left(3600\eta t^* \frac{P}{u_d}, 9.8066\mu M_{ta}\right) - \left(R_a(u_d) + R_r(u_d) + R_g(u_d)\right)}{M} = 0 \qquad \text{(III.8)}$$

The proposed throttle function was calibrated for each driver individually. As it can be observed from Table 2, most of the values adopted by the three parameters of the model fall between 0 and 1 (some exceptions for $t_3$ values). The next step consisted on investigating if there is any correlation and relationships between $t_1$, $t_2$ and $t_3$. Figure 3 plots these parameters against each other and makes it easy to see that no strong relationships exist between them. In fact, it was found that the relationship that might be significant would be a linear model between $t_1$ and $t_3$. However, seen the small number of participants, no conclusions can be confirmed and the model was kept as is.

**Table 2: Values of the different parameters of the throttle function for each driver**

| | $t_1$ | $t_2$ | $t_3$ |
|---|---|---|---|
| **Driver 1** | 0.5813 | 0.0187 | 0.9401 |
| **Driver 2** | 0.6400 | 0.0267 | 1.1586 |
| **Driver 3** | 0.8000 | 0.0333 | 0.9186 |
| **Driver 4** | 0.5333 | 0.0667 | 0.6615 |
| **Driver 5** | 0.6400 | 0.0267 | 1.1579 |
| **Driver 6** | 0.9184 | 0.0191 | 2.1088 |
| **Driver 7** | 0.5575 | 0.1925 | 0.0119 |
| **Driver 8** | 0.3967 | 0.2700 | 0.1182 |
| **Driver 9** | 0.3873 | 0.3399 | 0.322 |
| **Driver 10** | 0.4800 | 0.2700 | 0.4287 |
| **Driver 11** | 0.4898 | 0.1102 | 0.5838 |
| **Driver 12** | 0.5137 | 0.0863 | 0.5501 |
| **Driver 13** | 0.7456 | 0.0286 | 1.4957 |
| **Driver 14** | 0.7438 | 0.1937 | 1.2186 |

| | | | |
|---|---|---|---|
| **Driver 15** | 0.4444 | 0.3556 | 0.6349 |

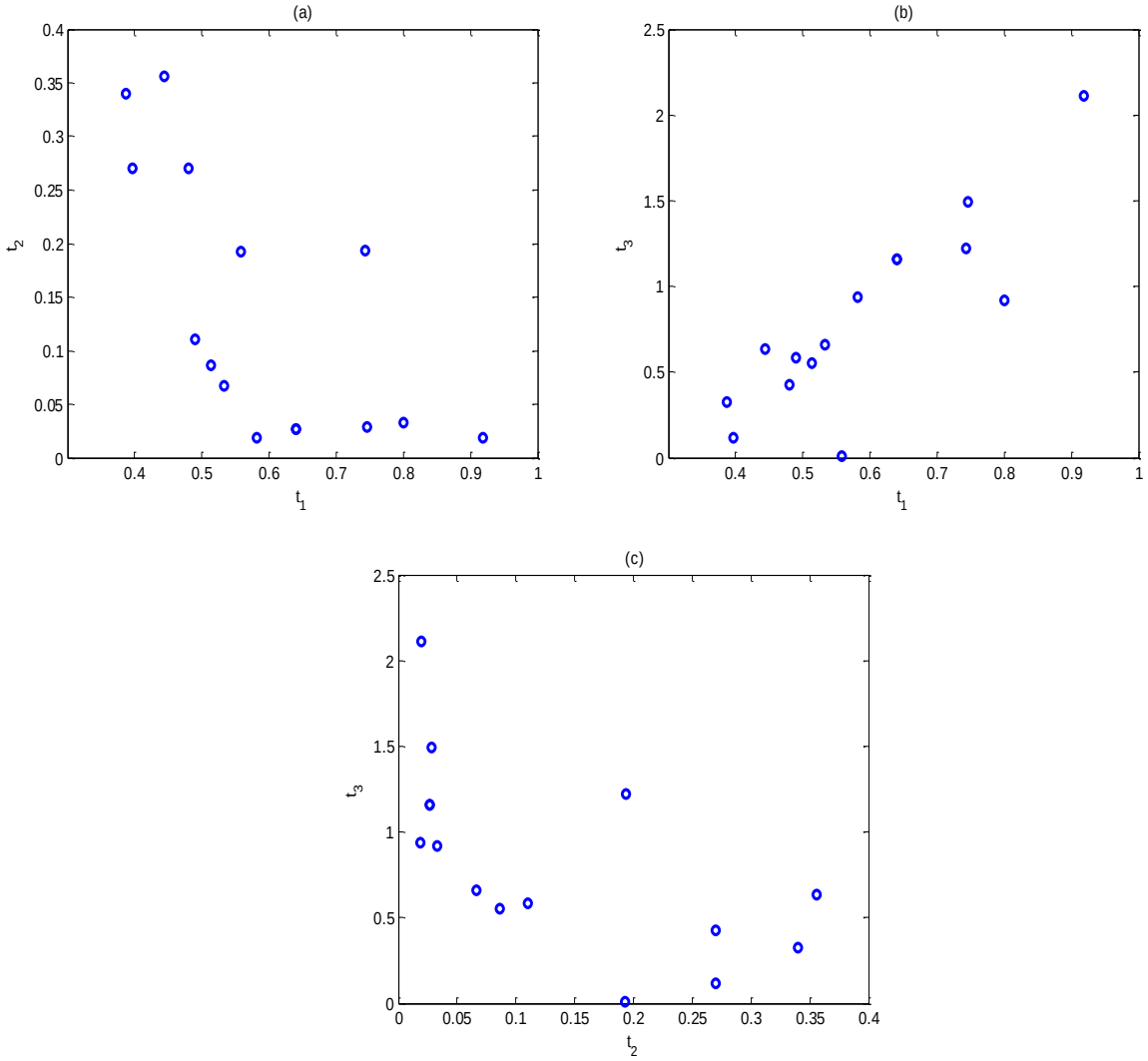


**Figure 3: Correlation between the model parameters: a. $t_1$ vs. $t_2$; b. $t_1$ vs. $t_3$; c. $t_2$ vs. $t_3$**

Having access to a throttle function that is specific to each driver, determining the acceleration function is straightforward by accounting for the throttle in the expression of the tractive force as presented by Equation III.9.

$$a(v) = \frac{\min\left(3600\eta t(v)\frac{P}{v}, 9.8066\mu M_{ta}\right) - \left(R_a(v) + R_r(v) + R_g(v)\right)}{M} \quad \text{(III.9)}$$

There are a lot of similarities between this model and the model proposed by Rakha et al. [17] for the estimation of typical accelerations. In fact, the throttle function can be looked at as a variable reduction factor to the maximum acceleration constant power model. However, the newly proposed model provides a more accurate representation than Rakha et al. model (as

will be discussed in the section dealing with the validation of the model) in that the power now varies as a function of the speed and the shape of the acceleration function is flexible as shown by Figure 4.

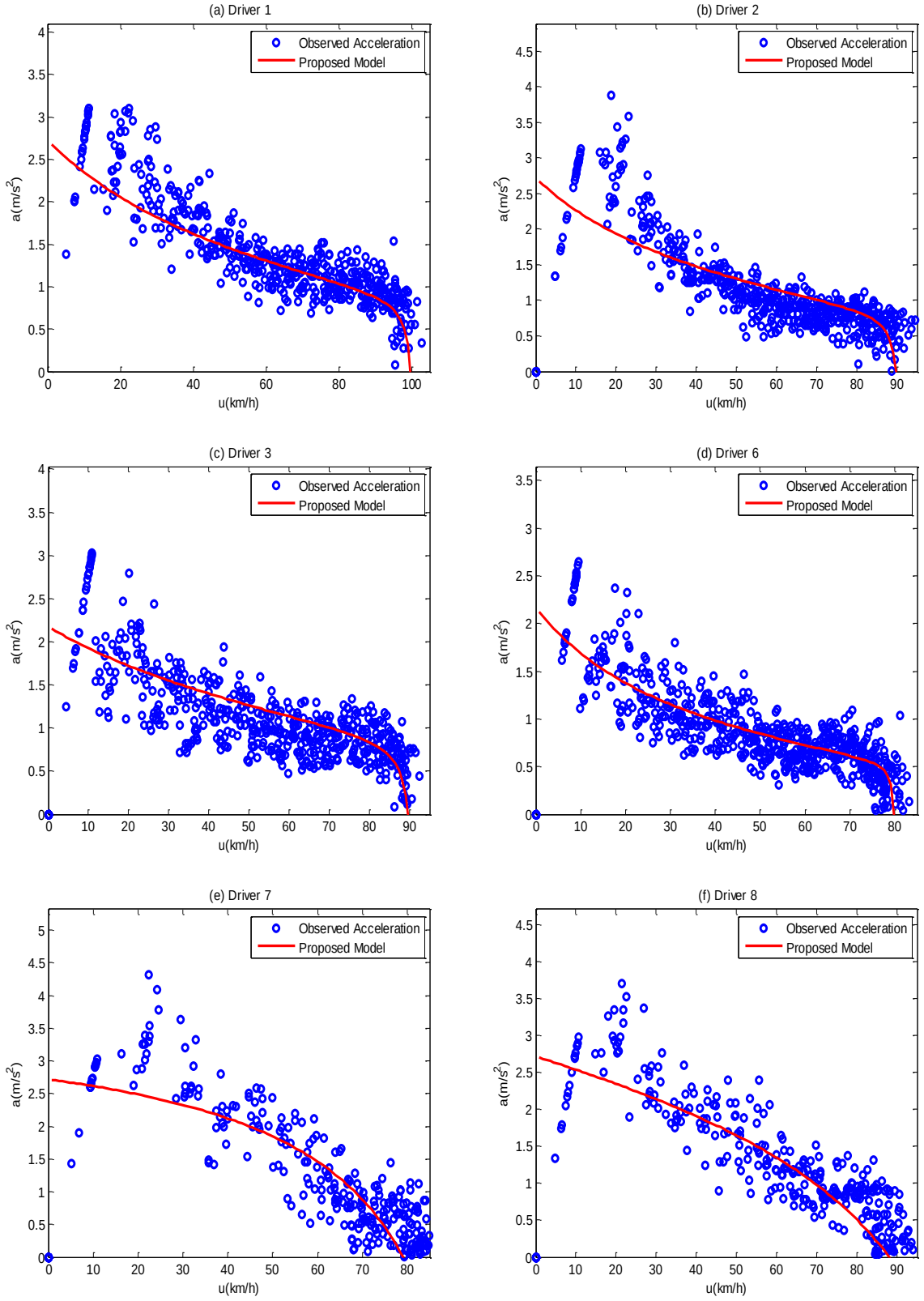


**Figure 4: Variation of the acceleration as a function of the speed for different drivers**

A special attention should be dedicated to the behavior of the developed model when the driver is close to his/her target speed. In fact, it is easily noticeable, from Figure 4, that the acceleration function has the ability to follow the driving pattern of the driver in terms of aggressiveness and convergence to $u_d$. Consequently, the change in the slope when the target speed is about to be hit is higher for aggressive drivers (Figure 4.a to Figure 4.d) than it is for standard drivers (Figure 4.e and Figure 4.f), whose acceleration functions are characterized by smoother concave functions.

### 3.4.3 Exponential Smoothing of the Model

Despite knowing Studies interested in the analysis of acceleration patterns revealed that the rate of acceleration is not maximum at time 0, but rather increases rapidly to the maximum acceleration after a short period of time. This behavior is not duplicated by the proposed model.

In order to fix this issue, the acceleration functions of the different drivers were exponentially smoothed with a smoothing coefficient α (α equal to zero would keep the original function unchanged). Instead of only taking a single smoothing coefficient α for all the drivers, which would anyway serve the main purpose of the procedure; the minimization of the error between the smoothed model and the acceleration data was also taken into account. Subsequently, α was changed for each driver from 0.01 to 0.99 with an increment of 0.01; and the optimal coefficient was selected for each driver.

The results of the combined exponential smoothing and the optimization, which are illustrated in Figure 5 and presented in Table 3 for some selected drivers, are quite interesting. In fact, besides forcing the acceleration rate to start at zero rather than the maximum value, the smoothed model is proved to result in a better fit to the experimental data. The root mean square error (RMSE) was used to compare the performance of both the original and the smoothed model. It is found that smoothing procedure results in decreasing the RMSE by at least 29% for all the participants (maximum observed improvement over the original model is equal to 51%).

While it is quite easy to come up with an explicit expression of the smoothed function, the research team judged it unnecessary and better to be avoided. This is due to the fact that the expression of a smoothed function will be purely mathematic; and thus lose the physical sense of the phenomenon that are captured in the expression of the unsmoothed model.

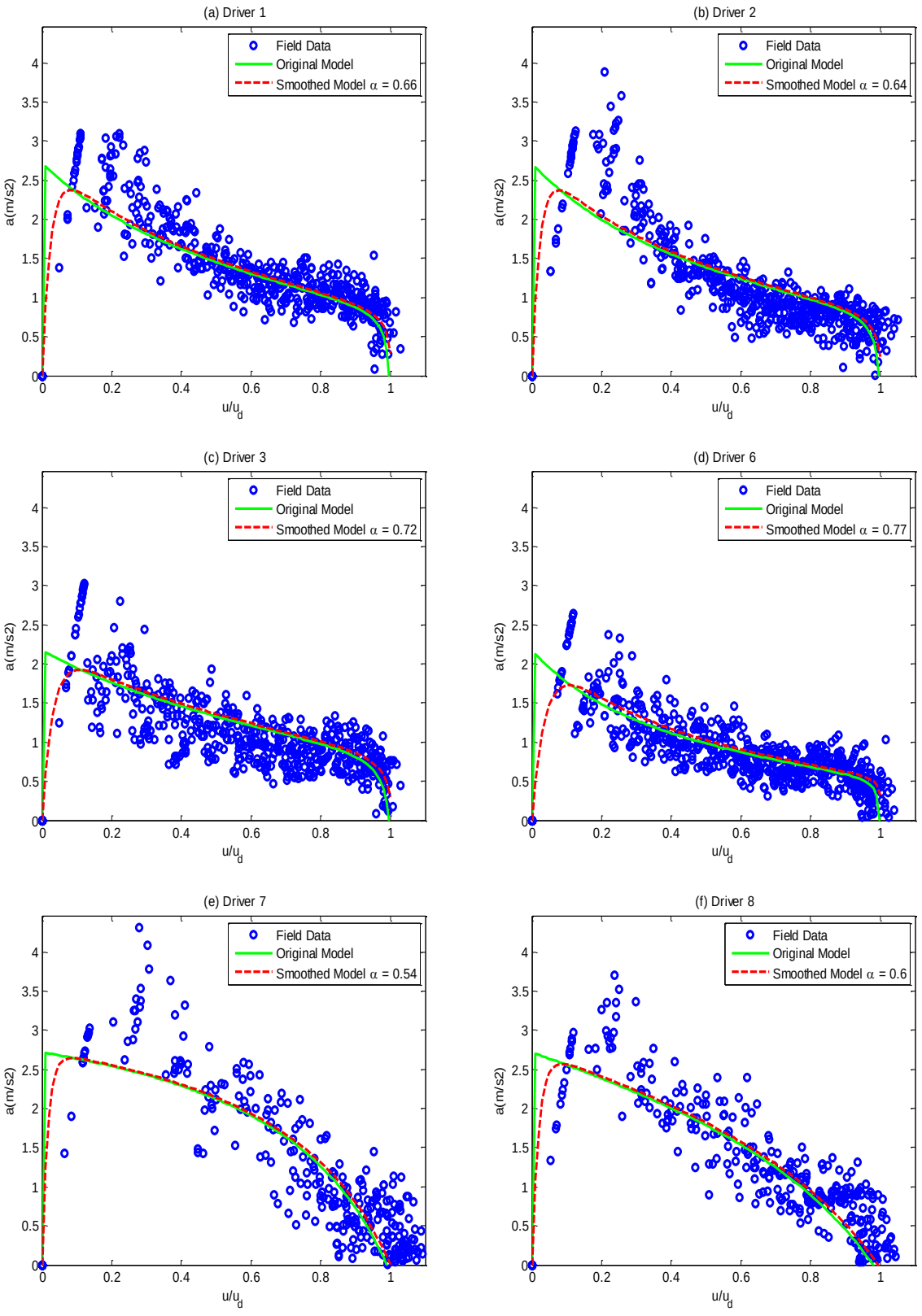


**Figure 5: Exponential smoothing of the resulting acceleration function for different drivers**

**Table 3: Comparison of the original model and the smoothed model**

| | Smoothed Model | | Original Model | Improvement Percentage (%) |
|---|---|---|---|---|
| | ***α*** | ***RMSE*** | ***RMSE*** | |
| **Driver 1** | 0.66 | **0.51** | 0.84 | 39 |
| **Driver 2** | 0.64 | **0.56** | 0.86 | 35 |
| **Driver 3** | 0.72 | **0.53** | 0.90 | 40 |
| **Driver 4** | 0.65 | **0.53** | 0.92 | 42 |
| **Driver 5** | 0.68 | **0.49** | 0.78 | 36 |
| **Driver 6** | 0.77 | **0.42** | 0.87 | 51 |
| **Driver 7** | 0.54 | **0.67** | 0.98 | 31 |
| **Driver 8** | 0.6 | **0.53** | 0.85 | 37 |
| **Driver 9** | 0.61 | **0.47** | 0.82 | 42 |
| **Driver 10** | 0.6 | **0.54** | 0.88 | 38 |
| **Driver 11** | 0.6 | **0.57** | 0.81 | 29 |
| **Driver 12** | 0.83 | **0.83** | 1.61 | 48 |
| **Driver 13** | 0.87 | **0.68** | 1.51 | 54 |
| **Driver 14** | 0.67 | **0.42** | 0.74 | 42 |
| **Driver 15** | 0.61 | **0.45** | 0.76 | 40 |

### 3.4.4 Comparison with Rakha Model and the IDM Model

In order to evaluate the performance of the proposed model, its results were compared to those obtained by two other existing and well-known models, namely the one proposed by Rakha et al. [17] dynamics model and the acceleration function of the IDM car-following model.

While the Rakha et al. model parameters were available to the research team as it was already fit to the same dataset [17], those needed for the acceleration function of the IDM model had to be calibrated for this study. In that context, both $a$ and $\delta$ (limited to an integer value between 2 and 5) were determined for each driver. The results of the calibration are presented in Table 4. The results confirm that the model developed in this study outperforms the other models since in most cases its RMSE was the lowest. In fact, the IDM model *significantly* performs better in the case of only two drivers (Driver 12 and Driver 13). However, it should be noted that, while calibrating the IDM model to the data, no constraints

were set on the value of its parameters resulting in maximum accelerations that are significantly lower than real-measured values, as illustrated in Figure 6.

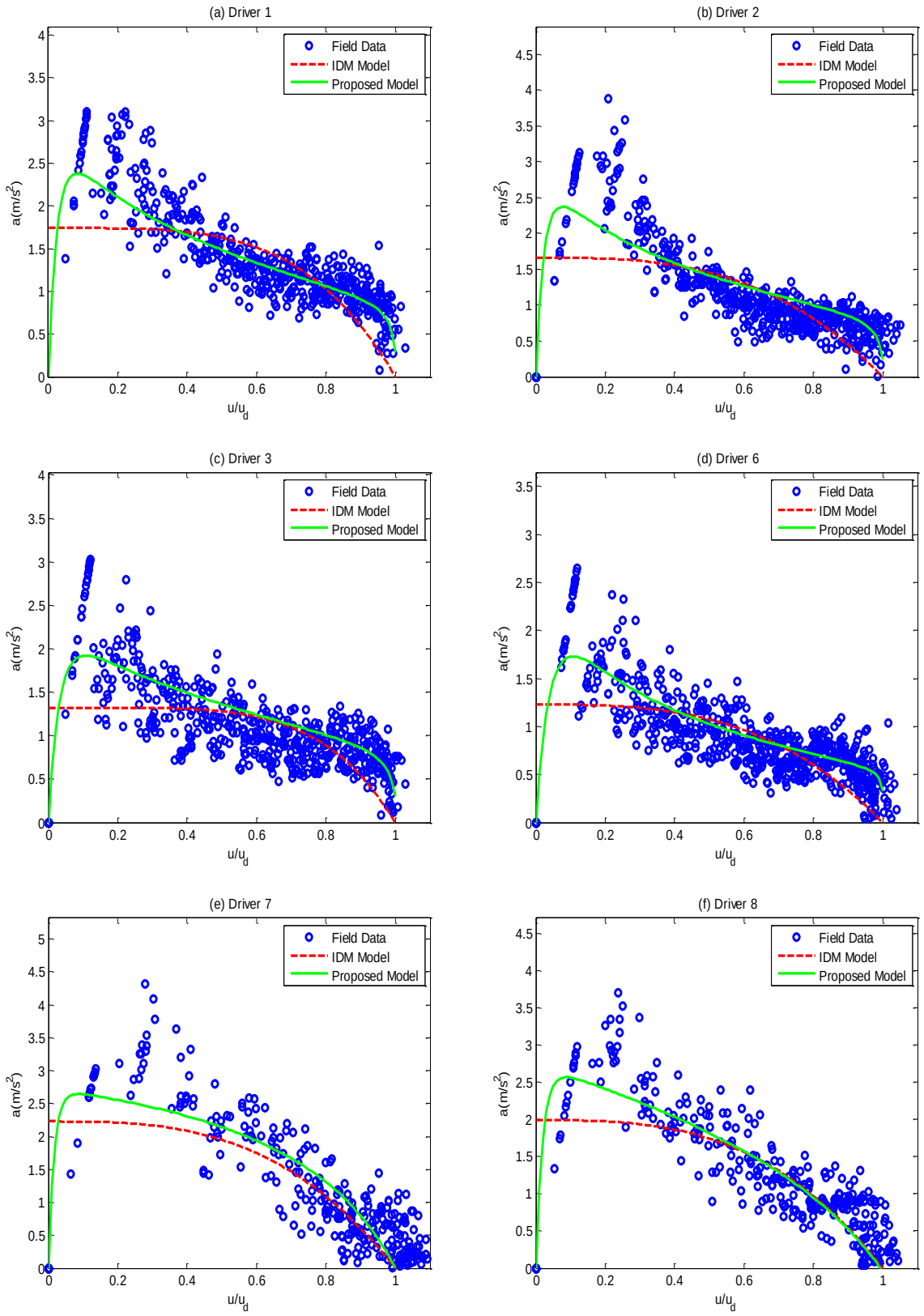


**Figure 6: Comparison of the proposed model with the acceleration function of the IDM model**

**Table 4: Results of the comparison to other models**

| | Smoothed Model | Rakha Model | IDM Model | | |
|---|---|---|---|---|---|
| | ***RMSE*** | ***RMSE*** | ***a*** | ***δ*** | ***RMSE*** |
| **Driver 1** | **0.51** | 0.73 | 1.74 | 4 | 0.59 |
| **Driver 2** | **0.56** | 0.71 | 1.66 | 3 | 0.60 |
| **Driver 3** | 0.53 | 0.81 | 1.32 | 5 | **0.52** |
| **Driver 4** | **0.54** | 0.69 | 1.77 | 5 | 0.62 |
| **Driver 5** | **0.50** | 0.73 | 1.46 | 4 | 0.51 |
| **Driver 6** | **0.42** | 0.72 | 1.23 | 3 | **0.42** |
| **Driver 7** | **0.68** | 0.89 | 2.23 | 3 | 0.76 |
| **Driver 8** | **0.54** | 0.73 | 1.99 | 3 | 0.63 |
| **Driver 9** | **0.48** | 0.76 | 1.89 | 3 | 0.57 |
| **Driver 10** | **0.54** | 0.80 | 1.92 | 3 | 0.64 |
| **Driver 11** | **0.58** | 0.74 | 1.73 | 3 | 0.59 |
| **Driver 12** | 0.83 | 0.73 | 1.93 | 4 | **0.68** |
| **Driver 13** | 0.68 | 0.75 | 1.55 | 3 | **0.57** |
| **Driver 14** | **0.43** | 0.72 | 1.34 | 3 | 0.47 |
| **Driver 15** | **0.46** | 0.81 | 1.6 | 3 | 0.51 |

One final result that should be mentioned is that the proposed model is able to follow the shape of the IDM model when adequate. This can be seen at the level of Figure 6.f where the proposed model overlaps the IDM model in the second portion of the data.

## 3.5 CONCLUSIONS

The research This paper extended on the constant power vehicle dynamics model proposed by Rakha et al. [16] for the prediction of maximum acceleration rates of light duty vehicles. The model was modified in such a way to make it suitable for estimating typical acceleration rates of different drivers. Besides providing a more realistic representation of the acceleration behavior in that a speed-dependent power is delivered by the engine, the proposed model is proved to significantly outperform other dynamics-based models for the estimation of typical accelerations. The model offers a good fit to field data in all the stages of the acceleration, has

a flexible shape that allows it to incorporate different types of variations that drivers can generate, and only requires a simple calibration of only four parameters (including a smoothing factor α).

In order to enhance the capabilities of the proposed model, further field experiments should be conducted with different vehicle types and for a larger group of drivers. That would result in a better understanding of the correlations that might exist between the model parameters. In an optimistic scenario, that would lead to the reduction of the number of needed parameters. Also, vehicles with manual transmission should be considered as driving a vehicle with an automatic transmission might limit the driver's ability to accelerate 'normally'. Finally, a similar procedure can be applied to the variable power vehicle dynamics model [48] proposed by Rakha et al. [34] for the prediction of maximum accelerations of trucks. That would results in a better understanding of typical accelerations of heavy duty vehicles.

## 3.6 ACKNOWLEDGEMENTS

The authors acknowledge the financial support provided by the Mid-Atlantic University Transportation Center (MAUTC) in funding this research effort.

# Chapter 4 An Enhanced Rakha-Pasumarthy-Adjerid Car-Following Model Accounting for Driver Behavior

**Authors:**

Karim Fadhloun

Hesham Rakha, Ph.D, P.Eng.

Abdessattar Abdelkefi, Ph.D.

Amara Loulizi, Ph.D, P.E.

*Presented at the 2017 TRB Annual Meeting and Published in the Compendium of Technical Papers.*

## 4.1 ABSTRACT

The biggest challenge facing traffic engineering researchers is how to account for human behavior, a non-physical parameter, in transportation modeling. In fact, a major drawback of existing car-following models is that the human-in-the-loop is not modeled explicitly. This is specifically important since the output from car-following models directly impacts several other factors and measures of effectiveness (MOE), such as vehicle emissions and fuel consumption levels. This paper describes a research effort that attempts to improve an existing car-following model by explicitly considering the characteristics of the vehicle as well as human driving behavior in its mathematical expression. The proposed model is an extension to the Rakha-Pasumarthy-Adjerid (RPA) car-following model, which uses a steady-state formulation along with acceleration and collision avoidance constraints to model the longitudinal motion of vehicles. The dataset used to calibrate and validate the model is extracted from the naturalistic data of the 100-Car study that was gathered by researchers at the Virginia Tech Transportation Institute. An analysis of the proposed modified variant using the aforementioned naturalistic driving data found that the modified formulation successfully integrated the human behavior component in the RPA model and that the new formulation slightly decreases the modeling error.

## 4.2 INTRODUCTION

Most phenomena in engineering fields involve physical variables that can potentially be predicted using simple or complex mathematical models. However, traffic engineers and researchers are faced with a complex challenge since they have to deal with the human element, which is difficult to model. The difficulty of mathematically modeling the vehicle and the driver as one unique component rather than two independent systems is due to two main reasons. First, there are numerous car models and types that make it difficult to determine the different parameters impacting the performance of the vehicle as they differ from vehicle to vehicle. Second, different driving patterns exist and the fact that they are mostly dependent on human behavior and psychology makes them very difficult to replicate mathematically.

A major issue that can be easily perceived in the literature is that the driver and the vehicle are rarely tied to each other. This is due to the fact that traffic engineers mostly rely on simulated data in their research due to the practicality and the simplicity of its acquisition. In other words, the success in modeling the driver/vehicle interaction aspect is related to the accuracy and the precision of the mathematical models implemented in the traffic simulation software producing these data. A main component of these types of software which has been a subject of several studies over the last fifty years is the car-following model. Car-following models predict the temporal and spatial behavior of a following vehicle when the time-space profile of the leading vehicle is known. It is noteworthy that the output from car-following models directly impacts several other factors and measures of effectiveness (MOE), such as vehicle emissions and fuel consumption levels.

This paper describes a research effort that attempts to improve an existing car-following model by explicitly considering the characteristics of the vehicle as well as human driving behavior in its mathematical expression. In addition to providing a brief comprehensive overview of the literature, the paper has the following two objectives:

1. Develop a car-following model that pioneers in terms of including a mathematical term, descriptive of human behavior, in its expression. The proposed model is an extension to the Rakha-Pasumarthy-Adjerid car-following model [12] (the RPA model) that already takes into account the characteristics of the vehicles. By explicitly including parameters that are reflective of different driving patterns, the model provides a more realistic representation of traffic.

2. Validate the proposed model by comparing its performance to that of the original RPA model in terms of goodness of fit. The dataset used in the validation procedure is extracted from the naturalistic data of the 100-Car study that was conducted by Virginia Tech Transportation Institute [49].

Concerning the layout, this paper is organized as follows. First, a brief description of the RPA car-following model and the dataset used is provided as it constitutes the pillar of this study. After that, the analysis related to the calibration procedure as well as the validation process of the proposed model is presented. Finally, the conclusions of the paper are drawn and insights for future work are provided.

## 4.3 THE RPA CAR-FOLLOWING MODEL

Car-following models are an important topic of traffic flow theory and a main component of micro-simulation software. Some example of models included in such software include Gipps' model [7], the RPA model [12] and the Intelligent Driver Model [8]. The latter models which are, logically, among the most complicated (in terms of expression) can be cast as newer and more recent compared to the first models [28, 29] that were developed in the field of car-following [50].

The RPA model [12] is a car-following model that controls the longitudinal motion of the vehicles in the INTEGRATION traffic simulation software [14, 15]. The model can be mathematically defined as a second-order car-following model that is composed of three main components: the steady-state, the collision avoidance and the vehicle dynamics models. While having a more complicated expression than other car-following models (especially those based on kinematics), it offers a more realistic representation of traffic and takes into account most of its influencing factors, which are the mechanical characteristics of the vehicle, the steady-state conditions governing the roadway as well as the adoption of certain physical laws, such as collision avoidance. Investigating the RPA model ability to emulate the behavior of real traffic has been the subject of several previous studies. In fact, one can mention the work of Sangster and Rakha [51] in which they compared it to other existing known models. It was found that the RPA model better predicts naturalistic behavior. The present research utilizes the same data as the previous study with the main purpose of improving the RPA model by incorporating in its expression a function that models human behavior. The additional function attempts to replicate driver gas pedal input. The details of the methodology used to develop

and calibrate such a function is described elsewhere [52], but will be briefly presented in this paper.

Having the values of its three components, the RPA model computes the speed of the following vehicle as shown in Equation IV.1.

$$u_{n+1}(t) = min\left(u_{n+1}^{1}(t), u_{n+1}^{2}(t), u_{n+1}^{3}(t)\right) \quad \text{(IV.1)}$$

Here $u_{n+1}^{1}(t)$, $u_{n+1}^{2}(t)$and $u_{n+1}^{3}(t)$ are the speeds calculated using the three modules described previously and which expressions are given in what follows.

The logic behind the RPA model is pretty straightforward to understand. In fact, the model evaluates the speed to which the vehicle need to converge to maintain cruising in steady-state conditions versus the speed needed to avoid any collisions with the lead vehicle. Next, the minimum of the latter two speeds is compared to the maximum attainable speed related to the mechanics and the surroundings of the vehicle.

Once the speed profile of the following vehicle is determined, its trajectory as well as its acceleration profiles are easily computed using first-order Euler approximations, as demonstrated in Equation IV.2 and IV.3.

$$x_{n+1}(t) = x_{n+1}(t - \Delta t) + \Delta t. u_{n+1}(t - \Delta t) \quad \text{(IV.2)}$$

$$a_{n+1}(t) = \frac{u_{n+1}(t + \Delta t) - u_{n+1}(t)}{\Delta t} \quad \text{(IV.3)}$$

### 4.3.1 First-order Steady-state Car-following Model

The RPA model utilizes the Van Aerde nonlinear functional form to control the steady-state behavior of traffic. The latter model was proposed by Van Aerde and Rakha [33] and is formulated as presented in Equation IV.4.

$$\Delta x_{n \to n+1}(t) = c_1 + \frac{c_2}{u_f - u_{n+1}(t)} + c_3. u_{n+1}(t) \quad \text{(IV.4)}$$

Here $\Delta x_{n \to n+1}(t)$ is the spacing (in meters) between the leading vehicle *n* and vehicle *n+1* at time *t*, $u_{n+1}(t)$ is the speed of vehicle *n+1*, in (m/s), $u_f$ is the free-flow speed of the roadway expressed in m/s, which can be subsequently cast as the desired speed of the drivers, and $c_1$ (m), $c_2$ ($m^2$/s) and $c_3$ (s) are constants used for the Van Aerde steady-state model. The

three constants have been shown to be directly related to the macroscopic parameters defining the fundamental diagram of the roadway as presented in Equation IV.5.

$$c_1 = \frac{u_f}{k_j u_c^2}\left(2u_c - u_f\right) \quad c_2 = \frac{u_f}{k_j u_c^2}\left(u_f - u_c\right)^2 \quad c_3 = \frac{1}{q_c} - \frac{u_f}{k_j u_c^2} \tag{IV.5}$$

Here $u_c$ is the speed-at-capacity of the roadway, $k_j$ is the jam density, and $q_c$ is the roadway capacity.

Finally, it should be noted that from the perspective of car-following modeling, the main objective is to determine how the following vehicle responds to changes in the behavior of the leading vehicle. Subsequently, a speed formulation is adopted for the Van Aerde model, as demonstrated in Equation IV.6, which is easily derived from Equation IV.4 using basic mathematics.

$$u_{n+1}^1 = \frac{-c_1 + c_3 u_f + \Delta x_{n\to n+1}(t) - \sqrt{\left(c_1 - c_3 u_f - \Delta x_{n\to n+1}(t)\right)^2 - 4c_3\left(\left(\Delta x_{n\to n+1}(t) - c_1\right)u_f - c_2\right)}}{2c_3} \tag{IV.6}$$

### 4.3.2 Collision Avoidance Model

As its name implies, the collision avoidance model ensures that collisions do not occur between the leading vehicle and its follower [53]. This module of the RPA model becomes the governing term when the following vehicle is approaching the leading vehicle with a higher speed (non-steady conditions).

The expression of the collision avoidance term is shown in Equation IV.7 and is directly related to a simple derivation of the maximum distance that a vehicle can travel to decelerate from its initial speed to the speed of the vehicle ahead of it while ensuring that, in the case of a complete stop, the jam density spacing between the two vehicles is respected.

$$u_{n+1}^2(t) = \sqrt{\left(u_n(t)\right)^2 + 2b\left(\Delta x_{n\to n+1}(t) - \Delta x_j\right)} \tag{IV.7}$$

Here *b* is the maximum deceleration at which the vehicles are allowed to decelerate.

### 4.3.3 Vehicle Dynamics Model

The final component of the RPA model is the vehicle dynamics model that ensures that the vehicle's mechanical capabilities do not limit it from attaining the speeds that are dictated by

the steady-state component. It is noteworthy at this level to mention the fact that most car-following models in the literature completely ignore both the dynamics of the vehicle as well as the effect of the different resistive forces acting on it. The RPA model incorporates in its expression the constant power model that was developed by Rakha *et al*. [16, 34] and was proven to provide a good approximation for typical acceleration behavior. This model computes the typical acceleration of the following vehicle as the ratio of the resultant force to the vehicle mass *M* (Equation IV.8.1). The resultant force is computed as the difference between the tractive force acting on the following vehicle $F_{n+1}$ (Equation IV.8.2) and the sum of the resistive forces; namely the aerodynamics resistance $R_{a_{n+1}}$ (Equation IV.8.3), the rolling resistance $R_{r_{n+1}}$ (Equation IV.8.4) and the grade resistance $R_{g_{n+1}}$ (Equation IV.8.5).

$$a_{n+1}(t) = \frac{F_{n+1}(t) - \left(R_{a_{n+1}}(t) + R_{r_{n+1}}(t) + R_{g_{n+1}}(t)\right)}{M} \quad \text{(IV.8.1)}$$

$$F_{n+1}(t) = \min\left(3600\eta\frac{\gamma P}{u_{n+1}(t)}, 9.8066\mu.M_{ta}\right) \quad \text{(IV.8.2)}$$

$$R_{a_{n+1}}(t) = c_1 C_d C_h A u_{n+1}(t)^2 \quad \text{(IV.8.3)}$$

$$R_{r_{n+1}}(t) = 9.8066.C_r(c_2 u_{n+1}(t) + c_3)\frac{M}{1000} \quad \text{(IV.8.4)}$$

$$R_{g_{n+1}}(t) = 9.8066.M.i \quad \text{(IV.8.5)}$$

Here *P* is the engine power, *M* is the vehicle's mass, $\mu$ is the coefficient of friction between the tires and the pavement, $\gamma$ is the vehicle throttle level (taken as the percentage of the maximum observed throttle level that a certain driver uses), $u_{n+1}$ is the vehicle speed, $\eta$ is the power transmission efficiency, $M_{ta}$ is the vehicle mass on the tractive axle, $c_1$ is a constant equal to 0.047285, $C_d$ is the air drag coefficient, $C_h$ is an altitude coefficient, *A* is the frontal area of the vehicle, $C_r$, $c_2$ and $c_3$ are rolling resistance coefficients, *i* is the pavement vertical grade.

The acceleration computed using the dynamics model is then used to calculate the maximum feasible speed $u^{3}_{n+1}$ that the vehicle is able to reach from its current speed using the first Euler approximation of Equation IV.9.

$$u^{3}_{n+1}(t) = u_{n+1}(t - \Delta t) + \Delta t . a_{n+1}(t - \Delta t) \quad \text{(IV.9)}$$

### 4.3.4 The Modified RPA Model

A main shortcoming of the vehicle dynamics model presented in Equation IV.8 is that it only considers the mechanical characteristics of the vehicle in its expression. In other words, it completely ignores the driver and its 'unique' pattern of driving. Recognizing this deficiency, Fadhloun *et al*. [52] successfully improved the model to make it representative of different driving patterns. The idea behind their research is quite simple and resides in the fact that the power delivered from the engine during driving cannot be assumed to be equal to the maximum power that the engine is able to producing nor to a constant percentage of that maximum power as modeled by Rakha *et al*. [16]. In fact, it is well-known that the delivered engine power is directly sensitive to the percentage of the throttle opening, which itself is related to the speed of the vehicle and the way with which drivers press on the gas pedal. Subsequently, the study [52] was based on a very basic idea which consists on incorporating a throttle function in the constant power model of Equation IV.8.

The proposed throttle function, presented in Equation IV.10, is a hyperbolic model that requires the calibration of three parameters $t_1$, $t_2$, and $t_3$ for each driver.

$$t\left(u/u_d\right) = \frac{u/u_d}{t_1 + \frac{t_2}{1 - u/u_d} + t_3\, u/u_d} \quad \text{(IV.10)}$$

Here $t(u/u_d)$ is the throttle value, $u$ is the current vehicle speed and $u_d$ is the target speed of the driver. Implementing the throttle function in the vehicle dynamics model results in a slight modification of the acceleration function, and thus; of the resulting estimation of the speed of the following vehicle as presented in Equation IV.11 and Equation IV.12.

$$a^{*}_{n+1}(t) = \frac{F^{*}_{n+1}(t) - \left(R_{a_{n+1}}(t) + R_{r_{n+1}}(t) + R_{g_{n+1}}(t)\right)}{M} \quad \text{(IV.11.1)}$$

$$F^*_{n+1}(t) = \min\left(3600\eta\frac{t\left({}^{u_{n+1}(t)}/_{u_d}\right)P}{u_{n+1}(t)}, 9.8066\mu.M_{ta}\right) \quad \text{(IV.11.2)}$$

$$u^*_{n+1}(t) = u_{n+1}(t-\Delta t) + \Delta t.a^*_{n+1}(t-\Delta t) \quad \text{(IV.12)}$$

Other than the above modification, the modified RPA model is similar to the original formulation as presented in Equation IV.13.

$$u^m_{n+1}(t) = min\left(u^1_{n+1}(t), u^2_{n+1}(t), u^*_{n+1}(t)\right) \quad \text{(IV.13)}$$

## 4.4 DATASET USED

In order to validate car-following models, researchers have usually had used three types of data. Empirical car-following data could either originate from field experiments conducted in a testing facility in a closed environment, from driving simulators or from real traffic conditions (using loop detectors or by tracking individual vehicles over a short distance). Regardless of its origin, the collected data was either biased due to the experimental set up or it involved anonymous drivers about whom no information is available. Even more, the mechanical characteristics of the vehicles are not necessarily known. This makes the validation of car-following models that include a vehicle dynamics component a very difficult and approximate task.

Recent technological development in terms of data acquisition and its storage made the collection of naturalistic driving data feasible. In 2002, the Virginia Tech Transportation Institute (VTTI) initiated a study where 100 cars were instrumented and were driven by designated drivers around the DC area. By the end of the study, a database was developed from the 207,000 trips completed by the 108 drivers involved in the study. The latter number translates into 337,000 hours of data and approximately 12 billion database observations (the sampling frequency was equal to one tenth of a second).

For the purpose of this study, only the dataset extracted by Sangster and Rakha [51] was used. This dataset comes from seven drivers and was collected along an 8-mile section of the Dulles Airport access road. It includes 1,732 car-following events with a total time length of 789 minutes.

The aggregated data of the seven drivers can be visualized in Figure 7, which shows the data in the different domains of the fundamental diagram. The reason for which the data is scattered over a large region is due to the fact that it is inclusive of both steady-state and non-steady-state conditions. The large scattering of the data is also reflective of the presence of different levels of aggressiveness among the sample of the considered drivers.

Noteworthy is the fact that due to the naturalistic nature of the dataset, both the characteristics of the vehicle as well as certain aspects defining the driving pattern of the driver are known. This makes the determination of the different RPA model variables straightforward and thus minimizing the bias in the model calibration. Table 5 presents the values of those variables for the different drivers.

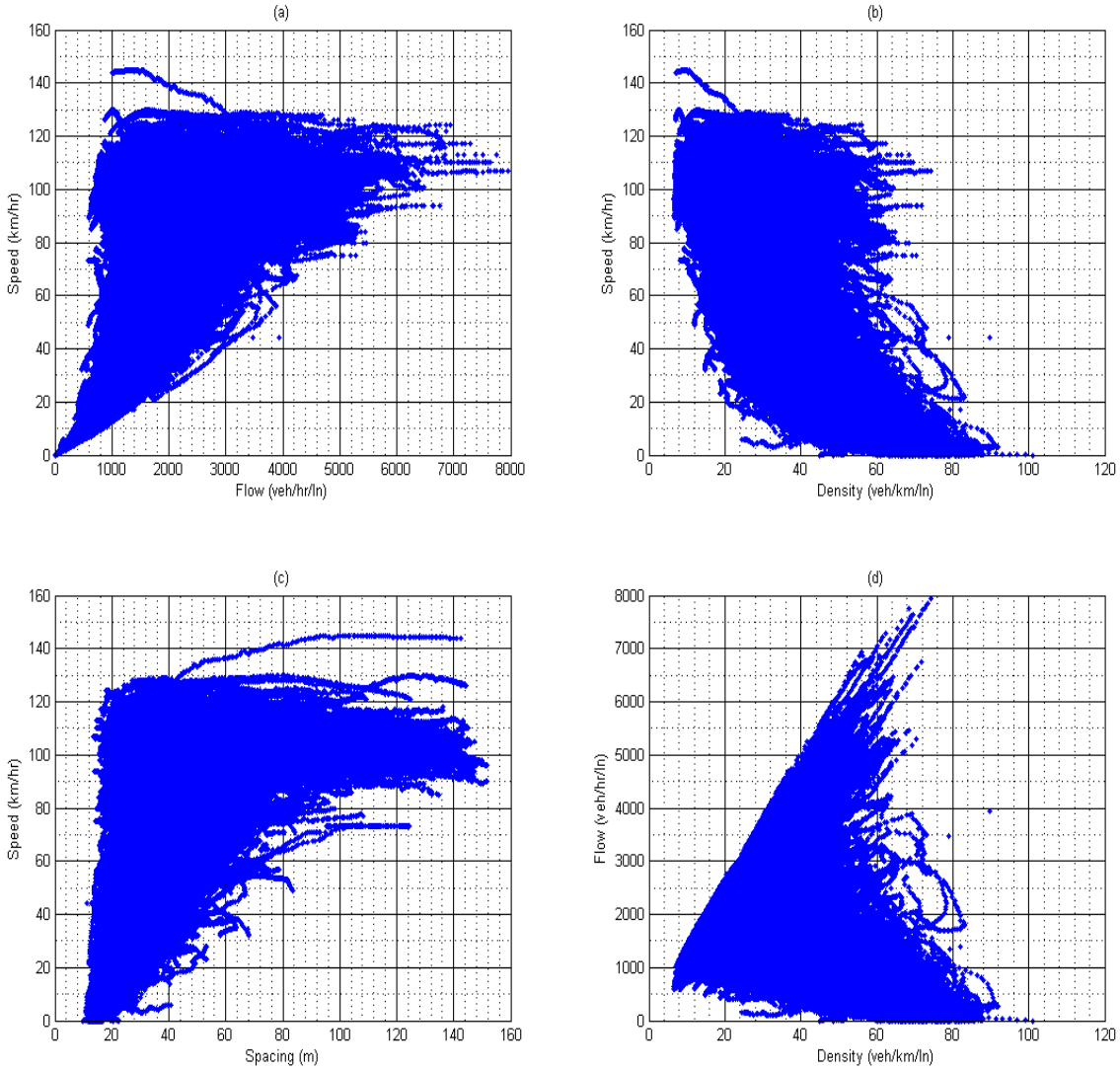


**Figure 7: Presentation of the aggregated data in different traffic domains: (a) Flow vs. Speed, (b) Density vs. Speed, (c) Spacing vs. Speed, and (d) Density vs. Flow**

## 4.5 ANALYSIS

The research described in this paper attempts to improve the RPA car-following model by explicitly incorporating the driver behavior in the mathematical expression of its dynamics-based acceleration model. By doing so, another degree of flexibility is added to the Rakha-Pasumarthy-Adjerid model in that it becomes able to model different types of variations of drivers in addition to its ability to model different vehicle types.

This section starts by describing the calibration procedure that was used for the RPA model and its proposed modified version. After that, the performance of the proposed modification is measured and quantified by comparing it to the performance of the original model.

### 4.5.1 Calibration of the RPA Model

The first decision that needed to be made in this research effort was to decide upon how to compare between the performances of the different models quantitatively. While a qualitative comparison that is based on graphical observation of how the simulated model covers the range of the collected data is useful in giving an initial insight of what is happening, it is usually not enough to support any conclusive results or comparisons. In that context, the first challenge that the authors dealt with consisted on choosing the optimization function that will be used to calibrate the different variants of the model. There are several error functions that are frequently used in car-following modeling. Among the most used tests, one can mention the Root Mean Square Error (*RMSE*) and the Root Mean Square Percentage Error (*RMSPE*) which are both easy to conduct and implement.

Noticing that the naturalistic data includes the observed speeds and positions of the leading and following vehicles and the fact that the primary output of the RPA model is the speed of the follower (from which the spacing is approximated using $\Delta t$ ), the authors opted to use the coefficient of variation (*CV*) of the *RMSE* as an error function (Equation IV.14).

$$\varepsilon\left(u^{s}{}_{n+1}\right)=\frac{\sqrt{n\sum\left(\left(u^{s}{}_{n+1}(t)-u^{o}{}_{n+1}(t)\right)^{2}\right)}}{\sum\left(u^{o}{}_{n+1}(t)\right)} \tag{IV.14}$$

Here $u^{o}{}_{n+1}(t)$ and $u^{s}{}_{n+1}(t)$ denote the observed and the simulated velocity of the following vehicle respectively.

With that in mind, the steady-state component of the RPA model was calibrated using a heuristic optimization software, SPD-CAL [54]. The final result of the optimization consists

of four parameters for each driver, namely the free-flow speed, the speed-at-capacity, the jam density and the capacity of the roadway. The values of the different calibrated parameters for the seven drivers are given in Table 6.

**Table 5: Characteristics of the vehicles and driving pattern**

| | | | *Vehicle Characteristics* | | | |
|---|---|---|---|---|---|---|
| **Driver** | ***b* ($m/s^2$)** | ***γ*** | ***P* (kW)** | ***M* (kg)** | **$C_d$** | **$A_f$ ($m^2$)** |
| **Driver_124** | 4.630 | 0.631 | 90 | 1190 | 0.36 | 2.06 |
| **Driver_304** | 2.778 | 0.600 | 90 | 1090 | 0.40 | 2.00 |
| **Driver_316** | 3.472 | 0.710 | 90 | 1090 | 0.40 | 2.00 |
| **Driver_350** | 5.556 | 0.537 | 90 | 1090 | 0.40 | 2.00 |
| **Driver_358** | 5.556 | 0.576 | 145 | 1375 | 0.40 | 2.18 |
| **Driver_363** | 4.861 | 0.529 | 145 | 1375 | 0.40 | 2.18 |
| **Driver_462** | 2.451 | 0.639 | 119 | 1900 | 0.50 | 2.94 |

**Table 6: Results for the Van Aerde steady-state model**

| **Driver** | ***kj* (veh/m)** | ***qc* (veh/s)** | ***uc* (m/s)** | ***uf* (m/s)** |
|---|---|---|---|---|
| **Driver_124** | 0.091 | 0.865 | 22.22 | 29.33 |
| **Driver_304** | 0.130 | 0.833 | 19.00 | 29.33 |
| **Driver_316** | 0.075 | 0.464 | 21.36 | 26.94 |
| **Driver_350** | 0.080 | 0.529 | 21.28 | 26.67 |
| **Driver_358** | 0.087 | 0.550 | 22.53 | 30.92 |
| **Driver_363** | 0.075 | 0.904 | 25.69 | 30.56 |
| **Driver_462** | 0.065 | 1.000 | 27.77 | 29.16 |

For illustrative purposes, the collected data of Driver_316 is drawn in Figure 8 along with the calibrated model. Qualitatively speaking, it can be seen from Figure 8 that the Van Aerde steady-state model successfully captures the average behavior of the driver as it is centered on the empirical data. However, the simulated data fails to provide a good fit to the surrounding variability. The latter can be observed in all the traffic domains and is especially obvious in the flow-density diagram for the area for which the observed flow is comprised between the capacity and about three folds of it. The concerned area is representative of the capacity drop that occurs when discharging from congestion and it is understandable that the

Van Aerde steady-state fails to model it since it is a first-order model. In fact, even certain second-order models are not able to capture such an effect.

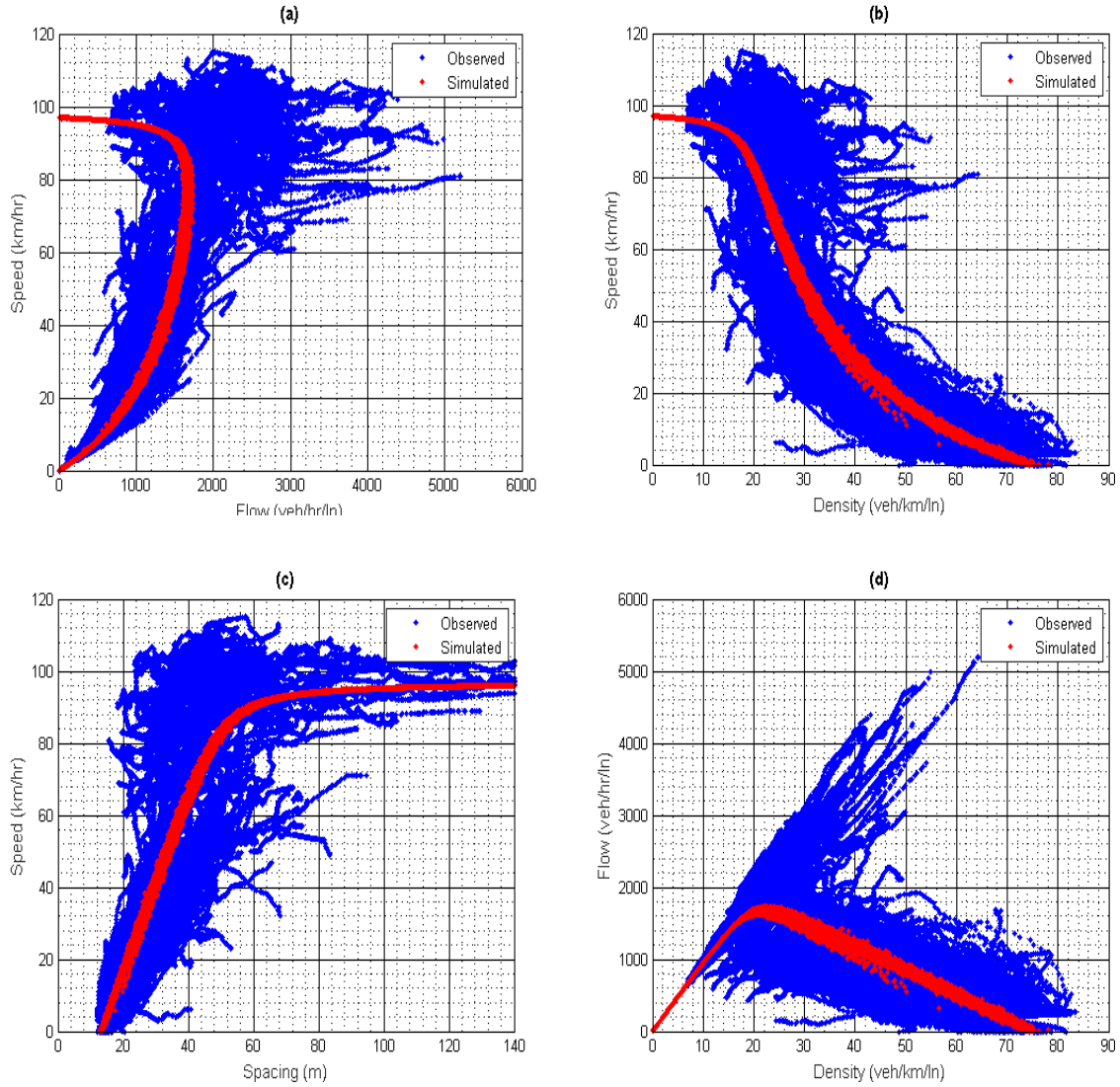


**Figure 8: Results of the VA steady-state model for Driver_316 in different traffic domains: (a) Flow vs. Speed, (b) Density vs. Speed, (c) Spacing vs. Speed, and (d) Density vs. Flow**

Speaking of second-order models, the next task was to calibrate the RPA model by investigating the effect of complementing the Van Aerde model by the collision avoidance and the vehicle dynamics modules. This would ensure a relatively better representation of real traffic conditions and the non-steady-state conditions that usually govern it. Concerning the vehicle dynamics model, the task was straightforward and simple due to the fact that the model is only sensitive to the characteristics of the roadway that are easy to calculate and to the

mechanical characteristics of the vehicle that are already known. The concerned variables and their values were already presented in Table 6.

The last calibration effort for the RPA model was with regards to the collision avoidance module. For that purpose, the maximum deceleration with which the vehicles are allowed to decelerate was set equal to the maximum deceleration that was attained by each driver (the parameter *b* in Table 5. The latter choice is relatively logical as it ensures consistency with what is happening physically.

The only challenge that was encountered at this level was with regards to a big deviation between the observed and simulated data at high speed levels as illustrated in Figure 9.a. After investigation, the reason was discovered to be related to the choice of the free-flow speed. In fact, for a significant number of events, the different drivers adopted a desired speed that is significantly higher or lower than the calibrated free-flow speed. This resulted in the discrepancies observed at high speeds as the simulated data is concentrated around the six values of $u_f$ obtained from Table 6. The issue was resolved by isolating the events that are creating the bias and replacing the original free-flow speed with the desired speed of the drivers under steady-state conditions. It should be noted that the original value in the case a certain car-following event does not manifest steady-state behavior. By doing the above, the six original $u_f$ values were substituted by a distribution of speeds that represent the desired speeds of the drivers for each event (Figure 9.b). A substantial amount of those speeds are still equal to the original values of Table 6. Supported by Figure 9.a, it can be stated that the issue was correctly approached and that the simulated speeds better match the empirical data. Finally, it should be noted that it is true that the adopted approach would result in decreasing the error of the RPA model resulting in improving its performance when compared to the Van Aerde model previously calibrated. However, that would not be of big importance especially for this study as it is already a known fact that the RPA model offers a better fit than the VA model. In addition to that, the main purpose of this paper is the comparison of the RPA model to the proposed variant subject of this paper.

Qualitatively speaking, it can be observed, in Figure 9 (Figure 9.c to Figure 9.f), that the RPA model offers a better fit to the data in terms of how it covers it and how it captures the naturalistic driver behavior. The most notable result is related to the fact that the RPA model constitutes a much better descriptor of conservative driving behavior. Graphically, this concerns the area for which the lines representing steady-state serve as an upper bound in Figure 9.f. Analytically, the cause of such a behavior is that either the collision avoidance or

the vehicle dynamics module has kicked in. On one hand, the collision avoidance module might have been activated to ensure a safety buffer between the following and the leading vehicle; thus, resulting in a divergence from the steady-state behavior that is dictated by the Van Aerde model. On the other hand, the steady-state behavior might have been unattainable due to the constraints imposed by the vehicle dynamics model, which are directly related to the mechanical capabilities of the vehicle.

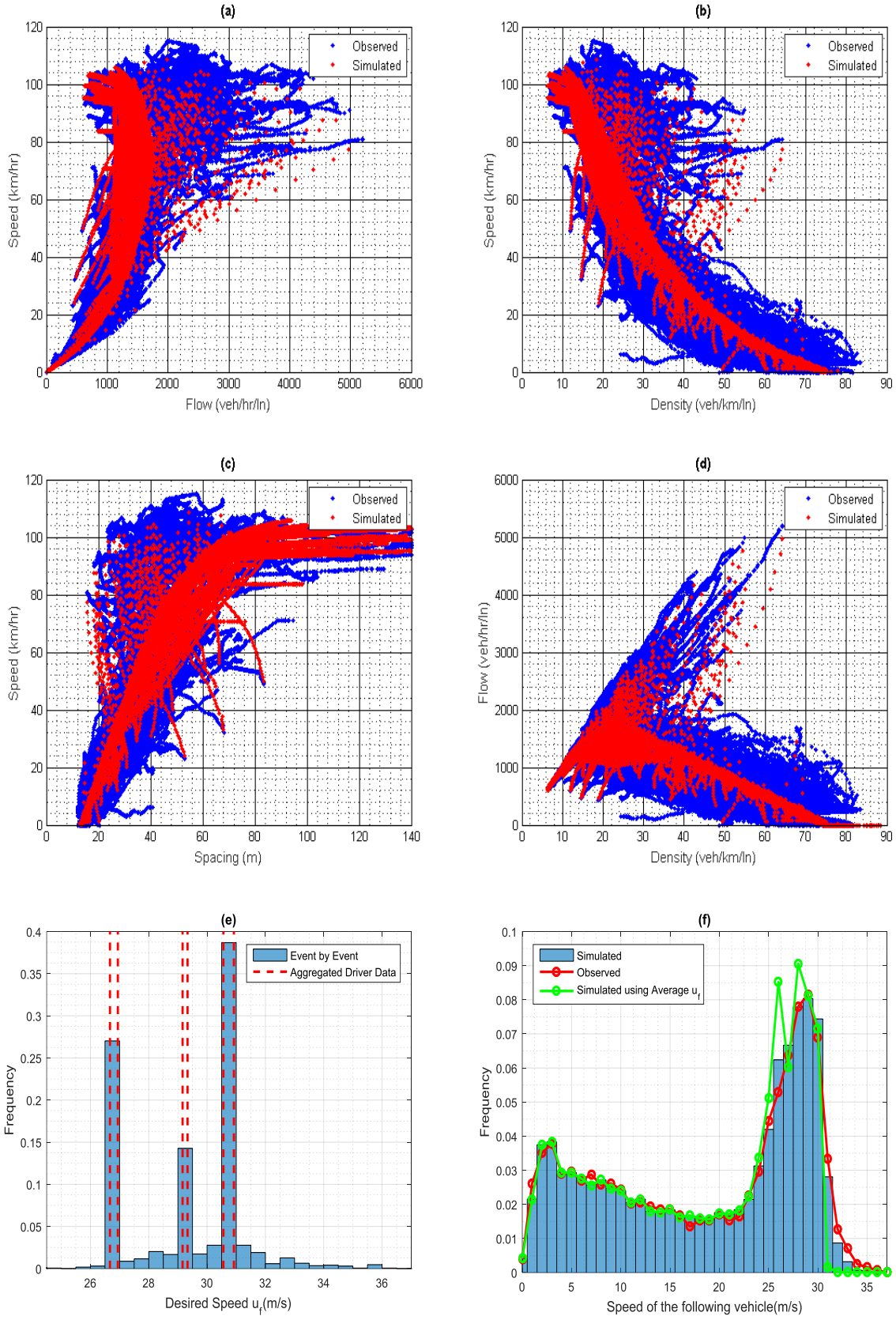


**Figure 9: Results of the RPA model for Driver_316 in different traffic domains: (a) Flow vs. Speed, (b) Density vs. Speed, (c) Spacing vs. Speed, and (d) Density vs. Flow**

### 4.5.2 Modified RPA Model Results

As already mentioned, the only change that is needed in the RPA model to make it representative of human behavior and the different driving patterns that a driver can adopt consists of a straightforward implementation of the throttle function in the expression of the tractive force as presented in Equation IV.11.2. The methodology for calibrating the throttle function, which can be cast as a variable reduction factor to the power consisted on finding the set of parameters $t_1$, $t_2$ and $t_3$ that minimizes the optimization function for each event. Next, having access to the different combinations of optimal parameters, the possibility of the existence of any relationships and/or correlation was explored. Figure 10.a to Figure 10.c, which plots the variation of $t_1$, $t_2$ and $t_3$ against each other, makes it easy to identify certain patterns related to the range of variation of the throttle function parameters. First, it is relatively clear in Figure 10.a and Figure 10.c that there is a concentration of $t_2$ values near zero (mostly between 0 and 0.01) and that it remains positive at all points which holds true for $t_1$ as well (but not $t_3$ which is negative for a significant percentage of the scenarios). Second, the different regions bounding the different parameters seem not to be random and suggest the existence of analytical functions that govern the relations between $t_1$, $t_2$ and $t_3$. Determining the latter functions and analytically confirming the observed boundaries would probably result, among others, in the reduction of the time needed to come up with the optimal solution in comparable studies (those interested in calibrating the model to observed data). Subsequently, an analytical investigation of the mathematics of the model would constitute an interesting and useful complement to this study.

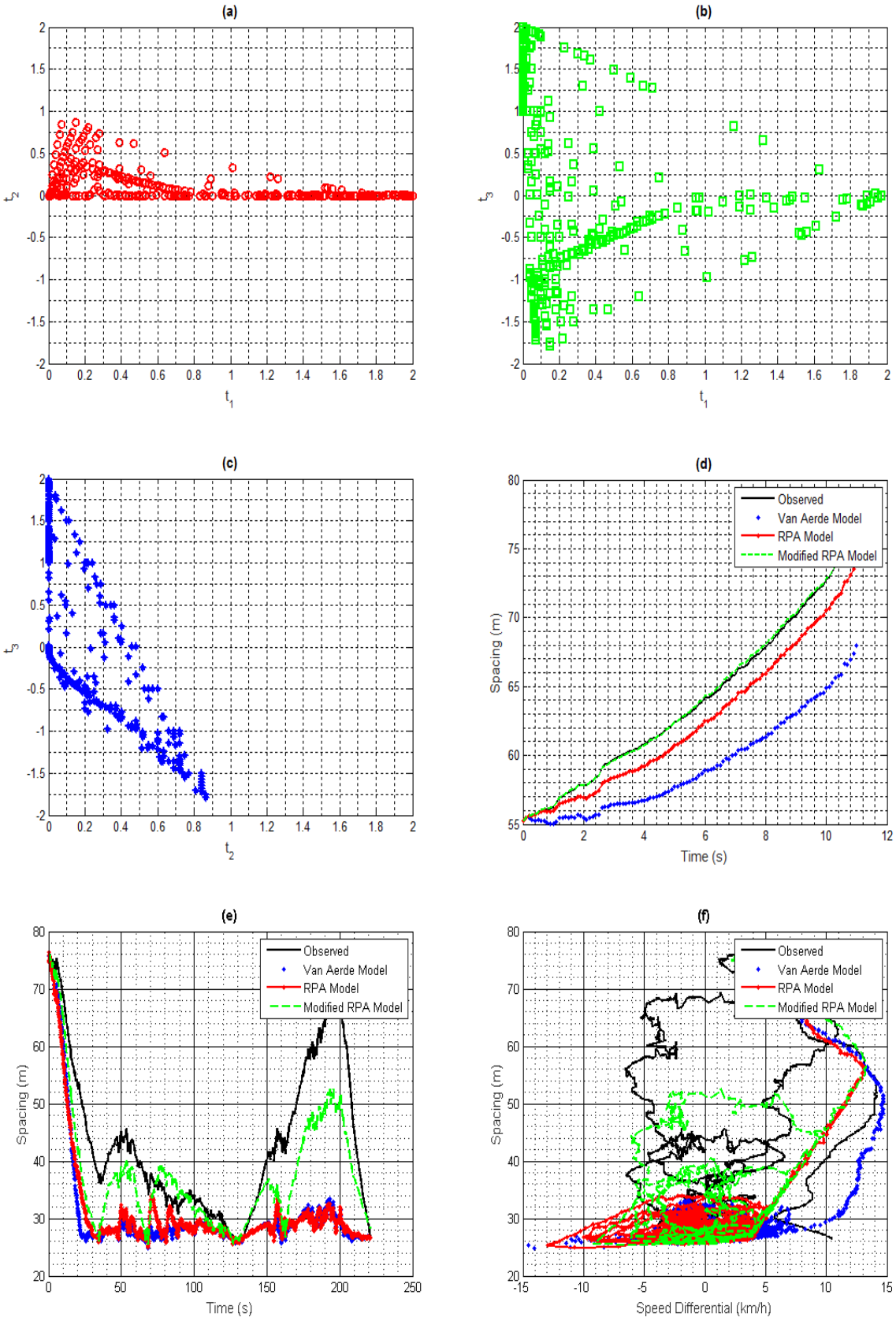


**Figure 10: Variation of the throttle function parameters against each other: a. t1 vs. t2; b. t1 vs. t3; c. t2 vs. t3; d. and e. Variation of the spacing as a function of the time for**

**events 22247.02 and 22247.04 ; f. Variation of the spacing as a function of the speed differential for event 22247.04**

From a qualitative standpoint, Figure 10.d and Figure 10.e illustrate the variation of the spacing as a function of the time difference between two sample events. Both figures can be cast as a proof of the success of the modified RPA model in improving the fit to the empirical data compared to the original formulation of the model and to the first-order steady-state model. Figure 10.d concerns an event for which the spacing is continuously increasing over time and demonstrates that the proposed model almost fits perfectly to the observed spacing. The second sample event, presented in Figure 10.e, is related to an event in which the spacing decreases and increases considerably over time. Here again, the modified RPA model is demonstrated to outperform the two other models especially in the way that it is able to follow the variations of the empirical data. This is further confirmed by Figure 10.f in which the variation of the spacing as a function of the speed differential between the two vehicles is presented.

In an attempt of computing an overall evaluation of the performance of the proposed model, its results were compared to those obtained by the Van Aerde steady-state model and the RPA model. The frequencies at which each of the three modules were activated for the RPA model are presented in Table 7 while those related to the modified model are given in Table 8. The results for the RPA model show that the steady-state behavior presented by the VA model could not be attained 7% of the time due to the mechanical inability of the vehicle to reach it and that, for about 2% of the observations, a collision between the two vehicles had to be prevented using the collision avoidance model. Furthermore, one can also conclude that Driver_462 is the most aggressive driver in the dataset and is apparently applying abrupt accelerations and decelerations (DYN: 21.92% and CA: 16.61%). For the modified model, on the other hand, it can be seen from Table 8 that the frequencies have significantly changed. In fact, the results confirm that the introduction of the throttle function in the RPA model has served its purpose successfully in that the utilization of the vehicle dynamics model became equal to more than 300% of the previous case. This is understandable and can be explained by the fact that the acceleration function of the original formulation serves as an upper bound to the new one. Finally, no significant change is observed in the utilization of the collision avoidance was observed as expected and the mentioned aggressiveness of Driver_462 is further confirmed (DYN: 57.66% and CA: 10.61%).

Next, a comparative analysis to compare the performance of the different models is performed. The computed comparative errors are presented in Table 9. The most important

outcome from this study is the fact that the error related to the modified RPA model is always smaller than that of the original formulation (as well as the expected improvement over the Van Aerde model). In fact, it is demonstrated that the new formulation that is representative of human behavior in its expression results in a 10% decrease in the error on average when compared to the original formulation (about 17% for Driver_462). What even makes the latter finding more important is the fact that a big number of combinations of the coefficients defining the throttle function were found to be resulting in a better statistical fit to the dataset than the RPA model. This makes the modified RPA model appropriate for the modeling of the variations between drivers in a car-following context. In other words, the variability due to the human input in the driving maneuver could be modeled explicitly and completely in the expression of the car-following model controlling the different longitudinal interactions between the vehicles in the system.

**Table 7 : Frequency of utilization of the Van Aerde model, the vehicle dynamics model and the collision avoidance model in the RPA model**

| **Driver** | ***VA (%)*** | ***DYN (%)*** | ***CA (%)*** |
|---|---|---|---|
| **Driver_124** | 87.20 | 7.05 | 5.75 |
| **Driver_304** | 91.54 | 3.71 | 4.76 |
| **Driver_316** | 96.08 | 3.73 | 0.19 |
| **Driver_350** | 86.06 | 13.75 | 0.19 |
| **Driver_358** | 94.21 | 5.68 | 0.11 |
| **Driver_363** | 89.59 | 8.73 | 1.68 |
| **Driver_462** | 61.47 | 21.92 | 16.61 |
| **Aggregate** | 91.01 | 7.02 | 1.97 |

**Table 8: Frequency of utilization of the Van Aerde model, the vehicle dynamics model and the collision avoidance model in the modified RPA model**

| Driver | *VA (%)* | *DYN (%)* | *CA (%)* |
|---|---|---|---|
| **Driver_124** | 68.98 | 25.83 | 5.19 |
| **Driver_304** | 83.84 | 12.07 | 4.09 |
| **Driver_316** | 89.67 | 10.18 | 0.15 |
| **Driver_350** | 74.08 | 25.78 | 0.14 |
| **Driver_358** | 86.15 | 13.75 | 0.09 |
| **Driver_363** | 62.28 | 36.39 | 1.32 |
| **Driver_462** | 31.73 | 57.66 | 10.61 |
| **Aggregate** | 77.07 | 21.36 | 1.57 |

**Table 9: Comparative error results between the Van Aerde model, RPA model and the modified RPA model**

| | **VA** | | **RPA** | | **RPA_modified** | |
|---|---|---|---|---|---|---|
| **Driver** | ***RMSE*** | **ε (%)** | ***RMSE*** | **ε (%)** | ***RMSE*** | **ε (%)** |
| **Driver_124** | 2.46 | 9.77 | 1.53 | 6.09 | *1.37* | *5.45* |
| **Driver_304** | 1.65 | 6.50 | 1.15 | 4.52 | *1.09* | *4.30* |
| **Driver_316** | 1.48 | 13.20 | 1.32 | 11.71 | *1.27* | *11.29* |
| **Driver_350** | 2.35 | 13.01 | 1.88 | 10.40 | *1.69* | *9.38* |
| **Driver_358** | 1.45 | 10.84 | 1.27 | 9.54 | *1.18* | *8.81* |
| **Driver_363** | 1.28 | 4.82 | 1.03 | 3.87 | *0.89* | *3.37* |
| **Driver_462** | 1.34 | 5.52 | 1.56 | 6.44 | *1.31* | *5.38* |

## 4.6 CONCLUSIONS AND FUTURE RESEARCH

The paper extended the RPA car-following model proposed in Rakha *et al*. [12] to the human-in-the-loop making it a pioneer in terms of capturing human behavior. Besides providing a more realistic representation of traffic in that a speed-dependent power is delivered by the engine as opposed to a constant power used in the original formulation, the proposed model is demonstrated to outperform the original RPA model, from which it was derived, for the

prediction of vehicle trajectories and speed profiles. While it is true that the calibration procedure is more complicated by adding three additional model parameters, the sensitivity and the importance of the subject that this paper tries to address makes its contribution noteworthy to traffic flow theory. As a matter of fact, the proposed variant of the RPA model can be used in traffic simulation to directly model the variation and the randomness between the different drivers rather than using a speed coefficient of variation. Subsequently, the characteristics of the vehicle and the input of the driver are modeled as a unique component rather than two independent systems. However, a better understanding of the throttle function and the different correlations and relationships between its different parameters is a must before achieving such a goal. In addition to that, while this research succeeded in developing a car-following model that would allow for the generation of several different vehicle trajectories and speed profiles using the same vehicle in the same road environment, a very important aspect needs to be investigated. The concerned aspect relates to studying how the different generated driving patterns differ from each other. In other words, the way with which randomness is induced in the new model needs to be understood. That would constitute a very interesting and innovative addition to the contribution of this research paper if achieved. Finally, the authors suggest that this study be followed by a stability analysis of the model in order to evaluate its capabilities to recreate certain traffic phenomena while, at the same time, being able to avoid others.

## 4.7 ACKNOWLEDGEMENTS

The authors acknowledge the financial support provided by the Mid-Atlantic University Transportation Center (MAUTC) in funding this research effort.

# Chapter 5 A Novel Car-Following Model: Model Development and Preliminary Testing

**Authors:**

Karim Fadhloun

Hesham Rakha, Ph.D, P.Eng.

*Published in the International Journal of Transportation Science and Technology, 2019*

## 5.1 ABSTRACT

The research presented in this paper proposes and develops a new car-following model, which we term the Fadhloun-Rakha (FR) model. The FR model incorporates the key components of the Rakha-Pasumarthy-Adjerid (RPA) model in that it uses the same steady state formulation, respects vehicle dynamics, and uses very similar collision-avoidance strategies to ensure safe following distances between vehicles. The main contributions of the FR model over the RPA model are the following: (1) it models the driver throttle and brake pedal input; (2) it captures driver variability; (3) it allows for shorter than steady-state following distances when following faster leading vehicles; (4) it offers a much smoother acceleration profile; and (5) it explicitly captures driver perception and control inaccuracies and errors. Besides describing the methodology and the role of each of the model parameters, this study evaluated the performance of the new model using a naturalistic driving dataset. A brief comparative analysis was performed to validate the model with regard to replicating empirical driver and vehicle behavior. Through a quantitative and qualitative evaluation, the proposed FR model demonstrated a significant decrease in the modeling error when compared to the original RPA model and generated trajectories that are highly consistent with empirically observed car-following behavior.

## 5.2 INTRODUCTION

Developing mathematical models for the accurate estimation and prediction of longitudinal vehicle behavior is a central challenge in traffic engineering. As a pillar of traffic flow theory, the analysis of car-following behavior informs geometric roadway design by predicting vehicle acceleration levels and their impact on a roadway facility during the different phases of its life.

The output of a car-following model is also important to the traffic analysts responsible for managing an existing facility. Furthermore, car-following models constitute the core component of microscopic simulation software. The data and results generated by these programs are highly dependent on the car-following model implemented in their algorithms and are used in a significant part of traffic analysis. The accurate prediction of vehicle accelerations is not only necessary to get correct estimations of travel times and delays, but it also directly impacts the precision of predicting other measure of effectiveness such as fuel consumption and emissions, which are very sensitive to acceleration levels.

The reason that modeling car-following behavior is a challenge for traffic researchers relates to the large number of parameters that are involved and have an effect on the acceleration produced by a vehicle, such as the vehicle's mechanical characteristics, type of roadway on which the vehicle is traveling, and randomness in human driving behavior. Among those factors, human driving behavior contributes the most to the complexity of modeling vehicle acceleration behavior. In other words, the biggest challenge facing traffic engineering researchers relates to how to account for human behavior, a non-physical parameter, in the modeling of the longitudinal motion of vehicles. In fact, a major drawback of existing car-following models is that the human-in-the-loop is not modeled explicitly.

As a result of its importance and the diversity of its applications, extensive research has been conducted on the longitudinal motion of vehicles over the last fifty years, leading to the development of several car-following models [1-13] that aim to emulate the way with which drivers/vehicles follow each other. The main objective of these models is to generate vehicle trajectories that mimic empirical driving behavior as realistically as possible. While existing car-following models are numerous and have evolved gradually in terms of accuracy and complexity of their mathematical expression, significant research is still needed to improve their mathematical representations.

Car-following models can be categorized into collision avoidance models [7, 8], psycho-physical models [9-11], and Gazis-Herman-Rothery (GHR) family models [3]. Alternatively, they can also be categorized based on whether they include vehicle dynamics in their expression. Kinematics-based models attempt to replicate the car-following behavior of vehicles as it occurs in the field, but ignore the mechanical characteristics of the vehicle, which represents one of their major weaknesses. Notable state-of-the-art kinematic models include the Gipps model [7] and the Intelligent Driver Model (IDM) [8]. On the other hand, car-following models [12, 13] that consider vehicle dynamics explicitly in their expressions

account for both the tractive and resistive forces that act on the vehicle. These models are more complicated in terms of mathematical representation and development. A state-of-the-practice vehicle dynamics model is the Rakha-Pasumarthy-Adjerid (RPA) model [12], which controls the car-following behavior used in the INTEGRATION software [55, 56].

The success of a car-following model to capture observed traffic behavior as realistically as possible is not the sole criterion of its performance. In fact, as with any other prediction model, the validity and the suitability of a certain car-following model for traffic simulation depends on achieving that goal with the smallest number of calibration parameters while, at the same time, not ignoring most of the parameters significantly influencing traffic. In that regard, finding the optimal balance between complexity and simplicity is the key starting point in achieving an "ideal" car-following model. Such a model would be one with the most straightforward and simple mathematical expression without any compromise in its ability to replicate reality.

This paper describes research performed to develop a new acceleration-based car-following model, the Fadhloun-Rakha (FR) model, which attempts to capture vehicle dynamics, the human-in-the-loop, and the randomness associated with human driving behavior. From a technical standpoint, the FR model and the RPA model share the same steady state formulation, respect vehicle dynamics, and use very similar collision-avoidance strategies to ensure a safe following distance between vehicles. The main contribution and key enhancements of the FR model over the RPA model, besides offering a better fit to empirical data, are the following: (1) it models the driver throttle and brake pedal input; (2) it captures driver variability; (3) it allows for shorter than steady-state following distances when following faster leading vehicles; (4) it offers a much smoother acceleration profile; and (5) it explicitly captures driver perception and control inaccuracies and errors.

Besides describing the methodology and the procedure that led to the development of the functional form of the FR model, this paper provides a brief validation of the new model relative to the RPA model in terms of goodness of fit. The validation work presented in this paper is not extensive and is mainly provided for illustrative purposes. A detailed validation of the FR model against other state-of-the practice models, such as the Gipps and Wiedemann models, will be described in future work.

This paper is organized as follows. First, a comprehensive overview of the RPA model is provided. After that, the new model formulation is presented along with an explanation of the theory underlying it and the role of each of its terms. Next, using naturalistic traffic data,

the new model's performance is evaluated against that of the RPA model. Finally, the conclusions of the paper are drawn and insights for future work are provided.

## 5.3 THE RPA CAR-FOLLOWING MODEL

The RPA model [12] is a car-following model that models the longitudinal motion of vehicles in the INTEGRATION traffic simulation software [55, 56]. The model can be mathematically defined as a second-order car-following model that is composed of three main sub-models: steady state, collision avoidance, and vehicle dynamics. While having a more complicated expression compared to traditional car-following models, it offers a more realistic representation of traffic while accounting for the mechanical characteristics of the vehicle, the steady-state conditions governing the roadway, and string stability.

Several previous studies have investigated the RPA model's ability to emulate the behavior of real traffic. Using the speed estimates from its three components, the RPA model computes the speed of the following vehicle as shown in Equation V.1.

$$u_{n+1} = min(u_{n+1}^{VA}, u_{n+1}^{CA}, u_{n+1}^{DYN}) \quad \text{(V.1)}$$

Where $u_{n+1}^{VA}$, $u_{n+1}^{CA}$, and $u_{n+1}^{DYN}$ are the speeds calculated using the three sub-models described previously and whose expressions are given below.

The logic behind the RPA model is straightforward to understand. The model evaluates the speed to which the vehicle needs to converge to maintain cruising in steady-state conditions versus the speed needed to avoid any collisions with the lead vehicle. Next, the minimum of the latter two speeds is compared to the maximum attainable speed related to the mechanics and the surroundings of the vehicle.

Once the speed profile of the following vehicle is determined, its trajectory and its acceleration profiles are easily computed using first-order Euler approximations.

### 5.3.1 Collision Avoidance Model

The collision avoidance model implemented in the RPA model is the component that ensures that the following vehicle does not collide with the vehicle ahead of it [53] and, as a result, the reason that the RPA is a crash-free model (for longitudinal motion).

The collision avoidance term is activated in certain conditions in which the leading vehicle is being approached by its follower. However, having a following vehicle with a higher

speed than the leader is only a necessary and not a sufficient condition for the collision avoidance model to be utilized. In fact, in addition to a decreasing spatial gap between the two vehicles (non-steady-state traffic), a rear-end collision would have to be unavoidable for the collision avoidance model to intervene.

The expression of the model is related to a derivation of the maximum distance that a vehicle can travel to decrease its current speed to the speed of the vehicle ahead of it while decelerating at an acceptable maximal allowable deceleration level, $b_{max}$. From a physical standpoint, it is the distance that ensures that the work done by the brakes, assuming a deceleration equal to $b$, is able to dissipate the change in the vehicle's kinetic energy resulting from the speed difference. An additional term, $s_j$, is added to the latter distance, as demonstrated by Equation V.2, to ensure that the jam density spacing between the two vehicles is respected in the case of a complete stop.

$$s_{n+1}^{CA} = s_j + \frac{u_{n+1}^2 - u_n^2}{2b_{max}} \tag{V.2}$$

Here, $s_j$ is the jam density spacing.

Since the main objective of car-following modeling consists of determining the effects of the changes in the behavior of the leading vehicle on the following vehicle's speed, a speed formulation is adopted for the collision avoidance model, resulting in Equation V.3. The transition between the two equations is straightforward using basic mathematics.

$$u_{n+1}^{CA} = \sqrt{u_n^2 + 2b_{max}\left(s_{n+1} - s_j\right)} \tag{V.3}$$

Finally, it is worth noting that the value of the parameter $b_{max}$ can be either determined by looking at collected data or by conducting a statistical analysis. However, the chosen value has to be bound by the value of the gravitational acceleration $g$ multiplied by the coefficient of friction of the roadway $\mu$.

### 5.3.2 First-Order Steady State Model

The RPA model utilizes the Van Aerde nonlinear functional form to control the steady-state behavior of traffic. The latter model was proposed by Van Aerde and Rakha [33] and is formulated as presented in Equation V.4. The model aims to get an estimate of the steady-state spacing $s_{n+1}^{VA}$ at the next time step using the known speed of the following vehicle.

$$s_{n+1}^{VA} = c_1 + \frac{c_2}{u_f - u_{n+1}} + c_3.u_{n+1} \quad \text{(V.4)}$$

Here, $c_1$, $c_2$, and $c_3$ are model coefficients that can be computed using key roadway traffic stream parameters (Equation V.5) [57]: namely, the roadway free-flow speed, $u_f$; the speed-at-capacity, $u_c$; roadway capacity, $q_c$; and the roadway jam density, $k_j$ (the inverse of the jam density spacing, $s_j$).

$$c_1 = \frac{u_f}{k_j u_c^2}\left(2u_c - u_f\right) \quad c_2 = \frac{u_f}{k_j u_c^2}\left(u_f - u_c\right)^2 \quad c_3 = \frac{1}{q_c} - \frac{u_f}{k_j u_c^2} \quad \text{(V.5)}$$

Similar to the collision avoidance model, the function of Equation 2 is used to derive the speed formulation of the Van Aerde model that is presented in Equation V.6. The model computes the steady-state speed using the estimated spacing $s_{n+1}$.

$$u_{n+1}^{VA} = \frac{-c_1 + c_3 u_f + s_{n+1} - \sqrt{\left(c_1 - c_3 u_f - s_{n+1}\right)^2 - 4c_3\left((s_{n+1} - c_1)u_f - c_2\right)}}{2c_3} \quad \text{(V.6)}$$

### 5.3.3 Vehicle Dynamics Model

The third component of the RPA model is the vehicle dynamics model that ensures that the vehicle's mechanical capabilities are respected. The RPA model incorporates in its expression the constant power model that was developed by Rakha et al. [16, 34] and was proven to capture maximum vehicle acceleration behavior. This model computes the typical acceleration of the following vehicle as the ratio of the resultant force to the vehicle mass *M* (Equation V.7). The resultant force is computed as the difference between the tractive force acting on the following vehicle $F_{n+1}$ (Equation V.8) and the sum of the resistive forces $R_{n+1}$ (Equation V.9); namely the aerodynamics resistance, the rolling resistance and the grade resistance.

$$a_{max} = \frac{F_{n+1} - R_{n+1}}{M} \quad \text{(V.7)}$$

$$F_{n+1} = \min\left(3600\frac{\eta\gamma\beta P}{u_{n+1}}, M_{ta}g\mu\right) \quad \text{(V.8)}$$

$$R_{n+1} = \frac{\rho C_d C_h A_f g u_{n+1}^2}{2} + MgC_{r0}(C_{r1}u_{n+1} + C_{r2}) + MgG \quad \text{(V.9)}$$

Rakha and Lucic [58] introduced the $\beta$ factor in order to account for the gearshift impacts at low traveling speeds when trucks are accelerating. This factor is set to 1.0 for light duty vehicles [59]. Other parameter definitions are: $\eta$ is the driveline efficiency (unitless); $P$ is the vehicle power (kW); $\gamma$ is a constant reduction factor of the vehicle power aiming to represent the throttle level (when the objective is to determine the maximum acceleration that a vehicle is able to achieve, the value of this factor is set equal to 1); $M_{ta}$ is the mass of the vehicle on the tractive axle (kg); $g$ is the gravitational acceleration (9.8067 m/s$^2$) and $\mu$ is the coefficient of road adhesion or the coefficient of friction (unitless); $\rho$ is the air density at sea level and a temperature of 15◦C (1.2256 kg/m$^3$); $C_d$ is the vehicle drag coefficient (unitless), typically 0.30; $C_h$ is the altitude correction factor equal to 1-0.000085$h$ where $h$ is the altitude in meters (unitless); $A_f$ is the vehicle frontal area (m$^2$), typically 0.85 multiplied by the height and width of the vehicle; $C_{r0}$ is a rolling resistance constant that varies as a function of the pavement type and condition (unitless); $C_{r1}$ is the second rolling resistance constant (h/km); $C_{r2}$ is the third rolling resistance constant (unitless); $M$ is the total vehicle mass (kg); and $G$ is the roadway grade (unitless).

A main shortcoming of the vehicle dynamics model presented in Equation V.7 is that it only considers the mechanical characteristics of the vehicle in its expression. In other words, it completely ignores the driver and its 'unique' pattern of driving. Recognizing this deficiency, Fadhloun *et al*. [52] successfully improved the model to make it representative of different driving patterns. The idea behind their research is quite simple and resides in the fact that the power delivered from the engine during driving cannot be assumed to be equal to the maximum power that the engine is able to produce nor to a constant percentage of that maximum power as modeled by Rakha *et al*. [16]. In fact, it is well-known that the delivered engine power is directly sensitive to the percentage of the throttle opening, which itself is related to the speed of the vehicle and the way with which drivers press on the gas pedal. Subsequently, the study [52] was based on a very basic idea which consists on incorporating a variable throttle function in the expression of the tractive force presented in Equation V.8.

The proposed throttle function, presented in Equation V.10, is a hyperbolic model that requires the calibration of three parameters $t_1$, $t_2$, and $t_3$ for each driver.

$$\gamma\left(\frac{u_{n+1}}{u_f}\right) = \frac{u_{n+1}/u_f}{t_1 + \frac{t_2}{1 - u_{n+1}/u_f} + t_3\, u_{n+1}/u_f} \tag{V.10}$$

Replacing the parameter $\gamma$ with the variable throttle function in the expression of the tractive force of Equation V.8 and then implementing the modified equation in Equation V.7 results in a modified acceleration function as shown by Equation V.11. The resulting equation allows modeling the typical acceleration behavior resulting from different driving patterns. In other words, the inclusion of the variable throttle function in the model makes it representative of the human behavior component and the randomness associated with it.

$$a_{n+1} = \frac{\min\left(3600.\gamma\left(\frac{u_{n+1}}{u_f}\right).\frac{\eta\beta P}{u_{n+1}}, M_{ta}g\mu\right) - R_{n+1}}{M} \tag{V.11}$$

Next, $u_{n+1}^{DYN}$ (the output speed of the vehicle dynamics model as defined in Equation V.1) is approximated from the acceleration of the following vehicle (Equation V.11) using a first Euler approximation.

Finally, it is noteworthy to mention that, in the 'Model Evaluation' section of this paper, we opt to use the RPA model formulation in which the vehicle dynamics component is governed by the acceleration function of Equation V.11 that is inclusive of the variable throttle function of Equation 10. By doing so, we ensure that, in worst case scenario, the performance of the model would be equal to that of the model using a constant throttle level $\gamma$.

## 5.4 PROPOSED MODEL FORMULATION

This research effort was initiated mainly for the purpose of investigating possible enhancements to the RPA model that would result in a better and smoother fit to observed acceleration behavior and would capture driver perception and control inaccuracies. It was determined that the majority of the estimation errors between modeled and observed accelerations are due to the discontinuities caused by the presence of the minimum function in the RPA model formulation. To the authors' best knowledge, the RPA model is one of very few car-following models that incorporate vehicle dynamics constraints. Consequently, the discontinuities in the acceleration behavior, caused by the fact that the modeled speed using the RPA model is chosen as the minimum of its three components, do not significantly affect the model's performance.

In fact, the RPA model was recently validated from a fuel consumption and emissions perspective by comparing its performance to that of other widely used car-following models. The study [60] found that the RPA model outperformed other models (Wiedemann, Gipps, and IDM) in terms of approximating the actual fuel consumption and emissions rates. In addition, the acceleration disruptions of the RPA model were found to be less than those observed in the other models. For instance, significant and omnipresent acceleration cliffs are observed in psycho-physical car-following models, which define the acceleration levels based on several traffic regimes, resulting in instantaneous abrupt changes of acceleration levels whenever the following vehicle moves from one regime to another.

Through the evaluation of several alternatives and modifications, it was found that the best approach to address the shortcomings of the RPA model would be the development of a new car-following model, the FR model. The model's main output would be the acceleration of the following vehicle rather than its speed.

Besides providing a smoother and a more realistic representation of the acceleration behavior in all stages, the FR model needed to address and/or respect the following:

- It should be governed by the Van Aerde steady-state model, which has been demonstrated to replicate empirical data.
- It would need to respect the vehicle dynamics model incorporated in the RPA model. Whenever a speed is not attainable due to the mechanical abilities of the vehicle or to the action of the resistive forces acting on it, the developed model should be able to capture that and respond accordingly.
- The developed model should be inclusive of a collision avoidance strategy that ensures that the modeled traffic is collision-free. Here, it is not necessary to use the same collision avoidance strategy as the RPA model. From a collision-avoidance perspective, the adopted algorithm does not matter as much as the model maintaining string stability.
- The number of calibration parameters should be kept as low as possible.
- The model should be as simple as possible with a mathematical expression that could be easily handled analytically in terms of derivation and integration.
- The model should capture driver perception and variability across different drivers.
- Finally, the model should separate terms associated with modeling the acceleration and the deceleration behaviors.

### 5.4.1 Vehicle Longitudinal Motion Modeling

Microscopic simulation software uses car-following models to capture the interaction of a subject vehicle and its preceding vehicle traveling in the same lane. The process of car-following is modeled as an equation of motion for steady-state conditions (collision avoidance for steady-state conditions) plus a non-steady-state collision avoidance term. In addition, a non-steady-state constraint is added to model the vehicle dynamics while accelerating.

To model the impact of trucks and driver distraction on driver car-following behavior, we introduce the following variables: $n$ is the index of the lead vehicle; $n+1$ is the index of the subject following vehicle; $x_{n+1}, u_{n+1},$ and $a_{n+1}$ are the subject vehicle (vehicle $n+1$) position, velocity, and acceleration, respectively; $u_f$ is the vehicle's desired speed (also known as the roadway free-flow speed); $d_{desired}$ is a desired comfortable vehicle deceleration level (typically taken to be $-3$ m/s$^2$); $s_{n+1}$ is the vehicle spacing from the back bumper of the subject vehicle to the back bumper of the lead vehicle; $s_j$ is the vehicle spacing at a speed of zero (i.e., the jam density spacing); and $\tau$ is the driver's perception-reaction time.

The typical car-following model implemented in commercial adaptive cruise control systems entails attempting to follow the lead vehicle at a constant headway, which is typically taken to be equal to the vehicle reaction time or the driver perception-reaction time $\tau$, as illustrated in Equation V.12. This model is also known as the Pipes or GM-1 model [61-63]. This time headway ensures that the subject vehicle $n+1$ follows its lead vehicle at a safe spacing in order to avoid a collision under state-state conditions (i.e., when both vehicles are traveling at the same constant velocity and assuming that the subject vehicle's deceleration maneuver starts $\tau$ seconds after the lead vehicle decelerates).

$$\tilde{s}_{n+1} = s_j + \tau u_{n+1} \tag{V.12}$$

Van Aerde [64] and Van Aerde and Rakha [65] proposed a more general formulation that reflects empirical driver behavior better than existing traffic stream models. This formulation combines the Pipes (Equation V.7) and the Greenshields models to generate a more general formulation [57, 66, 67], as was presented in Equation V.4 and Equation V.5.

Incorporating Equation V.5 in Equation V.4 and solving for the driver perception-reaction time, Equation V.13 is derived. This equation is critical, given that it characterizes how the driver's perception-reaction time varies as a function of the roadway parameters

$(u_f, u_c, q_c, k_j)$ and the vehicle's speed. The Van Aerde formulation would then be identical to Equation 12, except that the driver perception-reaction time will be that of Equation V.13.

$$\tau = \frac{1}{k_j u_c^2}\left[\frac{k_j u_c^2}{q_c} - u_f + \frac{\left(u_f - u_c\right)^2}{u_f\left(u_f - u_{n+1}\right)}\right] \tag{V.13}$$

If the lead vehicle is traveling at a higher velocity (non-steady-state conditions) then the desired safe following spacing can be computed using Equation V.14. This allows the driver to drive at a spacing less than the steady-state spacing when the vehicle ahead of it is driving at a higher speed.

$$\tilde{s}_{n+1} = \max\left(c_1 + \frac{c_2}{\left(u_f - u_n\right)} + c_3 u_n - \frac{u_{n+1}^2 - u_n^2 - \sqrt{(u_{n+1}^2 - u_n^2)^2}}{4d_{des}}, s_j\right) \tag{V.14}$$

Finally, the vehicle acceleration behavior is governed by the maximum acceleration computed using Equation V.7 to ensure that vehicle accelerations are realistic.

To capture the driver throttle input, the $f_p$ factor is introduced, which ranges between 0.0 and 1.0. The final expression of the FR model, which considers vehicle deceleration to avoid a collision with a slower traveling lead vehicle, is cast using Equation V.15. This equation includes two terms. The first term is the vehicle acceleration term, while the second term is the vehicle deceleration term. Both terms ensure that the vehicle does not collide with its lead vehicle. Improvements to the model could include relaxing this assumption and allowing collisions to occur.

$$a_{n+1} = f_p a_{max} + \frac{\left[u_{n+1}^2 - u_n^2 + \sqrt{(u_{n+1}^2 - u_n^2)^2}\right]^2}{16(d_{desired} + gG)\left(s_{n+1} - s_j\right)^2} \tag{V.15}$$

Here, $f_p$ is computed using Equation V.16, and $X_{n+1}$ is calculated using Equation V.17.

$$f_p = e^{-aX_{n+1}}\left(1 - X_{n+1}^b e^{b(1-X_n+1)}\right)^d \tag{V.16}$$

$$X_{n+1} = \frac{\tilde{s}_{n+1}}{s_{n+1}} \cdot \frac{u_{n+1}}{\tilde{u}_{n+1}} \tag{V.17}$$

where $\tilde{s}_{n+1}$ is the desired spacing for the current speed (computed using Equation V.12); $\tilde{u}_{n+1}$ is the desired speed for the current spacing (computed in a similar manner to Equation V.5 by inverting Equation V.12); *a*, *b*, and *d* are model parameters that are calibrated to a specific driver and model the driver input to the gas pedal.

Before proceeding to the following sections in which the model formulation is explained in more detail and its performance verified against that of the RPA model, a brief comparative summary of the parameters involved in the two models is provided. As a reminder, one of the stated requirements for the new model relates to the number of calibration parameters which should be kept as low as possible. Ensuring that the FR model formulation respects the latter point is of the utmost importance. In fact, the significance of any increase of accuracy offered by a certain model with regards to another is strongly correlated to the difference between the numbers of their respective calibration parameters. Subsequently, the purpose of this section is to verify that the number of parameters of the FR model is at most equal to that of the RPA model. That would completely out rule the effect of the number of calibration parameters on any potential increase of accuracy. Table 10 provides an exhaustive summary of the different parameters involved in the two models.

**Table 10: Parameters of the RPA model and the FR model**

| | RPA Model | FR Model |
|---|---|---|
| Steady State Parameters | $u_f, u_c, q_c, k_j$ (inverse of $s_j$) | |
| Vehicle and Road Parameters | $M, \eta, P, M_{ta}, \mu, \rho, C_d, C_h A_f, C_{r0}, C_{r1}, C_{r2}, G$ | |
| Human Behavior Parameters | $t_1, t_2, t_3$ | $a, b, d$ |
| Collision Avoidance | $b_{max}$ | $d_{des}$ |

The table highlights the fact that the number of parameters involved is equal for the two models both on the aggregate level and on the categorized level (steady state, vehicle and road characteristics, human behavior, and collision avoidance). Furthermore, the RPA model and the FR model share the same parameters that are representative of the steady state behavior, the vehicle model, and the road characteristics. The first observed differences are at the level of the human behavior modeling in which each model requires the calibration of three different parameters ($t_1, t_2, t_3$ for the RPA model and $a, b, d$ for the FR model). The other difference relates to using a maximum deceleration level in the collision avoidance module of the RPA model versus a desired deceleration level in that of the FR model.

### 5.4.2 Deceleration Component Formulation

Looking at Equations V.2 and V.3 presenting the collision avoidance logic of the RPA model, the "unknown" variable that needs to be determined is expressed as a function of parameters related to the previous time step for which all computations were completed. In other words, one can solve for any of the respective variables at the next time step using the remaining parameters. For instance, if the deceleration level is set as the unknown variable, its value could be determined by Equation V.18, which is easily derived through simple mathematical operations of Equation V.2 or V.3.

$$d_{kinematics} = \frac{\left[u_{n+1}^2 - u_n^2 + \sqrt{(u_{n+1}^2 - u_n^2)^2}\right]}{4\left(s_{n+1} - s_j\right)} \tag{V.18}$$

From a physical perspective and assuming that the following vehicle is approaching the leading vehicle, $d_{kinematics}$ denotes the deceleration level that is needed in order for the following vehicle to decrease its speed to the speed of the leading vehicle with the stopping distance being equal to the distance gap separating them.

To maintain collision-free traffic, the following vehicle needs to decelerate at a level that is at least equal to $b_{kinematics}$ whenever its speed exceeds that of the leading vehicle. However, opting for a collision avoidance strategy that just uses $d_{kinematics}$ for braking would not be optimal as this would not allow for the modeling of different levels of braking aggressiveness. Under the latter scheme, all drivers would behave in a similar fashion whenever a braking maneuver is needed.

In order to allow the FR model to capture different braking patterns and the heterogeneity in driver behavior, the adopted braking strategy uses a desired deceleration level $d_{desired}$ that is set by the user in addition to $b_{kinematics}$. The collision avoidance of the FR model, presented in Equation V.19, ensures that the function *CA* computes the needed deceleration to apply as the ratio of the square of the kinematics deceleration $d_{kinematics}$ needed to decelerate from the current speed to the leading vehicle speed and the desired deceleration level $d_{desired}$.

$$CA(u_{n+1}, s_{n+1}, \Delta u_{n+1}) = \frac{d_{kinematics}^2}{(d_{desired} + gG)} \tag{V.19}$$

The above collision avoidance logic is very similar in shape to that proposed in the IDM [8]. However, physically speaking it is more meaningful. The adopted strategy ensures that collisions do not occur between vehicles. In fact, one can notice that in the case that $d_{desired}$ is

less than $d_{kinematics}$, the applied deceleration is greater than the desired deceleration level. Conversely, when the desired deceleration is greater than $d_{kinematics}$, the deceleration converges smoothly towards $d_{desired}$.

The cause of the described behavior is determined by looking at the derivative of the *CA* function with regard to time. In fact, the only critical point and root of the latter function occurs at the point $d_{desired}$. The function is increasing on one side of $d_{desired}$ and decreasing on the other. That ensures a smooth transition between the different deceleration levels in order to avoid collisions whenever needed and decelerate at the desired level whenever possible.

Finally, a modified deceleration expression is included as the second term in Equation V.15 in order to ensure that the braking strategy is activated only when the following vehicle speed is higher than that of the leader and to account for the effect of the road grade on the desired deceleration level.

### 5.4.3 Acceleration Component Formulation

When developing the function governing the acceleration regime, the research team investigated several functions, starting from the simplest to the most complicated. The main commonality between the functions that were considered is that they were mostly developed using exponential functional forms. The primary reason that exponential functions were used relates to the relative simplicity of their expression, their dampening effect, and their flexible shape.

The biggest challenge in this task resides in the fact that the chosen functional form should be able to ensure that the steady-state behavior is respected and the vehicle dynamics as well as allowing the modeling of different patterns of driving. After thorough investigation, the function presented by Equation V.16 multiplied by the maximum acceleration level (Equation V.7) was found to be the best in terms of achieving the previous objectives. The proposed function requires the calibration of three parameters *a*, *b*, and *d* that are responsible for modeling several driving patterns.

The term $f_p$, which models the driver input to the gas pedal, ensures that two objectives are met. First, it ensures that the steady state model governing the FR model is the same as the RPA model formulation. Second, it attempts to model human behavior and the different patterns of driving by acting as a reduction factor to the vehicle dynamics model.

To better explain the second objective, the $f_p$ functions corresponding to different value sets for *a*, *b*, and *d* are used for illustration purposes. The variation of the resulting functions

plotted against the ratio $X_{n+1}$ in Figure 11. The figure shows that, regardless of the values of the aforementioned three parameters, the root of the function is fixed and occurs at $X_{n+1}$= 1, which is basically equivalent to the traffic being in steady-state conditions. That would result in the overall acceleration computed from Equation V.15 to be equal to zero, demonstrating that the FR model is governed by the Van Aerde fundamental diagram and forcing the vehicle to continue cruising in steady state conditions once it reaches it as long as the behavior of the leading vehicle remains unchanged. Alternatively, the Van Aerde model is the only solution to the equation describing steady-state conditions. Furthermore, when the following vehicle is at a complete stop ($X_{n+1}$= 1), the full vehicle mechanical capabilities are used, as $f_p$ would be equal to 1.0 in that case. Additionally, given that $f_p$ is bounded by 0.0 and 1.0 for the entire acceleration domain (corresponding to $X_{n+1} \in [0, 1]$), the vehicle dynamics model of the RPA model can be cast as an upper envelope to the proposed acceleration function. For each set of parameters a, b and d, a different unique function with the same values at 0 and 1 is defined. That allows modeling the variability across different drivers as a unique driving pattern is defined when the $f_p$ function is multiplied by the maximum acceleration function of Equation 7.

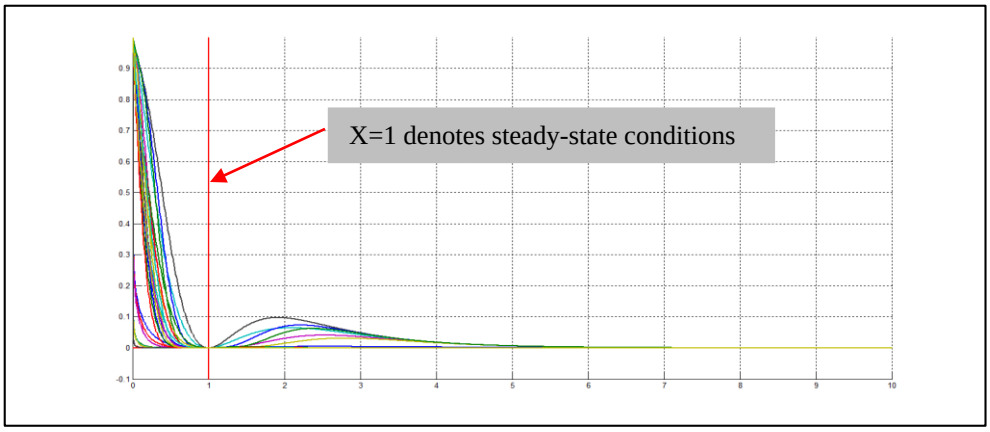


**Figure 11: Example $f_p$ functions resulting from several (*a*, *b*, *d*) combinations.**

Finally, the human behavior modeling that needs to be addressed by the FR model is demonstrated by the significant breadth of coverage of the acceleration domain by the different $f_p$ functions plotted in Figure 11. The latter effect attributed to the *a*, *b*, and *d* parameters is exemplified through the addition of three noise variables to capture driver perception and control inaccuracies. To model the driver perception error in estimating the leading vehicle speed and spacing between the two vehicles, two Wiener processes are incorporated in the model formulation as presented in Equation 20 and 21. On one hand, Equation V.20 emulates the fact that a driver is not able to have an exact estimation of the immediate leader ahead of

him. On the other hand, Equation V.21 simulates the error a driver commits while estimating the spacing separating him from the car in front of him/her. Additionally, a white noise signal, presented in Equation V.22, is added to the model's expression to capture driver imperfection while applying the gas pedal (control error). The compounding effect of these three signals makes the model output more representative of human driving behavior. The model output is computed as the sum of Equation V.22 and Equation V.15 in which $\widetilde{u_n}(t)$ and $\widetilde{s_{n+1}}(t)$ are used instead of $u_n$ and $s_{n+1}$.

$$\begin{cases} \widetilde{u_n}(t) = u_n(t-\Delta t) - 0.01\left(s_{n+1} - s_j\right)\left(e^{-0.01}.W_l(t-\Delta t) + \sqrt{0.02}.N(0,1)\right) \\ W_l(1) = N(0,1) \end{cases} \quad \text{(V.20)}$$

$$\begin{cases} \widetilde{s_{n+1}}(t) = s_{n+1}(t-\Delta t) \times e^{0.1\left(e^{-0.01}.W_s(t-\Delta t) + \sqrt{0.02}.N(0,1)\right)} \\ W_s(1) = N(0,1) \end{cases} \quad \text{(V.21)}$$

$$\breve{a}_n(t) = N(0, 0.25) \quad \text{(V.22)}$$

The next objective that the FR model needs to meet relates to separating the acceleration term from the deceleration term. That was initially planned to be achieved through the use of maximum and minimum functions. However, a coincidental finding that the maximum achieved by $f_p$ in the deceleration domain ($1 < x_{n+1}$) is relatively small led the authors to proceed differently. In fact, an iterative procedure that derives an approximation of the maximum of $f_p$ in the deceleration domain was developed. The iterative procedure, presented in Equation V.23, is only approximate and converges relatively fast (four to five steps) to the location of the maximum of $f_p$, which is then verified to be below a very low threshold ε (for instance, ε = 0.01). By doing so, it is decided whether the chosen values for the parameters *a*, *b*, and *d* are accepted or rejected. Of course, this procedure was only adopted after ensuring that the number of the different combinations of (*a*, *b*, *d*) that would result in $f_p(x_{n+1}) < \varepsilon = 0.01$ is significant.

$$\begin{cases} X_0 = 3.\left(-1 + \sqrt{2ln(3)}\right) \\ X_{k+1} = 3.\left[-1 + \sqrt{2ln\left(3 \times \left[1 + \frac{bd}{a}\left(1 - \frac{1}{X_k}\right)\right]^{1/b}\right)}\right] \end{cases} \quad \text{(V.23)}$$

## 5.5 MODEL EVALUATION

In this section, a brief comparative analysis between the performance of the FR model and the RPA model is provided to allow the reader to visualize and evaluate the performance of the proposed model using naturalistic driving data. Besides the characteristics of the different vehicles as well as certain aspects defining the driving pattern of the driver, which are known due to the naturalistic nature of the dataset, the FR model and the RPA model require the calibration of three additional parameters (*a*, *b*, and *d* for the FR model and $t_1$, $t_2$, and $t_3$ for the RPA model).

It should be noted that the calibration of the parameters considered the speed root mean square error (RMSE) as the objective function and was conducted on an event-by-event basis rather than for the dataset as a whole. Such a choice was made so that each model's outputs incorporated the effect of its strength points. As for the Van Aerde steady-state model parameters, which are the same for the two models, they were calibrated using the procedure described in [54].

Finally, given the presence of noise in the proposed model, the calibration was conducted using a bi-level procedure. First, the model parameters were calibrated deterministically without consideration of the noise signals. Next, to model the effect of the noise, the optimized parameters of the first step were used to run a total of 1,000 simulations in order to have valid model outputs and to determine the 95% confidence interval of the results.

### 5.5.1 Naturalistic Dataset

The data used herein represent a small subset that was extracted from the naturalistic driving database generated by the 100-Car study [68] that was conducted by the Virginia Tech Transportation Institute (VTTI) in 2002. Specifically, VTTI initiated a study where 100 cars were instrumented and driven by a total of 108 drivers around the District of Columbia (DC) area. The resulting database from the 100-Car study [68] contains detailed logs of more than 207,000 completed trips with a total duration of around 20 million minutes of data.

The naturalistic dataset that was used to validate the proposed model contains information relating to 1,659 car-following events that span a duration of approximately 13 hours, which is significant for the task of validating car-following models. The car-following data come from six different drivers and were collected on a relatively short segment of the

Dulles Airport access road (an approximately 8-mile-long section) in order to maintain facility homogeneity.

### 5.5.2 Results

Having access to the calibrated parameters, the speed profiles were obtained for each car-following event of the naturalistic dataset. The corresponding speed outputs ensure a minimal RMSE between a model's predictions and the empirical data over its whole timespan. The error results for the RPA model and the FR model are shown in Table 11 and Table 12 which present the main distribution characteristics of the speed RMSE and the acceleration respectively. The results demonstrate that the FR model results in an increase of accuracy compared to the RPA model both in terms of fitting the speed and acceleration profiles. In fact, the mean, median and standard deviation for the FR model are smaller than those achieved by the RPA model. The performance of the FR model is further supported by the histograms of Figure 12 and Figure 13 which allows visualizing the distribution of the absolute speed and acceleration error values. The figures confirm that the FR model results in a narrower more compacted distribution especially on the acceleration level.

**Table 11: Distribution characteristics of the speed RMSE**

| | **Mean** | **Median** | **Std Deviation** |
|---|---|---|---|
| FR Model | 1.00 | 0.85 | 0.73 |
| RPA Model | 1.60 | 1.13 | 1.44 |

**Table 12: Distribution characteristics of the acceleration RMSE**

| | **Mean** | **Median** | **Std Deviation** |
|---|---|---|---|
| FR Model | 0.60 | 0.56 | 0.20 |
| RPA Model | 0.93 | 0.84 | 0.51 |

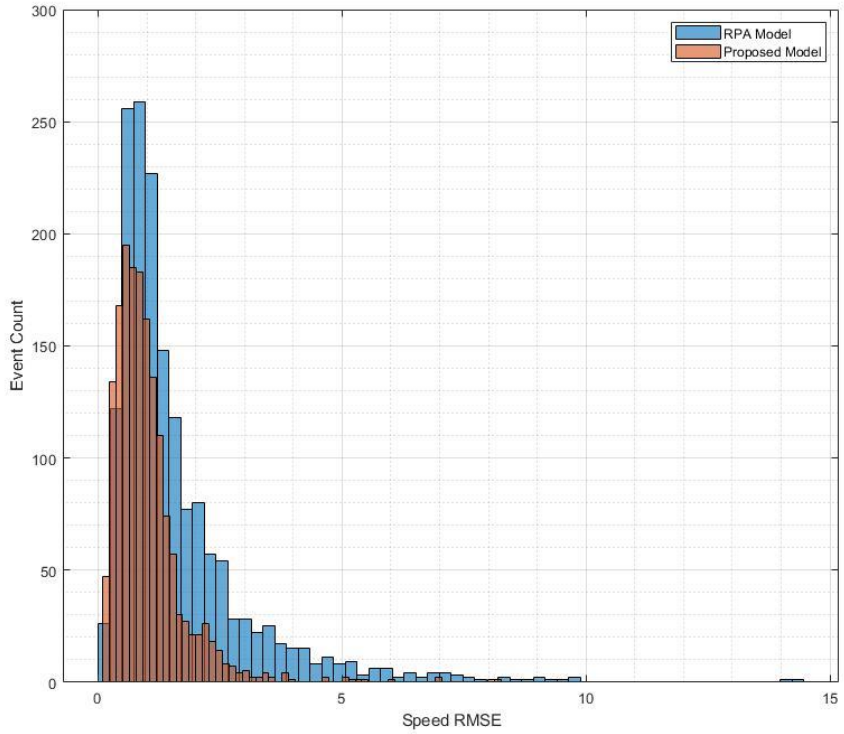


**Figure 12: Histogram showing the distribution of the speed RMSE**

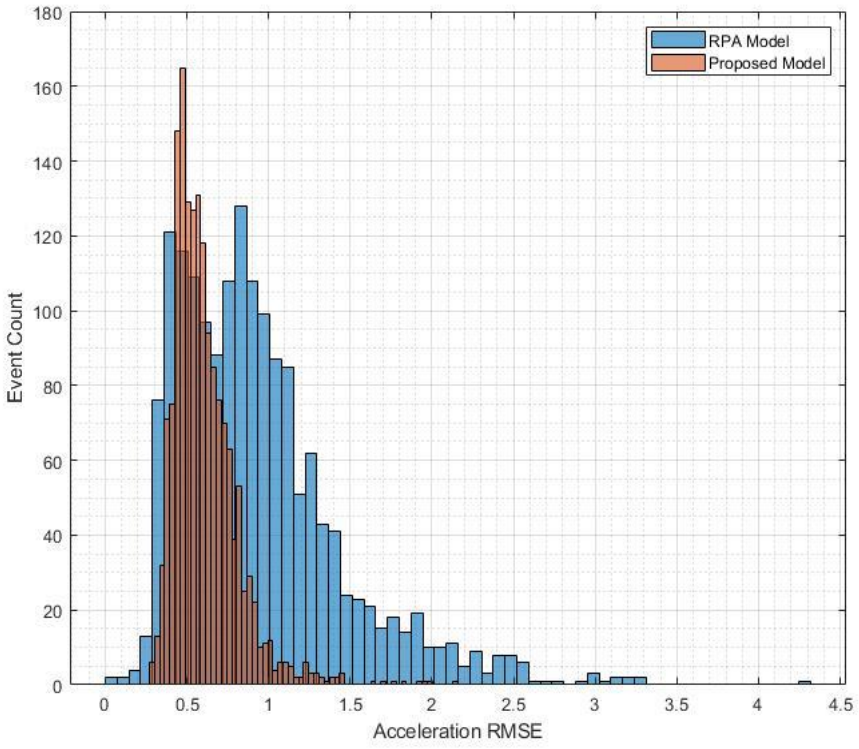


**Figure 13: Histogram showing the distribution of the acceleration RMSE**

To better statistically quantify the difference in performance between the proposed model and the RPA model, the rank of the new model was determined for each event based on the calculated RMSE value (taken as the resulting mean of the 1,000 trials). In doing so, it was found that the proposed FR model significantly outperformed the RPA model approximately 80% of the time, and its speed RMSE was less than that found using the RPA model. To better quantify the percentage by which the error function was reduced, key measures of the distribution of the relative percentage decrease in the speed RMSE were calculated (Table 13). It was found that for the events for which the proposed model formulation outperformed the RPA model, the error reduction percentage had a mean and a median equal to 57% and 55%, respectively. The significance of those results is accentuated given that the RPA model only resulted in a mean and median decrease of 31% and 28% for the remaining 20% of the events for which it outperformed the FR model.

**Table 13: Distribution characteristics of the decrease of percentage in speed RMSE for head-to-head comparisons.**

| | **Best Model** | **Mean** | **Median** | **Std Deviation** |
|---|---|---|---|---|
| **80% of events** | FR Model | 54.92 | 57.01 | 28.00 |
| **20% of events** | RPA Model | 31.70 | 28.15 | 22.23 |

To complement the above results, the resulting acceleration data from the optimized speed profiles were investigated as well. It was found that the proposed FR model resulted in a significant improvement over the acceleration profiles of the RPA model. In fact, the FR model resulted in a better fit to observed acceleration data in about 87% of the cases, with an average and median percentage decrease slightly above 50%.

In order to examine the performance of the two models qualitatively, the resulting simulated speeds and accelerations are presented for three sample events in Figure 14, Figure 15 and Figure 16. Both figures plot the variation of the observed and simulated speed and acceleration profiles resulting from the calibration of the two models over time. Looking at the speed profiles of Figure 14 and Figure 15, the two models appear to successfully generate a speed profile for the following vehicle that emulates empirical data such that the resulting error is at its minimum. More importantly, the FR formulation traced the actual acceleration profile the best for both events. For the event of Figure 16, the FR model capture the speed profile in a much better way than the RPA model. The same could be said also for the related acceleration profile.

Generally speaking, the new model was found to be the best in terms of mimicking real-driver behavior as it successfully avoided the acceleration fluctuations produced by the RPA model that are far in excess of those observed at the level of the empirical data. Overall, as a qualitative measure for the acceleration data, the two sample events are consistent with the goodness-of-fit results presented earlier.

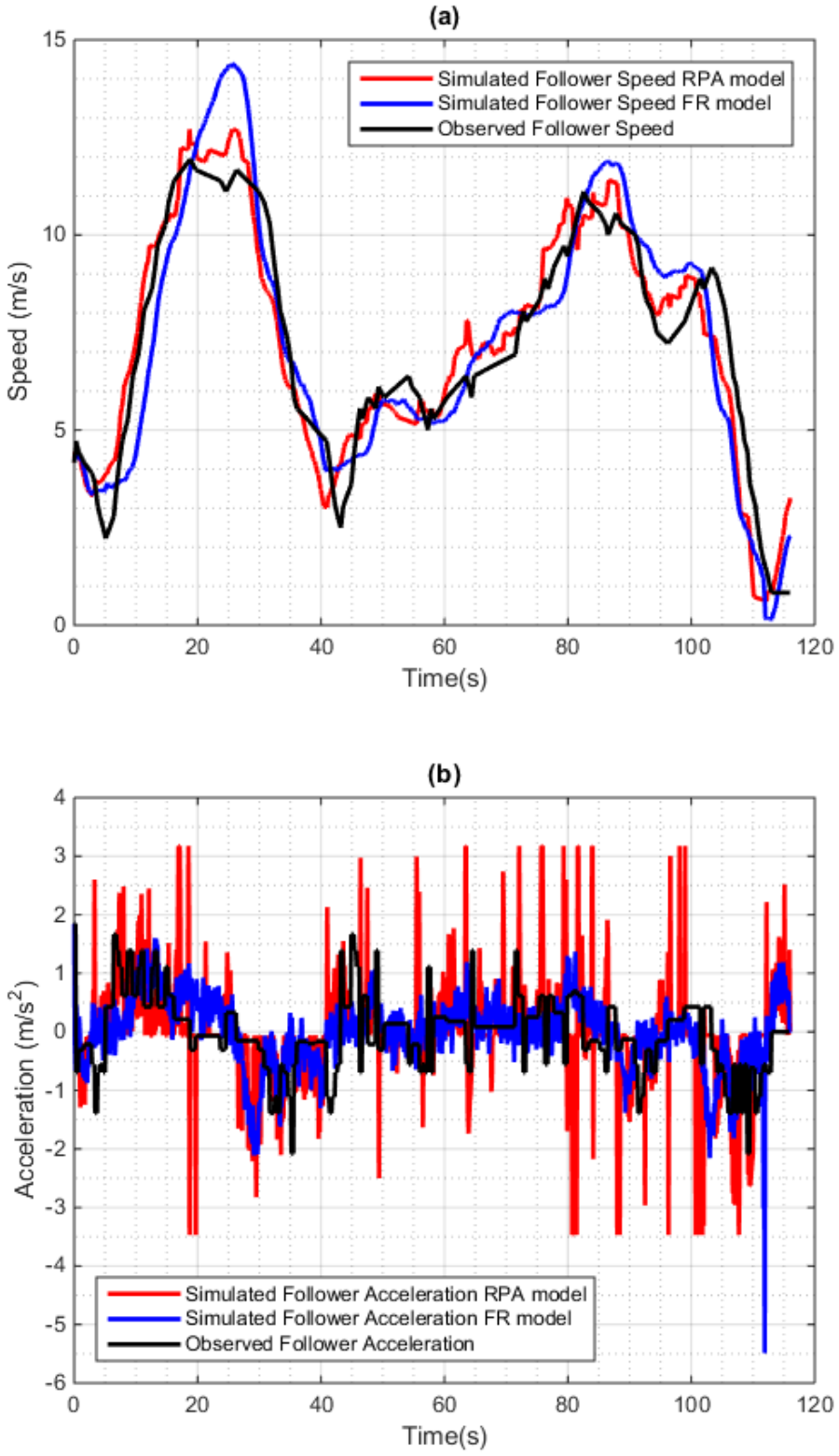


**Figure 14: Sample event data. (a) Speed profile. (b) Acceleration profile.**

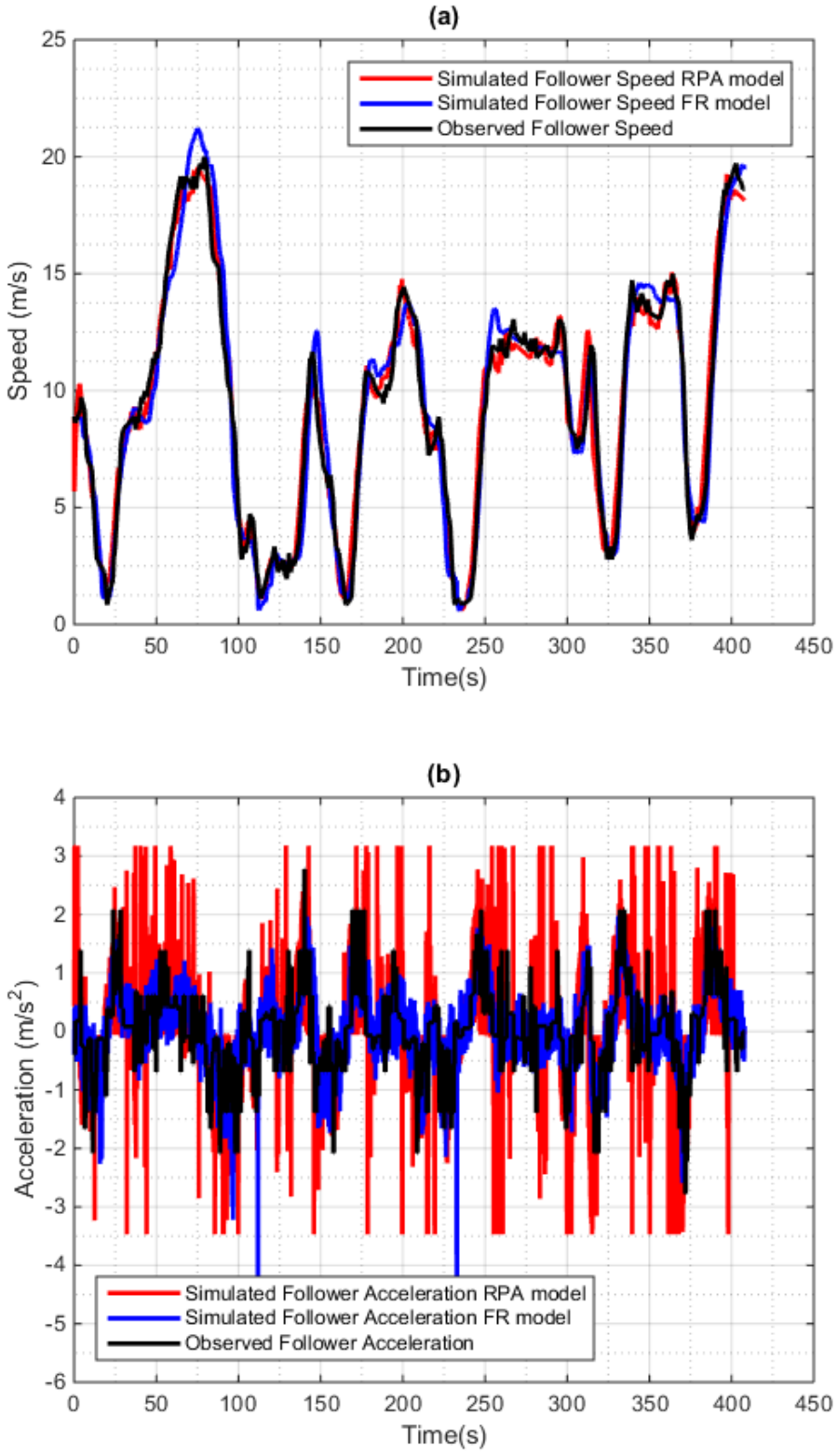


**Figure 15: Sample event data. (a) Speed profile. (b) Acceleration profile.**

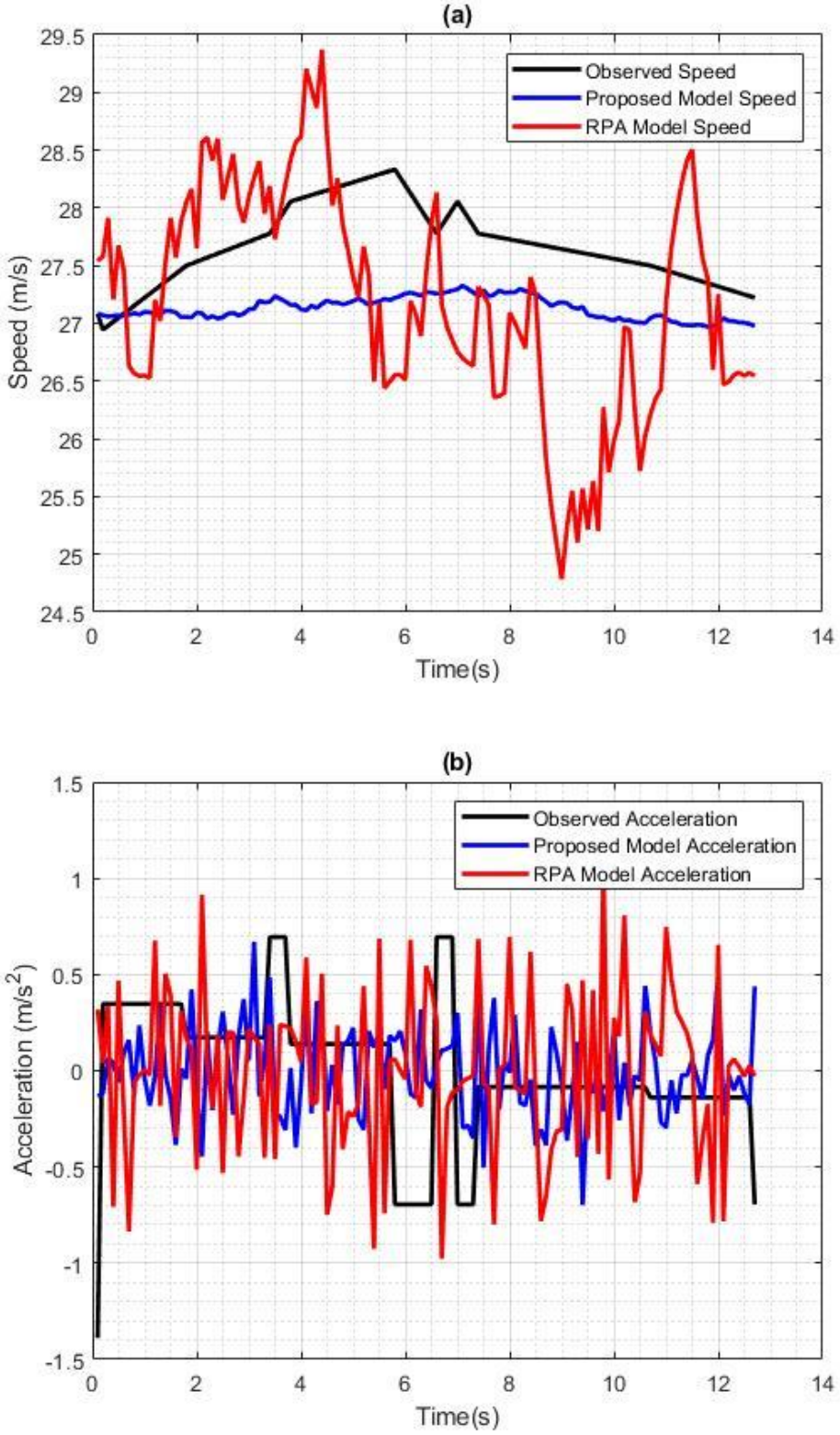


**Figure 16: Sample event data. (a) Speed profile. (b) Acceleration profile.**

## 5.6 CONCLUSIONS

This paper described the methods and procedures leading to the development of a new car-following model that is derived from the RPA model. The proposed FR model is an enhancement to the original RPA model. In fact, the FR model maintains the key components of the RPA model. As a result, the two models are governed by the same steady state formulation (i.e., the Van Aerde first-order model), respect vehicle dynamics constraints, and use very similar collision-avoidance strategies to ensure a safe following distance between vehicles. In addition, the FR model explicitly captures human driving variability in its acceleration function. The model term responsible for modeling different driving patterns is complemented with three noise signals that attempt to emulate the effects of human estimation errors and driving imperfections.

This research effort was initiated mainly for the purpose of investigating possible enhancements to the RPA model that would result in a better and smoother fit to observed acceleration behavior and also capture driver perception and control inaccuracies. It was determined that the majority of estimation errors between modeled and observed accelerations are due to the discontinuities caused by the presence of the minimum function in the RPA model formulation. Through the evaluation of several alternatives and modifications, the FR model formulation was found to be the best in terms of successfully addressing the aforementioned objectives. Despite providing a more realistic representation of the acceleration behavior in all stages, the FR model only requires the calibration of three parameters *a*, *b*, and *d* (besides the vehicle and roadway parameters, which are typically known).

## 5.7 DATA AVAILABILITY

The data used to support the findings of this study have not been made available because Institutional Review Board (IRB) approval is required to access the data.

## 5.8 CONFLICTS OF INTEREST

The authors declare that there are no conflicts of interest regarding the publication of this paper.

## 5.9 FUNDING STATEMENT

The authors acknowledge the financial support provided by the University Mobility and Equity Center (UMEC) and the Department of Energy through the Office of Energy Efficiency and Renewable Energy (EERE), Vehicle Technologies Office, Energy Efficient Mobility Systems Program under award number DE-EE0008209.

# Chapter 6 Validating the Fadhloun-Rakha Car-Following Model

**Authors:**

Karim Fadhloun

Hesham Rakha, Ph.D, P.Eng.

Amara Loulizi, Ph.D, P.E.

Jinghui Wang, Ph.D.

*Submitted for presentation at the 2020 TRB Annual Meeting and publication in the Transportation Research Record: Journal of the Transportation Research Board, 2020.*

## 6.1 ABSTRACT

The research presented in this paper investigates and validates the performance of a new car-following model (the Fadhloun-Rakha (FR) model). The FR model incorporates the key components of the Rakha-Pasumarthy-Adjerid (RPA) model in that it uses the same steady-state formulation, respects vehicle dynamics, and uses very similar collision-avoidance strategies to ensure safe following distances between vehicles. The main contributions of the FR model over the RPA model are the following: (1) it explicitly models the driver throttle and brake pedal input; (2) it captures driver variability; (3) it allows for shorter than steady-state following distances when following faster leading vehicles; (4) it offers a much smoother acceleration profiles; and (5) it explicitly captures driver perception and control inaccuracies and errors. In this paper, a naturalistic driving dataset is used to validate the FR model. Furthermore, the model performance is compared to that of five widely used car-following models, namely: the Wiedemann model, the Frietzsche model, the Gipps model, the RPA model and the Intelligent Driver Model (IDM). A comparative analysis between the different model outputs is used to determine the performance of each model in terms of its ability to replicate the empirically observed driver/vehicle behavior. Through quantitative and qualitative evaluations, the proposed FR model is demonstrated to significantly decrease the modeling error when compared to the five aforementioned models and to generate trajectories that are highly consistent with empirically observed driver following behavior.

## 6.2 INTRODUCTION

Due to the continuous technological advancement and proliferation of computational tools both at the level of hardware and software, traffic engineering is becoming more and more simulation-oriented. Relying on computerized traffic simulations for planning, urbanization and environmental purposes can be cast as a two-edged activity. On the one hand, microscopic simulation software allow the user to evaluate and estimate the outcomes of different potential scenarios in a fast and cost effective manner and, most importantly, without inducing any bottlenecks or disrupting the flow of vehicles in the real world. On the other hand, it is imperative to not forget that the results returned by traffic simulators are directly correlated to the accuracy and precision of the different models and logics incorporated in them. Subsequently, it is necessary to ensure that whatever implemented in this type of software, would constitute good descriptors of real traffic conditions and empirical behavior.

A main component of microscopic simulation software is the car-following model. Car-following models [1-6, 8, 9] predict the temporal and spatial behavior of a following vehicle when the time-space profile of the leading vehicle is known. The output of car-following models directly impact several other factors and measures of effectiveness (MOE), such as vehicle energy/fuel consumption and emissions.

This paper describes a research effort that aims to validate a new innovative acceleration-based car-following model, which is the Fadhloun-Rakha model [18]. The methodology and the procedure that led to the functional form of the model was described extensively in a previous work by Fadhloun and Rakha [18]. The validation of the proposed model is conducted by comparing its performance against the performance of other car-following models. Gipps [7], Frietzsche [9], Wiedemann [10, 11], the IDM model [69] and the RPA model [12] were selected as controls of the proposed model because of their wide use and their implementation in some of the most famous traffic simulators (*AIMSUN* [25], *PARAMICS* [27], *VISSIM* [26] and *INTEGRATION* [14, 15]). The dataset used in the validation procedure is extracted from the naturalistic data of the 100-Car study that was conducted by the Virginia Tech Transportation Institute [68].

Concerning the layout, this paper is organized as follows. First, an overview of the Fadhloun-Rakha (FR) model [18] is provided along with the other state-of-the-practice car-following models mentioned above. Subsequently, the dataset used in this study is briefly described and the analysis related to the calibration procedure as well as the validation process

of the FR model is presented. Finally, the conclusions of the paper are drawn and insights into future work are provided.

## 6.3 BACKGROUND

In this section, a brief description of the logic behind each of the studied models is provided in a chronological order.

### 6.3.1 Wiedemann Model

Wiedemann model [10] is a psycho-physical car-following model that is widely known in the traffic engineering community due to its integration in the microscopic multi-modal traffic simulation software *VISSIM* [26]. The initial formulation of the model [10], proposed in 1974, was calibrated mostly based on conceptual ideas rather than real traffic data. As a result, a much-needed recalibration of the model [11] was performed in the early-1990s using an instrumented vehicle.

The Wiedemann model framework, as implemented in *VISSIM*, uses five bounding functions in the $\Delta v - \Delta x$ domain —*AX*, *ABX*, *SDX*, *SDV* and *OPDV*— to define the thresholds between four traffic regimes — free driving, closing-in, following and emergency — as presented in Figure 17.a. The figure illustrates the Wiedemann model logic graphically by showing how a following vehicle would behave as it is approaching a lead vehicle. Depending on the traffic regime in which the following vehicle is located, the acceleration is set equal to a predefined specific rate as illustrated in Figure 17.a. The mathematical expressions of the five regime thresholds are given in Equations (VI.1- VI.5).

$$AX = L_{n-1} + [AX_{add} + AX_{mult} \times RND1] \quad \text{(VI.1)}$$

$$ABX = AX + [BX_{add} + BX_{mult} \times RND1]\sqrt{\min(u_{n-1}, u_n)} \quad \text{(VI.2)}$$

$$SDX = AX + [EX_{add} + EX_{mult} \times (NRND - RND2)] \times [BX_{add} + BX_{mult} \times RND1]\sqrt{\min(u_{n-1}, u_n)} \quad \text{(VI.3)}$$

$$SDV = \left(\frac{\Delta x - L_{n-1} - AX}{CX}\right)^2 \quad \text{(VI.4)}$$

$$OPDV = SDV \times [-OPDV_{add} - OPDV_{mult} \times NRND] \quad \text{(VI.5)}$$

Where *RND1*, *RND2*, *RND3*, *RND4* and *NRND* are normally distributed parameters that aim to model the randomness associated with different driving patterns and behaviors, $L_{n-1}$ is the length of the leading vehicle in meters, $u_{n-1}$ is the leading vehicle speed in (*m/s)*, $\Delta x$ is the spacing between the lead and the following vehicles, and *CX* is a model parameter that is

assumed to be equal to 40. Finally, the remaining variables, named using the standard format $P_{add}$ or $P_{mult}$, are the model parameters requiring calibration.

It is noteworthy to mention that the formulations of Equations (VI.1- VI.5) could be further simplified by removing the random driver-dependent parameters for the specific case of this study. In fact, the randomness inducing parameters are of no use when calibrating the model against empirical data of a single driver. With that being said, Equations (VI.1- VI.5) are modified by applying the generic transformation of Equation 6 resulting in a significant reduction of the number of calibration parameters. The resultant set of equations, defined in Equations (VI.7- VI.11), requires the calibration of a total of four parameters.

$$P_{cal} = P_{add} + P_{mult} \times P_{rand} \quad \text{(VI.6)}$$

$$AX = L_{n-1} + AX_{cal} \quad \text{(VI.7)}$$

$$ABX = AX + BX_{cal}\sqrt{\min(u_{n-1}, u_n)} \quad \text{(VI.8)}$$

$$SDX = AX + EX_{cal} \times BX_{cal}\sqrt{\min(u_{n-1}, u_n)} \quad \text{(VI.9)}$$

$$SDV = \left(\frac{\Delta x - L_{n-1} - AX}{40}\right)^2 \quad \text{(VI.10)}$$

$$OPDV = -SDV \times OPDV_{cal} \quad \text{(VI.11)}$$

### 6.3.2 Gipps Model

Gipps model [7], developed in the late-1970s and implemented in the traffic simulation software *AIMSUN* [70] , is formulated as a system of differential difference equations. Using a time step $\Delta t$ that aims to model the reaction time of drivers, the model computes the following vehicle speed $u_n$ at time $t+\Delta t$ as a function of its speed and the leading vehicle speed $u_{n-1}$ at the preceding time step $t$.

As shown in Equation VI.12, the speed of the following vehicle is estimated by determining the minimum of two arguments. The first term governs the cases characterized by uncongested traffic and relatively large headways. Under such conditions, the following vehicle speed increases until the free-flow speed of the facility $u_f$ is reached. The model formulation is also inclusive of a condition that ensures that $u_f$ is never exceeded once achieved. The second argument of the model is attained when congestion prevails and speeds are constrained by the behavior of the vehicles ahead of them. Due to the collision avoidance mechanism it implements, the congested regime branch is the one responsible for making the Gipps model collision-free.

$$u_n(t+\Delta t) = min\left(\begin{array}{c} u_n(t) + 2.5.A_{max}^{des}.\Delta t\left(1-\frac{u_n(t)}{u_f}\right)\sqrt{0.025+\frac{u_n(t)}{u_f}} \\ D_{max}^{des}.\Delta t + \sqrt{\left(D_{max}^{des}.\Delta t\right)^2 - D_{max}^{des}\left[2(\Delta x - L_{n-1}) - \Delta t.u_n(t) - \frac{u_{n-1}^2(t)}{\widehat{D}_{n-1}}\right]} \end{array}\right) \quad \text{(VI.12)}$$

Where $A_{max}^{des}$ and $D_{max}^{des}$ are the respective desired maximum acceleration and deceleration of the following vehicle in m/s$^2$, and $\widehat{D}_{n-1}$ denote the maximum deceleration rate of the leading vehicle in m/s$^2$. Those three parameters are the ones requiring calibration for Gipps model.

### 6.3.3 Frietzsche Model

Frietzsche model [9] is a car-following model that shares the same structure as Wiedemann model. In this model, six threshold parameters are used to define five driving regimes. The thresholds are defined for four gap ($\Delta x$) values and two differences in speed ($\Delta v$) values between the leader and the follower vehicles. The four gap threshold parameters, *AR*, *AS*, *AD*, and *AB* are presented in Equations (VI.13- VI.16); while the two differences in speed thresholds, *PTP* and *PTN*, are given in Equations (17-18). The five different driving regimes are shown by Figure 17.b along with the acceleration rates assigned for each regime. We note that the expression of the acceleration rate $a_n$ associated with the "closing in" regime is given in Equation (VI.19- VI.20).

$$AR = s_{n-1} + T_r \times u_{n-1} \quad \text{(VI.13)}$$

$$AS = s_{n-1} + T_s \times u_n \quad \text{(VI.14)}$$

$$AD = s_{n-1} + T_d \times u_n \quad \text{(VI.15)}$$

$$AB = AR + \frac{\Delta u^2}{\Delta b_m} \quad \text{(VI.16)}$$

$$PTP = K_{PTP}(\Delta x - s_{n-1})^2 + f_x \quad \text{(VI.17)}$$

$$PTN = -K_{PTN}(\Delta x - s_{n-1})^2 - f_x \quad \text{(VI.18)}$$

$$a_n = \frac{u_{n-1}^2 - u_n^2}{2d_c} \quad \text{(VI.19)}$$

$$d_c = \Delta x - AR + u_{n-1}.\Delta t \quad \text{(VI.20)}$$

Where $T_r$, $T_s$, $T_D$ and $\Delta b_m$ are calibration parameters expressed in seconds. For the remainder of this study, $d_{max}$, $f_x$, $K_{ptp}$ and $K_{ptn}$ are set equal to -6 m/s$^2$, 0.5, 0.002 and 0.001.

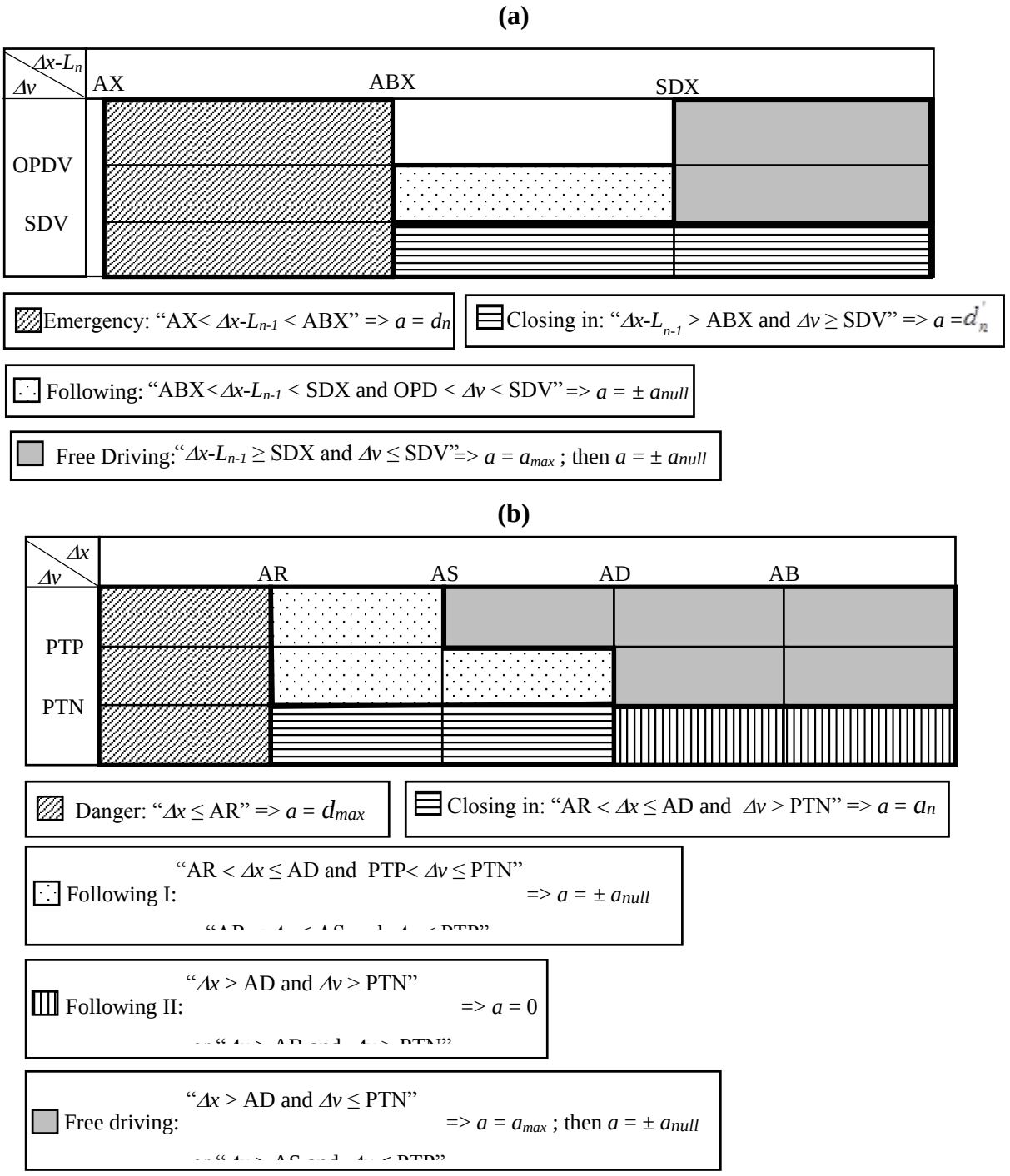


**Figure 17: Model structure of: a. Wiedemann model; b. Frietzsche model**

### 6.3.4 The Intelligent Driver Model

The IDM model [69] is a kinematics-based car-following model that is widely used for the simulation of freeway traffic. It was developed in 2000 by Treiber et al. [69] with the main objective of modeling the longitudinal motion of vehicles as realistically as possible under all traffic situations. The fame of this model is mainly due to its mathematical stability, which

results in stable vehicle trajectories and smooth acceleration profiles. The acceleration function of the intelligent driver model (IDM) car-following model is presented in Equations (VI.21-VI.22).

$$a_{n+1}(u_{n+1}, s_{n+1}, \Delta u_{n+1}) = a\left(1 - \left(\frac{u_{n+1}}{u_f}\right)^{\delta} - \left(\frac{s^*(u_{n+1}, \Delta u_{n+1})}{s_{n+1}}\right)^2\right) \quad \text{(VI.21)}$$

With

$$s^*(u_{n+1}, \Delta u_{n+1}) = s_j + u_{n+1}T + \frac{u_{n+1}\Delta u_{n+1}}{2\sqrt{a.\,b}} \quad \text{(VI.22)}$$

Where $s^*$ denotes the steady state spacing, $a$ is the maximum acceleration level, $b$ is the maximum deceleration level, $\delta$ is a calibration parameter and $T$ is the desired time headway.

### 6.3.5 Rakha-Pasumarthy-Adjerid Model

The RPA model [12] is a car-following model that controls the longitudinal motion of the vehicles in the INTEGRATION traffic simulation software [14, 15]. The model is composed of three main components: the steady-state, the collision avoidance and the vehicle dynamics models. Having the values of its three components, the RPA model computes the speed of the following vehicle as shown in Equation VI.23.

$$u_{n+1} = min(u_{n+1}^{VA}, u_{n+1}^{CA}, u_{n+1}^{DYN}) \quad \text{(VI.23)}$$

Here $u_{n+1}^{VA}$, $u_{n+1}^{CA}$and $u_{n+1}^{DYN}$ are the speeds calculated using the three modules described previously and which expressions are given in what follows.

#### *6.3.5.1 First-order Steady-state Car-following Model*

The RPA model utilizes the Van Aerde nonlinear functional form to control the steady-state behavior of traffic. The latter model was proposed by Van Aerde and Rakha [33] and is formulated as presented in Equation VI.24.

$$s_{n+1}^{VA} = c_1 + \frac{c_2}{u_f - u_{n+1}} + c_3 u_{n+1} \quad \text{(VI.24)}$$

Here $s_{n+1}^{VA}$ is the steady state spacing (in meters) between the leading and the following vehicles, $u_{n+1}$ is the speed of the follower, in (m/s), $u_f$ is the free-flow speed expressed in m/s, and $c_1$ (m), $c_2$ (m$^2$/s) and $c_3$ (s) are constants used for the Van Aerde steady-state model that have been shown to be directly related to the macroscopic parameters defining the fundamental diagram of the roadway.

Finally, it should be noted that from the perspective of car-following modeling, the main objective is to determine how the following vehicle responds to changes in the behavior of the leading vehicle. Subsequently, a speed formulation is adopted from the Van Aerde model, as demonstrated in Equation VI.25, which is easily derived from Equation VI.24 using basic mathematics.

$$u_{n+1}^{VA} = \frac{-c_1 + c_3 u_f + s_{n+1} - \sqrt{\left(c_1 - c_3 u_f - s_{n+1}\right)^2 - 4c_3\left(s_{n+1} u_f - c_1 u_f - c_2\right)}}{2c_3} \quad \text{(VI.25)}$$

### *6.3.5.2 Collision Avoidance Model*

The expression of the collision avoidance term is shown in Equation VI.26 and is directly related to a simple derivation of the maximum distance that a vehicle can travel to decelerate from its initial speed to the speed of the vehicle ahead of it while ensuring that, in the case of a complete stop, the jam density spacing between the two vehicles is respected.

$$u_{n+1}^{CA} = \sqrt{(u_{n+1})^2 + 2b\left(s_{n+1} - s_j\right)} \quad \text{(VI.26)}$$

Here $b$ is the maximum deceleration at which the vehicles are allowed to decelerate and $s_j$ is the spacing at jam density.

### *6.3.5.3 Vehicle Dynamics Model*

The final component of the RPA model is the vehicle dynamics model [16, 34] that ensures that the vehicle's mechanical capabilities do not limit it from attaining the speeds that are dictated by the steady-state component. This model computes the typical acceleration of the following vehicle as the ratio of the resultant force to the vehicle mass $M$ (Equation VI.27). The resultant force is computed as the difference between the tractive force acting on the following vehicle $F_{n+1}$ (Equation VI.28) and the sum of the resistive forces acting on the vehicle which include the aerodynamics, rolling and grade resistances.

$$a_{n+1}^{DYN} = \frac{F_{n+1} - \left(0.5\rho C_d C_h A_f g u_{n+1}^2 + MgC_{r0}(C_{r1} u_{n+1} + C_{r2}) + MgG\right)}{M} \quad \text{(VI.27)}$$

With

$$F_{n+1} = \min\left(3600\eta \frac{\gamma P}{u_{n+1}}, M_{ta} g\mu\right) \quad \text{(VI.28)}$$

Here $\eta$ is the driveline efficiency (unitless); $P$ is the vehicle power (kW); $M_{ta}$ is the mass of the vehicle on the tractive axle (kg); $\gamma$ is the vehicle throttle level (taken as the percentage of the maximum observed throttle level that a certain driver uses); $g$ is the gravitational acceleration (9.8067 m/s$^2$); $\mu$ is the coefficient of road adhesion or the coefficient of friction (unitless); $\rho$ is the air density at sea level and a temperature of 15°C (1.2256 kg/m$^3$); $C_d$ is the vehicle drag coefficient (unitless), typically 0.30; $C_h$ is the altitude correction factor equal to 1-0.000085$h$, where $h$ is the altitude in meters (unitless); $A_f$ is the vehicle frontal area (m$^2$), typically 0.85 multiplied by the height and width of the vehicle; $C_{r0}$ is a rolling resistance constant that varies as a function of the pavement type and condition (unitless); $C_{r1}$ is the second rolling resistance constant (h/km); $C_{r2}$ is the third rolling resistance constant (unitless); $m$ is the total vehicle mass (kg); and $G$ is the roadway grade (unitless).

The acceleration computed using the dynamics model is then used to calculate the maximum feasible speed $u_{n+1}^{DYN}$ using a first Euler approximation.

### 6.3.6 Fadhloun-Rakha Model

The Fadhloun-Rakha (FR) model [18] is an acceleration-based car-following model that uses the same steady-state formulation and respects the same vehicle dynamics as the RPA model. Additionally, the model uses very similar collision-avoidance strategies to ensure a safe following distance between vehicles.

The mathematical expression of the FR model, presented in Equation VI.29, estimates the acceleration of the following vehicle as the sum of two terms. The first term models the vehicle behavior in the acceleration regime, while the second governs the deceleration regime.

$$a_{n+1} = F \times a_{n+1}^{DYN} + CA(u_{n+1}, s_{n+1}, \Delta u_{n+1}) \quad \text{(VI.29)}$$

In the acceleration regime, the vehicle behavior is governed by the vehicle dynamics, as demonstrated in Equation VI.27 to ensure that vehicle accelerations are realistic. A reducing multiplier *F* (Equation VI.30), which ranges between 0.0 and 1.0, is then applied to the vehicle dynamics acceleration. The *F* factor is a function that is sensitive to $X_{n+1}$ (Equation VI.31) which represents the ratio of $u_{n+1}/s_{n+1}$ divided by the ratio of the steady state speed to the steady state spacing $u_{n+1}^{VA}/s_{n+1}^{VA}$. It aims to guarantee that two objectives are met. First, it ensures the convergence of the vehicles' behavior towards the Van Aerde steady state model. Second, it attempts to model human behavior and the different patterns of driving by acting as a reduction factor to the vehicle dynamics model.

$$F(X_{n+1}) = e^{-aX_{n+1}}\left(1 - X_{n+1}^{b} e^{b(1-X_n+1)}\right)^{d} \quad \text{(VI.30)}$$

$$X_{n+1} = \frac{s_{n+1}^{VA}}{s_{n+1}} \cdot \frac{u_{n+1}}{u_{n+1}^{VA}} \quad \text{(VI.31)}$$

Where *a*, *b*, and *d* are model parameters that are calibrated to a specific driver and model the driver input to the gas pedal.

The second term in the expression of the FR model considers vehicle deceleration to avoid a collision with a slower traveling lead vehicle as shown in Equations (VI.32- VI.33). As shown, collision avoidance is ensured by the function *CA* which computes the needed deceleration to apply as the ratio of the square of the kinematics deceleration needed to decelerate from the current speed to the leading vehicle speed at a desired deceleration level that is set by the user.

$$d_{kinematics} = \frac{\left[u_{n+1}^2 - u_n^2 + \sqrt{(u_{n+1}^2 - u_n^2)^2}\right]}{4\left(s_{n+1} - s_j\right)} \quad \text{(VI.32)}$$

$$CA(u_{n+1}, s_{n+1}, \Delta u_{n+1}) = \frac{d_{kinematics}^2}{(d_{desired} + gG)} \quad \text{(VI.33)}$$

Where $d_{des}$ is the desired deceleration level.

Finally, to model the effect of the driver error in estimating the leading vehicle speed and the distance gap between the two vehicles, two wiener processes are incorporated in the model formulation at the level of $u_n$ *and* $s_{n+1}$. Additionally, a white noise signal is added to the model's expression to capture the driver's imperfection while applying the gas pedal. The compounding effect of those three signals makes the model output more representative of human driving behavior.

## 6.4 NATURALISTIC DATASET

The data used herein represents a small subset that was extracted from the naturalistic driving database generated by the 100-Car study [68] that was conducted by the Virginia Tech Transportation Institute (VTTI) in 2002. In fact, VTTI initiated a study where 100 cars were instrumented and driven by a total of 108 drivers around the District of Columbia (DC) area. The resulting database from the 100-Car study [68] contained detailed logs of more than 207,000 completed trips with a total duration of around 20 million minutes of data.

The naturalistic dataset that was used to validate the proposed model contains information relating to 1,659 car-following events which spans over a duration of around 13

hours which is significant for the task of validation of car-following models. The car-following data composing the dataset comes from six different drivers and was collected on a relatively short segment of the Dulles Airport access road (approximately an 8-mile long section) in order to maintain facility homogeneity.

Finally, it is noteworthy to state that both the characteristics of the different vehicles are known due to the naturalistic nature of the dataset. This makes the determination of the different FR and RPA model variables straightforward and exclusive of bias.

## 6.5 PARAMETER CALIBRATION OF THE STUDIED MODELS

For each of the studied models, a certain number of inputs is needed. These inputs can be categorized into two groups. The first category comprises the inputs that are the same for the different models, namely the time-space and the time-speed profiles of the leading vehicle, the starting location and speed of the following vehicle as well as the free-flow speed ($u_f$) which was estimated specifically for each car-following event along with any other variables related to the roadway. The use of the free-flow speed distribution shown in Figure 18.a, instead of a constant value across all of the events, is justified by the significant heterogeneity of the driver behavior during the free driving phase. In fact, drivers do not necessarily drive at the speed limit of the facility when there is no vehicle ahead of them. Besides that, the desired speed of a certain naturalistic event was set equally across all of the studied models in order to maintain the homogeneity of driver behavior and road facility for that specific event. As a side remark, we note that the jam density $k_j$, the capacity $q_c$ and the speed-at-capacity $u_c$, which are needed to generate a simulated trajectory in the case of the formulations of the RPA model and the FR model, were estimated using the calibration procedure proposed by Rakha and Arafeh [54]. However, unlike the free-flow speed, those parameters were calibrated using the bulk data of each driver given their minor influence on the resulting model outputs. The estimated values for the latter driver-specific parameters are presented in Table 14 along with the needed vehicle-specific parameter values in Table 15.

**Table 14: Values of $k_j$, $q_c$ and $u_c$ for each driver**

| Driver | $k_j$ (veh/m) | $q_c$ (veh/s) | $u_c$ (m/s) |
|---|---|---|---|
| **Driver_124** | 0.091 | 0.865 | 22.22 |
| **Driver_304** | 0.150 | 0.833 | 19.00 |
| **Driver_316** | 0.075 | 0.464 | 21.36 |
| **Driver_350** | 0.080 | 0.529 | 21.28 |
| **Driver_358** | 0.087 | 0.447 | 19.53 |
| **Driver_363** | 0.131 | 0.906 | 23.69 |

**Table 15: Characteristics of the different vehicles**

| | *Vehicle Characteristics* | | | |
|---|---|---|---|---|
| **Driver** | ***P (kW)*** | ***M (kg)*** | $C_d$ | $A_f$ ($m^2$) |
| **Driver_124** | 90 | 1190 | 0.36 | 2.06 |
| **Driver_304** | 90 | 1090 | 0.40 | 2.00 |
| **Driver_316** | 90 | 1090 | 0.40 | 2.00 |
| **Driver_350** | 90 | 1090 | 0.40 | 2.00 |
| **Driver_358** | 145 | 1375 | 0.40 | 2.18 |
| **Driver_363** | 145 | 1375 | 0.40 | 2.18 |

The remaining input variables consist of model-specific parameters that require calibration. Since this study aims to validate a new car-following model by comparing its performance to that of other state-of-the-art models, the different parameters need to be calibrated such that the resulting simulated behavior of the following vehicle matches its observed behavior as closely as possible. The calibration procedure of the different parameters of each model was conducted heuristically taking the speed RMSE as the error objective function. The choice to optimize each model with regards to the speed RMSE is judged reasonable given that the optimization operation was done on an event-by-event basis. In fact, we opted to calibrate each model separately for each car-following event rather than for the dataset as a whole. Even though that increased the computation time exponentially, a more fair comparison between the results is made possible as each model was allowed to propose its best possible fit for each of the 1659 naturalistic events. Hence, the different model outputs are incorporative of the effect of the strength points of each model.

Finally, given the presence of noise in the proposed model, the calibration was conducted using a bi-level procedure. First, the model parameters were calibrated deterministically without the consideration of the noise signals. Next, to model the effect of the

noise, the optimized parameters of the first step were used to run a total of 1000 simulations in order to have valid model outputs and to determine the 95% confidence interval of the results.

## 6.6 RESULTS AND MODEL VALIDATION

Having access to the calibrated parameters, the speed profiles were obtained for each car-following event of the naturalistic dataset. The corresponding speed outputs ensure a minimal RMSE between a model's predictions and the measured data over its whole timespan. To illustrate the results, the probability distribution of the speed RMSE of the different models is plotted in Figure 18.b. The figure demonstrates that the FR model performs better overall in terms of fitting the observed data than the other models. That is demonstrated by the fact that its RMSE distribution is higher than those of the other models towards the lower end of the speed errors (between 0 and 0.5). Then, as the RMSE keeps getting bigger and bigger, the tendency is reversed and the RMSE distribution of the FR model becomes the smallest.

(a) (b)

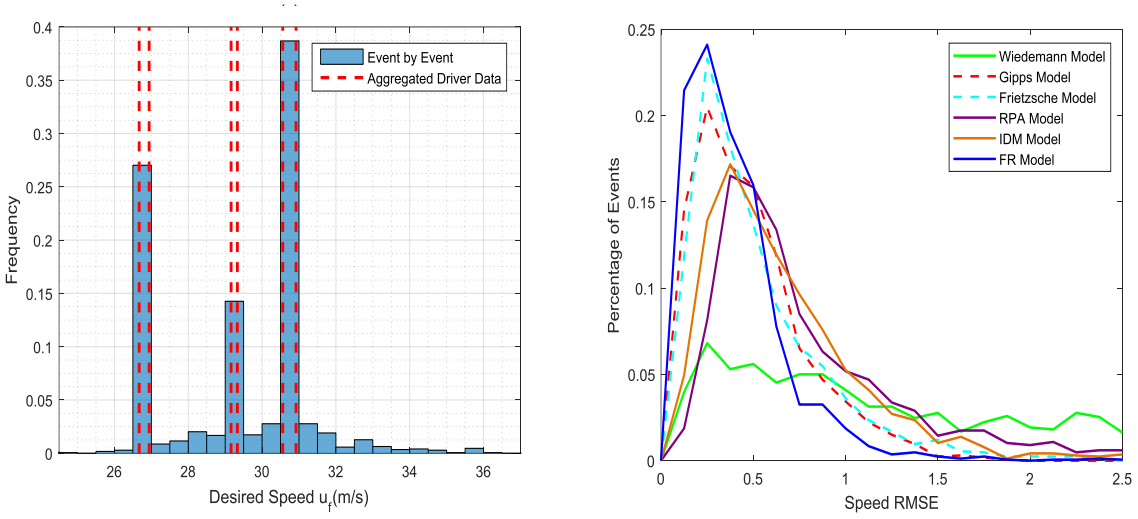


**Figure 18: a. Distribution of the free-flow speed for the naturalistic events; b. Probability distribution of the speed RMSE for the different models**

To better quantify statistically the difference in performance between the proposed model and the other five models, the rank of the new model was determined for each event based on the calculated RMSE value (the resulting mean of the 1000 trials). The ranking was sorted in an increasing direction of the RMSE value with the best model being the one offering the lowest error. Table 16 shows the results of this analysis where the rank distribution of the proposed model is presented. From the table, one can see that the FR model outperformed the other ones. In fact, this model offered the best fit to the empirical data for about half of the

considered events (735 out of 1659 events). Furthermore, the number of events for which the fit of the proposed model was in either the first or the second position, represents about two thirds of the total cases (1126 out of 1659 events).

The quantitative analysis was taken a step further as the proposed model was compared face-to-face with each of the studied models. That would allow for a better understanding of the new model's performance. Figure 19.a and Figure 19.b present the results of this comparison in terms of the optimized speed RMSE and the one computed from the resulting acceleration profiles, respectively. In terms of speed error, the FR model is demonstrated to significantly outperform the other models. In fact, its speed RMSE was smaller than that found using the RPA, Gipps, Wiedemann, Frietzsche, and the IDM models in 65% to 90% of the events. The previous stated values do not confer enough information about the new model performance by themselves as they do not quantify the percentages by which the error function was reduced. Consequently, the bar chart of Figure 19 is complemented by Table 17 which presents key measures (mean, median and standard deviation) about the distribution of the relative percentage decrease in the speed RMSE. For instance, it is found that for 90% of the total events for which the proposed model formulation outperformed the Wiedemann model, the error reduction percentage had a median equal to 85%. In the case of the RPA model, the FR model resulted in an average decrease of the RMSE that is around 56% for the 88% of the events for which it was the best.

When considering face-to-face comparisons in terms of the resulting acceleration data from the optimized speed profiles, only the Wiedemann and the IDM model outperformed the FR model as it can be observed in Figure 19.b. While the IDM model is known for its excellent fit to acceleration data due to its smooth expression, the results of the Wiedemann model seem intriguing at first. In fact, it is found that the results are justified by the structure of the Wiedemann model itself as it will be described later.

**Table 16: Rank of the FR model in terms of goodness of fit as a percentage of the total number of events using the speed RMSE**

| Rank | Rank Distribution (%) |
|---|---|
| **1** | 44.30 |
| **2** | 23.57 |
| **3** | 16.88 |
| **4** | 11.63 |
| **5** | 3.32 |
| **6** | 0.30 |

**Table 17: Distribution characteristics of the decrease in the speed RMSE for head-to-head comparisons**

| | Best Model | Mean | Median | Standard Deviation |
|---|---|---|---|---|
| **RPA Model** | FR Model | 56.33 | 58.68 | 23.76 |
| **Gipps Model** | | 45.43 | 46.97 | 22.45 |
| **Wiedemann Model** | | 77.02 | 85.72 | 20.96 |
| **Frietzsche Model** | | 45.65 | 46.91 | 22.78 |
| **IDM Model** | | 50.51 | 53.46 | 21.50 |
| | | | | |
| **RPA Model** | RPA Model | 26.62 | 22.76 | 18.76 |
| **Gipps Model** | Gipps Model | 43.25 | 45.66 | 23.33 |
| **Wiedemann Model** | Wiedemann Model | 43.94 | 45.49 | 24.41 |
| **Frietzsche Model** | Frietzsche Model | 35.97 | 35.87 | 22.10 |
| **IDM Model** | IDM Model | 30.36 | 27.54 | 20.87 |

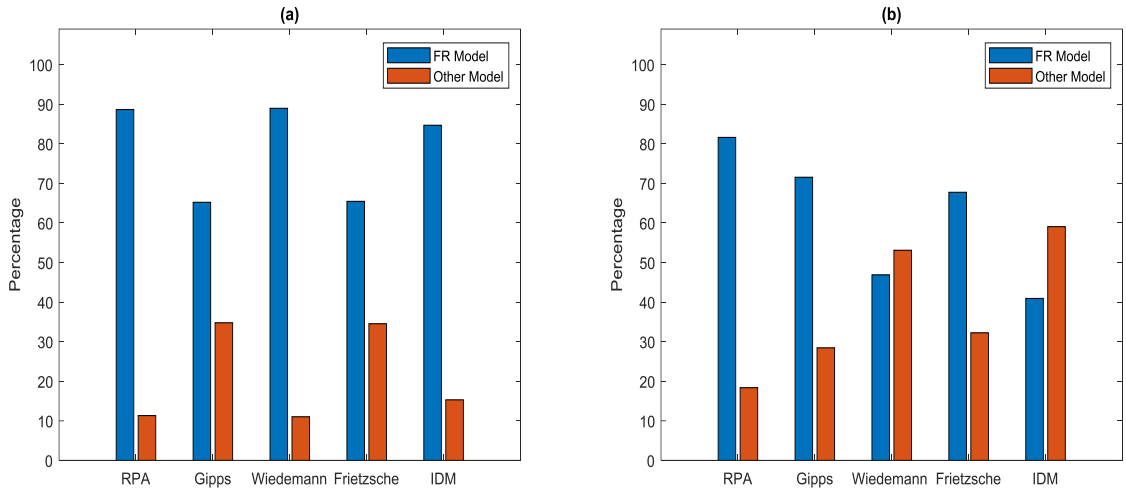


**Figure 19: Comparison of the proposed FR model formulation performance to the performance of the other models: a. Based on the speed RMSE; b. Based on the acceleration RMSE**

In order to examine the performance of the different models qualitatively, the resulting simulated speeds are presented for some sample events. Figure 20 plots the variation of the observed and simulated speed profiles for four different events over time. For each subplot (Figure 20.a through Figure 20.d), the results from the studied models are drawn in order to compare their predictions with the observed naturalistic behavior. For example, for the event presented in Figure 20.a, the driver accelerated from about 85 km/h to around 94 km/h, maintained his/her speed around that value, then re-accelerated to about 97 km/h and tried to maintain that speed until the end of the event. This behavior was well captured by most of the studied models, except that at the end of the event all models predicted a decrease in speed. This is mainly due to the fact that all the studied models take into account a minimum safe distance in order to avoid collision with the leading vehicle. Given that the collision avoidance logics of the models judged that the spacing maintained by the driver is unsafe for such high speeds, a decrease in speed was predicted to keep a safe distance and to ensure that the collision avoidance conditions are met. That opposes the actual driver behavior who maintained his/her driving speed despite being unsafely close to the leading vehicle. Looking roughly into this event, it is the FR model that traces better the actual driver behavior, followed by the IDM model, then Gipps, the RPA and Frietzsche models, and lastly Wiedemann model.

It is worth clarifying at this level the reasons behind the steep decrease in speed observed in the output of the Wiedemann model. The observed speed drop, which occurs 30 seconds after the start of the event, is due to the nomenclature of Wiedemann model itself. In fact, similar data cliffs were found to be present in a noticeable number of other events for this

model. Such behaviors result from the abrupt change in the acceleration value when transitioning from one traffic regime to another. Besides the latter aspect, the crossing of one of the boundaries delimiting the different regions of the Wiedemann model was found to result in another disparity in the model output when compared to most of the other models (FR, RPA, Gipps, IDM). The concerned disparity is observed when the following vehicle remains in the same traffic region for the entire duration of the car-following event, hence arising the possibility of having a constant acceleration over the entire duration of the car-following maneuver. The previous two drawbacks are also manifested in the Frietzsche model due to its similar structure, however their presence is not as prevalent. For instance, one such case in which the following vehicle remained within the same traffic regime for Frietzsche model is shown in Figure 20.c. The figure illustrates a scenario in which the driver was trying to maintain his/her desired speed of 100 km/h with minor fluctuations. Since the vehicle started and finished its trip within the "Free Driving" regime, the Frietzsche model resulted in a constant speed profile for the entire event. However, the latter aspects of Frietzsche and Wiedemann models do not necessarily connote an inability to propose a fitted speed that matches empirical data. As a matter of fact, while all the models captured the empirical behavior of the event presented in Figure 20.b, the Frietzsche model was the best in terms of tracing the actual speed profile. All other models slightly over-predicted the maximum reached speed.

Finally, concerning the event described by Figure 20.d, the speed profile suggests that the highway is heavily congested. The driver decelerated from about 32 km/h to come to an almost complete stop for a few seconds. This was followed by an oscillatory behavior due to a succession of accelerations and decelerations. Despite the repeating oscillations, the FR model traced almost perfectly the driver behavior for the entire timespan. The RPA model gave reasonable predictions for this event as well. Overall, as a qualitative measure, the different events presented in the figure are consistent with the goodness of fit results presented earlier. The Gipps model along with the FR and RPA model appear to capture the naturalistic data considerably well.

Next, the acceleration profiles derived from the calibrated speed data were examined. For illustration purposes, a sample event was chosen to visualize and compare the simulated acceleration profiles to empirical data. The different profiles are presented in Figure 21. For clarity of the figure as the overlap between the outputs of the studied models is significant, the results are presented in each sub-figure (Figure 21.a through Figure 21.f) along with the observed acceleration of the driver. During this 2-minute car-following event, the driver had

acceleration and deceleration maneuvers with maximum values of 1.6 $m/s^2$ and 2.1 $m/s^2$, respectively. As shown by Figure 21.a, the Wiedemann model results in a zero constant acceleration mainly because the modeled vehicle behavior remained within the boundaries of one of the traffic regimes for the total event duration.

More importantly, the illustrated constant acceleration behavior of the Wiedemann model, which was confirmed across several other car-following events, gives a plausible explanation of the extremely low values found when the RMSEs related to the acceleration data were computed. By avoiding the oscillatory behavior of the other models and, more importantly, staying within the maximum acceleration and deceleration values without overshooting, a constant acceleration profile would result in a better fit to the empirical behavior in terms of the RMSE value. Setting aside the car-following events with a constant simulated acceleration, the Wiedemann model resulted in a stepped acceleration profile similar to the acceleration-time diagram of the Frietzsche model plotted in Figure 21.b. As for Gipps model, the FR model and the RPA model (Figure 21.c, Figure 21.d, and Figure 21.e, respectively), they resulted in acceleration values that closely followed the field data even though the maximum predicted deceleration was relatively overestimated. More precisely, the IDM model traced the actual acceleration profile the best for this specific event followed by the FR model formulation. Generally speaking, the new model was found to be the best in terms of mimicking the real driver behavior as it successfully avoided the acceleration fluctuations produced by the other models that are far in excess of those observed at the level of the empirical data. Even more, the significance and contribution of the latter finding is further amplified given the fact that the FR model formulation is inclusive of three noise signals. Those noises attempt to account for the driver's errors related to estimating the model input variables — the distance gap to the leading vehicle along with its speed — as well as his/her imperfection while applying the gas pedal. Notwithstanding the fact that the other models are exclusive of such errors giving them a statistical edge, their predicted acceleration profiles were still outperformed by the acceleration predictions of the FR model except for the IDM model which provides comparable results.

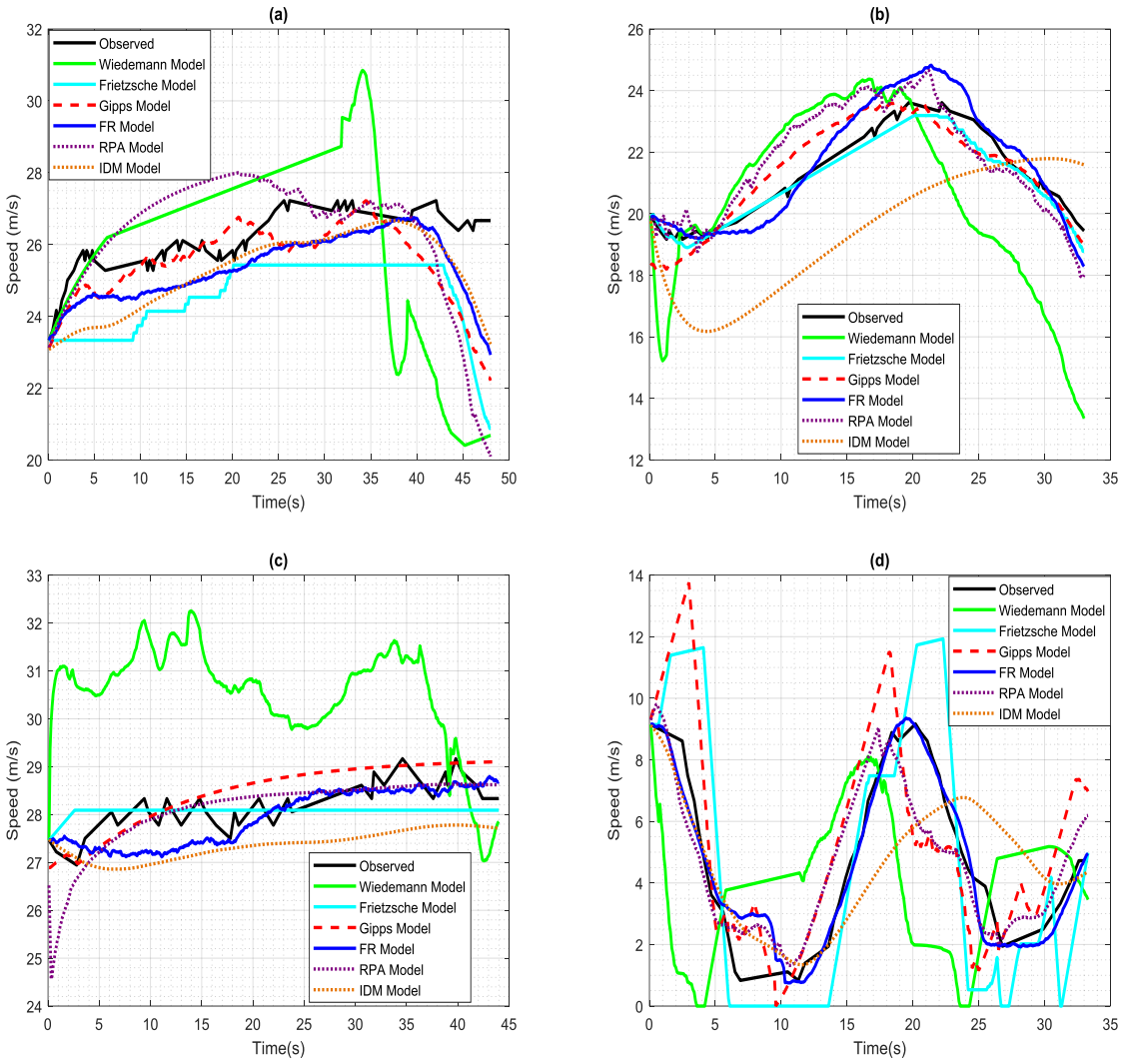


**Figure 20: Variation of the simulated speeds over time of four sample events**

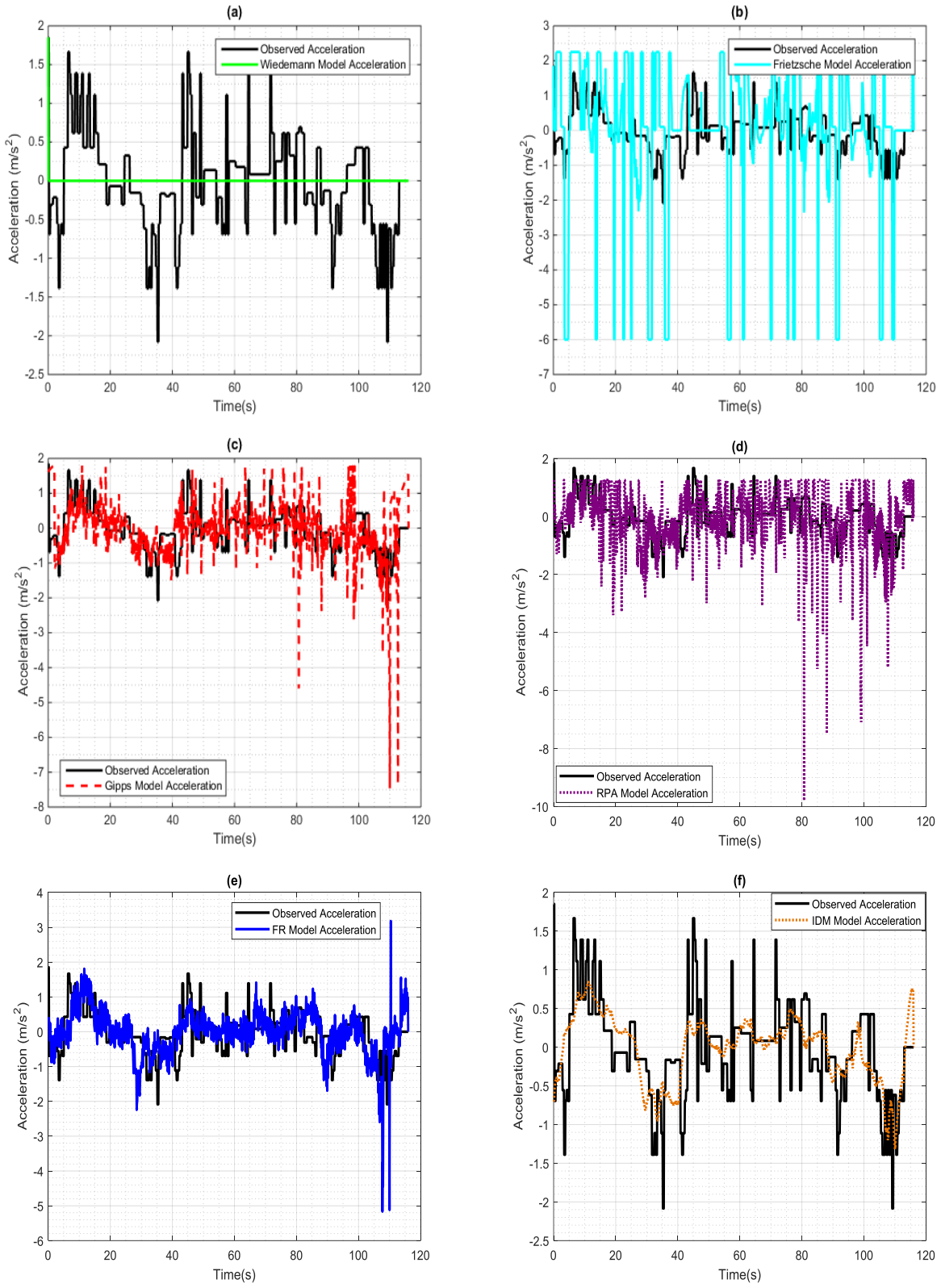


**Figure 21: Variation of the simulated acceleration over time of a sample car-following event: a. Wiedemann model; b. Frietzsche model; c. Gipps model; d. RPA model; e. FR model; f. IDM Model.**

From a traffic researcher standpoint, acceleration data can be cast as the most important output of a car-following model. In fact, acceleration information is the starting point for the computation of other measures of effectiveness (MOEs). Two specific MOEs that are very sensitive to the accuracy of predicted accelerations and quite important from an environmental perspective, are fuel consumption and emissions estimations. With that in mind, it seemed necessary to examine the behavior of the maximum acceleration distribution of the bulk dataset given its major impact on any fuel consumption or emissions calculation.

Subsequently, the observed and predicted maximum acceleration of each model were extracted for each event and plotted as shown in Figure 22. We note here that the maximum acceleration data is sorted from the highest value to the lowest for each model independently of the others. This means that the event numbered as one, for example, in the figure is not the same physical event for all the studied models or that calculated from the measured speed data. It is just the physical event that resulted in the highest maximum observed or modeled acceleration. In other words, the figure does not allow making event-by-event comparisons between the different models. The main purpose of the plot is to compare the empirical maximum acceleration distribution of the whole dataset to the ones resulting from the calibration of the different studied models.

As a side note, since 1000 simulations were run using the logic of the FR model to estimate the mean and the dispersion of the results, the simulated maximum acceleration using the new model formulation is plotted using the mean and the 95% confidence interval of the data which is shown by the light bounded area in Figure 22. Qualitatively speaking, the figure demonstrates the superiority of the FR model in terms of its ability of replicating the maximum acceleration behavior of the naturalistic dataset. In fact, the observed data appears to be successfully covered by the breadth of the 95% confidence interval of the model output.

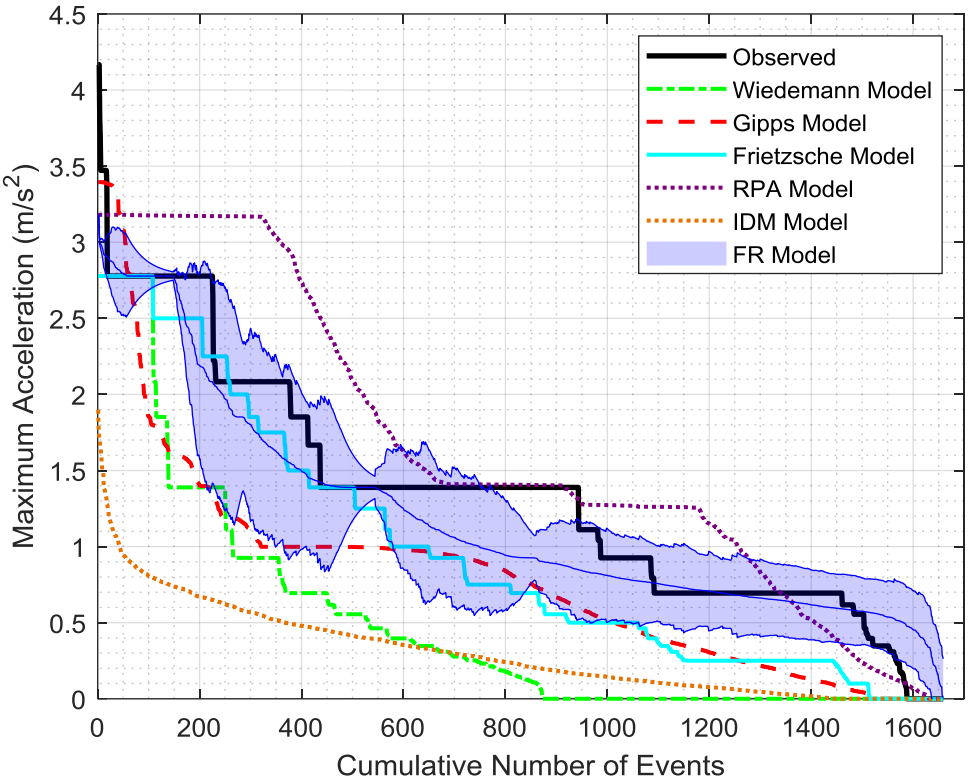


**Figure 22: Comparison of the maximum acceleration behavior of the naturalistic dataset to the outputs of the different models**

## 6.7 CONCLUSIONS AND FUTURE WORK

This research effort investigates and validates the statistical performance of the FR car-following model using naturalistic driving data from the 100-Car study. The validated model is an acceleration-based alternative formulation of the RPA model. In fact, the two models share the same steady state model, respect the same vehicle dynamics and use different, but very similar, collision-avoidance strategies to ensure a safe following distance between cars.

The considered naturalistic data of six drivers was used to calibrate the FR model along with five state-of-the-art car-following models, and a comparative analysis between the resulting model performances was conducted. By doing so, this study demonstrates that the FR model outperforms Gipps, Wiedemann, Frietzsche, the RPA and the IDM models in terms of statistically matching the empirical data on an event-by-event basis.

While the RMSE, used herein, is a good indicator to evaluate a car-following model from a statistical perspective, it is not generally enough to confirm that it would be the best with regards to every aspect of traffic engineering. In fact, the only solid conclusion that can be deducted from this study is that the FR model is the most flexible when compared to the

other ones in terms of its ability to generate a speed profile for the following vehicle that emulates empirical data such that the resulting error is at its minimum. Whether the FR model formulation would offer the best fit when considering other indicators, such as fuel consumption or emissions rates, is a completely separate problem that needs to be investigated before conclusions can be made.

## 6.8 ACKNOWLEDGMENTS

The authors acknowledge the financial support provided by the University Mobility and Equity Center (UMEC) and the Department of Energy through the Office of Energy Efficiency and Renewable Energy (EERE), Vehicle Technologies Office, Energy Efficient Mobility Systems Program under award number DE-EE0008209.

## 6.9 AUTHOR CONTRIBUTION STATEMENT

The authors confirm contributions to the paper as follows: study conception and design: Fadhloun, Loulizi and Rakha; data reduction: Fadhloun and Wang; model calibration; Fadhloun and Rakha; analysis and interpretation of results: Fadhloun, Loulizi, Wang and Rakha; draft manuscript preparation: Fadhloun, Loulizi, Wang and Rakha. All authors reviewed the results and approved the final version of the manuscript.

# Chapter 7 Car-Following Model Impacts On Light-Duty Vehicle Fuel Consumption Estimation

**Authors:**

Karim Fadhloun

Amara Loulizi, Ph.D, P.E.

Hesham Rakha, Ph.D, P.Eng.

## 7.1 ABSTRACT

This paper studies the effect of car-following predicted trajectories on light-duty vehicle fuel consumption estimates. The analysis is based on empirical naturalistic data collected on a 13-km section of the Dulles airport access road. The empirical data includes the instantaneous speed of the following and lead vehicles as well as the spacing between them. This data was collected for several events capturing congested and free-flow traffic conditions. In total 1180 events were used in this study. The empirical data are used with four car-following models to predict the trajectory of the following vehicle. The models considered in the study are the Wiedemann, Fritzsche, Gipps, and Fadhloun-Rakha models. The Virginia Tech Comprehensive Power-Based Fuel Consumption Model is used to estimate the fuel consumed by ten different gasoline cars. The same procedure is then used with the car-following model generated trajectories. In general, a significant difference between the observed fuel consumption and the simulated estimates are found. This difference is mainly caused by the variation in predicted speed profiles that leads to different acceleration behaviors. The maximum difference between observed and predicted consumed fuel reached 70% for some models, but the median never exceeded 30%. The newly developed Fadhloun-Rakha model showed very promising results in terms of estimating fuel consumption since its maximum error, for all considered events and all selected cars, never exceeded 25% with a median error less than 8%.

## 7.2 INTRODUCTION

With recent advances in computers' performances, road traffic micro-simulation tools are being increasingly developed and more and more used around the world. These tools simulate the longitudinal movements of individual vehicles in a given road network based mainly on

developed car-following and crash-avoidance rules. Micro-simulation software packages are becoming increasingly popular for evaluating geometric designs (layouts of interchange systems, geometry of roundabouts, etc.), traffic control devices (traffic light cycle lengths and phasing for instance), traffic management measures (ramp metering and toll plaza for examples), and many other traffic systems. The evaluation is usually based on estimated measure of effectiveness (MOE) such as average and total travel times, average and total delays, average travel speed, quantities of consumed fuel and emitted pollutants, and predicted number of accidents. Therefore, a good estimate of these MOEs is essential in order to have reliable and objective evaluations.

Estimations of the MOEs are mainly based on models that uses parameters from the simulated movements of the vehicles (such as speed and acceleration), road characteristics and geometry (such as roughness, friction, and grade), vehicle properties (such as engine type, number of cylinders, and engine displacement), and other factors. Hence, if it assumed that different micro-simulation software use the same models to estimate MOEs and use the same vehicles' properties and road characteristics and geometry, differences in the MOEs estimates would be only due to differences in vehicle trajectories simulated by their used car-following models. It is therefore interesting to quantify the effect of different car-following models on estimated MOEs, which is the main objective of this paper with the "fuel consumption" as the considered MOE.

Car-following models predict the position of a given vehicle with respect to the preceding one in the same lane given the trajectory of the leading vehicle. Different types of car-following models have been developed since the 1950s. As stated by Janson and Tapani [6], three groups are used, in general, to classify car-following models depending on the used reasoning for formulating the equations governing the output of the trajectory of the follower. These groups are: (1) the Gazis-Herman-Rothery models, which logic is based on the fact that the acceleration of the following vehicle is proportional to the speed of the leading vehicle, the difference in speed between the leading and following vehicles, and the space headway; (2) the safety-distance models which logic dictates a safe distance between the following and leading vehicle; and (3) the psycho-physical models which use some type of thresholds to define different regime regions for the following vehicle. In this study, 3 existing car-following models and a new model developed recently by Fadhloun and Rakha (FR) [18] were used to evaluate the effect of the different models' predicted trajectory of the following car on its estimated consumed fuel. This was achieved by using real collected trajectory events of a

following vehicle and the fuel consumed during these observed events was estimated. Then using the collected data of the leading vehicle, the trajectory of the follower was predicted, for all the events and for all studied car-following models. The fuel consumed during the simulated events was consequently calculated. A comparison was then performed using the distribution of the variable "absolute percentage difference between consumed fuel for the observed event and that obtained for the simulated one".

This paper is organized as follows. First, a brief description of the Virginia Tech Comprehensive Power-based Fuel Consumption Model is provided, as this model was used for calculating the fuel consumed during the observed vehicle trajectory events and that based on the simulated ones. The collected naturalistic data and the used gasoline vehicles are then described. Subsequently, only a brief description of the new FR car-following model is presented since the other three studied models are well-known and are described in many existing publications. Finally, the findings of the study and their interpretations are presented followed by the conclusions of the paper.

## 7.3 VIRGINIA TECH COMPREHENSIVE POWER-BASED FUEL CONSUMPTION MODEL

The Virginia Tech Comprehensive Power-Based Fuel Consumption Model (VT-CPFM) uses the Environmental Protection Agency (EPA) city and highway fuel economy ratings and publicly available vehicle characteristics to obtain calibration parameters for any type of vehicle. These calibration parameters are then used with calculated instantaneous vehicle power to estimate the instantaneous fuel consumption rate. The model has been proved to generate realistic and reliable fuel consumption predictions. In this model, the instantaneous power of the vehicle in kW, *P(t)*, is found based on calculated instantaneous resultant resistive force in N (*R(t)*), instantaneous acceleration in m/s$^2$ (*a(t)*), and instantaneous speed in km/h (*v(t)*), as shown in Equation VII.1.

$$P(t) = \left( \frac{R(t) + 1.04ma(t)}{3600\eta_d} \right) v(t) \qquad \text{(VII.1)}$$

Where $m$ is the mass of the vehicle in kg and $\eta_d$ is its driveline efficiency. The resultant resistive force on the vehicle is computed as the sum of the aerodynamic ($R_a$), rolling ($R_{rl}$), and grade resistance ($R_G$) forces as expressed in Equation VII.2. In this equation, $\rho$ is the density of air at sea level at a temperature of 15 °C, $C_d$ is the vehicle drag coefficient (unitless); $C_h$ is a correction factor for altitude (unitless) and computed as (1–0.085H) where H is the altitude

in km; $A_f$ is the vehicle frontal area in $m^2$; $C_r$, $c_1$, and $c_2$ are rolling resistance parameters that vary as a function of the road surface type, road condition, and vehicle tire type; and $G(t)$ is the instantaneous road vertical grade in m/m.

$$\begin{cases} R(t) = R_a + R_{rl} + R_G \\ R_a = \dfrac{\rho}{25.92} C_d C_h A_f v(t)^2 \\ R_{rl} = 9.81m \dfrac{C_r}{1000}\left(c_1 v(t) + c_2\right) \\ R_G = 9.81mG(t) \end{cases} \quad \text{(VII.2)}$$

The instantaneous fuel consumption rate in L/s, $FC(t)$, is calculated as shown in Equation VII.3. The $\alpha_0$, $\alpha_1$ and $\alpha_2$ are the vehicle-dependent model parameters.

$$FC(t) = \begin{cases} a_0 + a_1 P(t) + a_2 P(t)^2; & P(t) \geq 0 \\ a_0; & P(t) < 0 \end{cases} \quad \text{(VII.3)}$$

Since the objective of this study is to evaluate the effect of predicted car-following models trajectories on estimated fuel consumption, the rolling resistance parameters, $C_r$, $c_1$, and $c_2$ were assumed to be constants and were set equal to 1.75, 0.0328, and 4.575, respectively. The road grade was also assumed to be constant and was set equal to 0 (leveled road). A constant air density of 1.2256 $kg/m^3$ was also used. The mass, drag coefficient, and frontal area of the different studied vehicles were obtained from the manufacturers' published data with the frontal area taken as 0.85 times the product of the width and height of the vehicle.

The fuel consumed per event was calculated numerically. Specifically, for each event, the instantaneous speed data were used to calculate the corresponding acceleration. With the speed data and vehicle properties, all resistive forces could be calculated and using Equation VII.1, the instantaneous power is computed every second. The fuel consumption rate is then computed every second. The total fuel quantity ($FQ$) consumed per event is found using Equation VII.4.

$$FQ = \sum_{i=1}^{N} FC_i \times \Delta t \quad \text{(VII.4)}$$

Where $N$ is such that the time span of the event, $T$, is equal to $N \times \Delta t$ ($\Delta t$ is equal to 1 s).

## 7.4 COLLECTED NATURALISTIC DATA AND STUDIED GAZOLINE VEHICLES

Recent technological development in terms of data acquisition and its storage made the collection of naturalistic driving data feasible. In 2002, the Virginia Tech Transportation Institute (VTTI) initiated a study where 100 cars were instrumented and were driven by designated drivers around the Washington, DC area. By the end of the study, a database was developed from the 207,000 trips completed by the 108 drivers involved in the study. The latter number translates into 337,000 hours of data and approximately 12 billion database observations (the sampling period was equal to one tenth of a second).

For the purpose of this study, only the dataset relating to 1,180 car-following events that span over a duration of around 10 hours which is significant to fulfill the objective of this study. The car-following data composing the dataset comes from six different drivers and was collected on an approximately 13-km long segment of the Dulles Airport access road in order to maintain facility homogeneity. For each event, the collected naturalistic data used in this study includes the instantaneous speed of the following vehicle, the instantaneous speed of the leading vehicle, and the gap distance between the two vehicles. The instantaneous speed of and gap distance from the leading vehicle were measured using a radar system installed in the instrumented following vehicle. The instantaneous speed of the following vehicle was measured using its on-board diagnostic (OBD) system. Figure 23 shows a typical event used in this study where the instrumented follower is shown with a view of the leading vehicle.

**Figure 23: Photo of a typical collected data event used in this study (view from the testing follower vehicle)**

In order to study the vehicle effect on fuel consumption, the collected speed profiles were assigned to ten different types of gasoline vehicles: the 10 most-sold vehicles in the U.S. for the year 2015. A total of 3,002,316 sales represented the 10 most-sold vehicles in the U.S. For that year, the most-sold vehicle (Toyota Camry) accounted for 14% of the total U.S. top 10 sales. The tenth most-sold vehicle in the U.S. (Nissan Sentra) represented 7% of the top 10 sold vehicles in the U.S. Information on the selected vehicles was then taken from the manufacturers' specification sheets and the VT-CPFM calibration tool (a MATLAB code) was used to calibrate the VT-CPFM model parameters for the 10 selected vehicles. Table 18 shows the obtained values for all evaluated vehicles. In this table, note that the $\alpha_2$ value is independent of the vehicle type and has a constant value of $10^{-6}$, whereas the $\alpha_0$ and $\alpha_1$ values change from vehicle to vehicle.

**Table 18: Calibration Parameters for the Different Selected Vehicles**

| | $\alpha_0$ ($\times 10^{-6}$) | $\alpha_1$ ($\times 10^{-6}$) | $\alpha_2$ ($\times 10^{-6}$) |
|---|---|---|---|
| **U.S. Vehicles** | | | |
| Toyota Camry | 628.90 | 26.793 | 1.0 |
| Toyota Corolla | 452.81 | 44.243 | 1.0 |
| Honda Accord | 603.74 | 27.964 | 1.0 |
| Honda Civic | 452.81 | 66.304 | 1.0 |
| Nissan Altima | 628.90 | 17.938 | 1.0 |
| Ford Fusion | 628.90 | 27.522 | 1.0 |
| Hyundai Elantra | 452.81 | 46.239 | 1.0 |
| Chevrolet Cruze | 452.81 | 43.811 | 1.0 |
| Hyundai Sonata | 654.06 | 15.709 | 1.0 |
| Nissan Sentra | 452.81 | 47.621 | 1.0 |

## 7.5 STUDIED CAR-FOLLOWING MODELS AND CALIBRATION PARAMETERS

Wiedemann [10], Frietzsche [9], Gipps [7], and a new developed model by FR were selected for this study. The first three models are well-known since they are implemented in some of the most famous traffic simulators: VISSIM, PARAMICS, and AIMSUN, respectively. The FR new model, once validated, will be implemented in the INTEGRATION software.

The Wiedemann model [10] is a psycho-physical car-following model (group 2 of the previously presented car-following model classes). The initial formulation of the model, proposed in 1974, was calibrated mostly based on conceptual ideas rather than real traffic data. As a result, a much-needed recalibration of the model was performed in the early-1990s using an instrumented vehicle.

The Frietzsche model [9] belongs also to the psycho-physical group and shares the same structure as Wiedemann model. In this model, six threshold parameters are used to define five driving regimes. The thresholds are defined for four gap values and two differences in speed values between the leader and the follower vehicles.

Gipps model [7], developed in the late-1970s belongs to the safety-distance car-following model group and is formulated as a system of differential difference equations. Using a time step $\Delta t$ that aims to model the reaction time of drivers, the model computes the following vehicle speed $u_n$ at time $t+\Delta t$ as a function of its speed and the leading vehicle speed $u_{n-1}$ at the preceding time step $t$.

The newly developed FR model [18] captures the main characteristics of the Rakha-Pasumarthy- Adjerid (RPA) model in that they share the same steady-state formulation, respect the same vehicle dynamics and use very similar collision-avoidance strategies to ensure a safe following distance between vehicles. Contrary to the original model, which estimates the speed of the following vehicle, the FR mathematical expression, presented in Equation VII.5, estimates the acceleration of the following vehicle using the three functions $a_{max}$, $f_p$ and $CA$.

$$a_{n+1} = f_p a_{max} + CA \tag{VII.5}$$

Here, $f_p$ and $X_{n+1}$ are calculated using Equation VII.6. $CA$ is computed using Equation VII.7.

$$\begin{aligned} f_p &= e^{-aX_{n+1}}\left(1 - X_{n+1}^{b} e^{b(1-X_n+1)}\right)^{d} \\ X_{n+1} &= \frac{\tilde{s}_{n+1}}{s_{n+1}} \cdot \frac{u_{n+1}}{\tilde{u}_{n+1}} \end{aligned} \tag{VII.6}$$

$$CA = \frac{\left[u_{n+1}^2 - u_n^2 + \sqrt{(u_{n+1}^2 - u_n^2)^2}\right]^2}{16(d_{desired} + gG)\left(s_{n+1} - s_j\right)^2} \tag{VII.7}$$

The first term is nothing but the vehicle dynamics model [12][12][12][12]multiplied by a function that is sensitive to the ratio of $u_{n+1}/s_{n+1}$ that is divided by the ratio of the speed and

spacing computed using the Van Aerde steady state model using the simulated speed and spacing. The steady state spacing and speed are the same as proposed by the RPA model. The $f_p$-function ensures that two objectives are met. First, it ensures that the steady model governing the FR model is the same as the RPA model formulation. Second, it attempts to model human behavior and the different patterns of driving by acting as a reduction factor to the vehicle dynamics model.

Collision avoidance is ensured by the function CA (Equation VII.7) which computes the needed deceleration to apply as the ratio of the square of the kinematics deceleration needed to decelerate from the current speed to the leading vehicle speed at a desired deceleration rate that is set by the user.

Finally, to model the effect of the driver error in estimating the leading vehicle speed and the distance gap between the two vehicles, two wiener processes are incorporated in the model formulation at the level of $u_n$ and $s_{n+1}$. Additionally, a white noise signal is added to the model's expression to capture the driver's imperfection while applying the gas pedal. The compounding effect of those three signals makes the model output more representative of human driving behavior.

### 7.5.1 Calibration of the car-following models with the dataset

For each of the studied models, a certain number of inputs is needed. These inputs can be categorized into two groups. The first category comprises the inputs that are the same for the different models, namely the time-space and the time-speed of the leading vehicle, the starting location and speed of the following vehicle as well as the free-flow speed ($u_f$) which was estimated specifically for each car-following event along with any other variables related to the roadway. The desired speed of a certain naturalistic event was set equally across all of the studied models in order to maintain the homogeneity of driver behavior and road facility for that specific event.

The remaining input variables consists of model-specific parameters that require to be calibrated accordingly depending on the researcher's objectives. The different parameters were calibrated such that the resulting simulated behavior of the following vehicle matches its observed behavior as closely as possible. The calibration procedure of the different parameters of each model was conducted heuristically taking the speed RMSE as the error objective function. The optimization operation was done for the whole dataset rather than on an event-event basis.

Finally, given the presence of noise in the proposed model and the fact that 10 cars are considered, the effect of the noise was ignored.

## 7.6 RESULTS AND INTERPRETATION

Figure 24 shows, for illustration purposes, a typical result of the analysis performed on one of the 1180 studied events (Event No. 23 of the dataset) using the Toyota Camry as the follower vehicle. In this figure, the observed real speed as a function of time of the follower vehicle is plotted along with the predicted speed pattern as obtained from the four studied models. For this particular event, the driver of the follower car had an initial speed around 105 km/h, then he/she decelerated to about 25 km/h, then he/she accelerated to about 62 km/h. The event ended after 42 seconds with a reached speed of 72 km/h. In Figure 24.a, the Wiedemann model predicted a speed drop, which at first followed the observed behavior, however, this decrease in speed continued to reach a zero value indicating a full stop, which means that the model failed to detect the observed acceleration that occurred at around 15 seconds from the start of the event when the real speed was about 25 km/h. This drawback is a direct result of the nomenclature of the Wiedemann model itself. Such behaviors result from the abrupt change in the acceleration value when transitioning from one traffic regime to another. Besides the latter aspect, the crossing of one of the boundaries delimiting the different regions of the Wiedemann model was found to result in another disparity in the model output when compared to most of the other models (mainly Gipps and FR models). The concerned disparity is observed when the following vehicle remains in the same traffic region for the entire duration of the car-following event, hence arising the possibility of having a constant acceleration over an extended duration of the car-following maneuver. The previous two drawbacks are also manifested in the Fritzsche model due to its similar structure, however their presence is not as prevalent. For instance, one such case in which the following vehicle remained within the same traffic regime for a relatively long time is shown in Figure 24.b for Fritzsche model. The figure illustrates a scenario in which the driver cruised with a constant speed for about 12 seconds in the timeframe starting at 30 seconds from the start of the event. Since the following vehicle remained within the same traffic regime for the concerned time range, the Fritzsche model resulted in a constant speed profile. However, the latter aspects of Fritzsche and Wiedemann models do not necessarily connote an inability to propose a fitted speed that matches empirical data. Finally, while all the models relatively succeeded in capturing the empirical behavior of the vehicle, the FR model was the best in terms of tracing the actual speed profile. The FR

model is followed by Gipps model (Figure 24.c) which slightly over-predicted the minimum reached speed. The latter results are further confirmed in the associated acceleration profiles of Gipps and the FR model, drawn in Figure 25.c and Figure 25.d respectively. In fact, it can be observed that the latter two models resulted in acceleration values that closely followed the field data. In accordance with the corresponding speed profiles, the FR formulation traced the actual acceleration profile the best for this specific event. Generally speaking, the FR model was found to be the best in terms of mimicking the real driver behavior as it successfully avoided the acceleration fluctuations produced by the other models that are far in excess of those observed at the level of the empirical data.

Figure 26 shows the instantaneous observed fuel consumption rate along with that predicted by the four models using the same event which speed and acceleration profiles were shown in Figure 24 and Figure 25, respectively. As presented by Equation VII.2, an increase in speed and/or acceleration would increase the instantaneous power and therefore the fuel consumption rate. For example, the increase in speed and acceleration predicted by the Fritzsche model around 2 and 10 seconds from the event start (Figure 24.b and Figure 25.b), resulted in a jump in the fuel consumption rate at these instances (Figure 26.b). For the Wiedemann model the decrease in speed associated with a deceleration predicted from the start of the event until about 24 seconds results in a zero instantaneous power and therefore a minimum fuel consumption rate. After 24 seconds, the increase in speed associated with the acceleration resulted in an increase in the fuel consumption rate. For the Gipps and FR models, the close agreement of their predicted speed and acceleration profiles to the observed ones, lead to a similar trend in their predicted fuel consumption rates as compared to the observed one (Figure 26.c and Figure 26.d). From Figure 24, Figure 25, and Figure 26, it is noted, as expected, that the fuel consumption rate is very sensitive to the predicted speed and acceleration values.

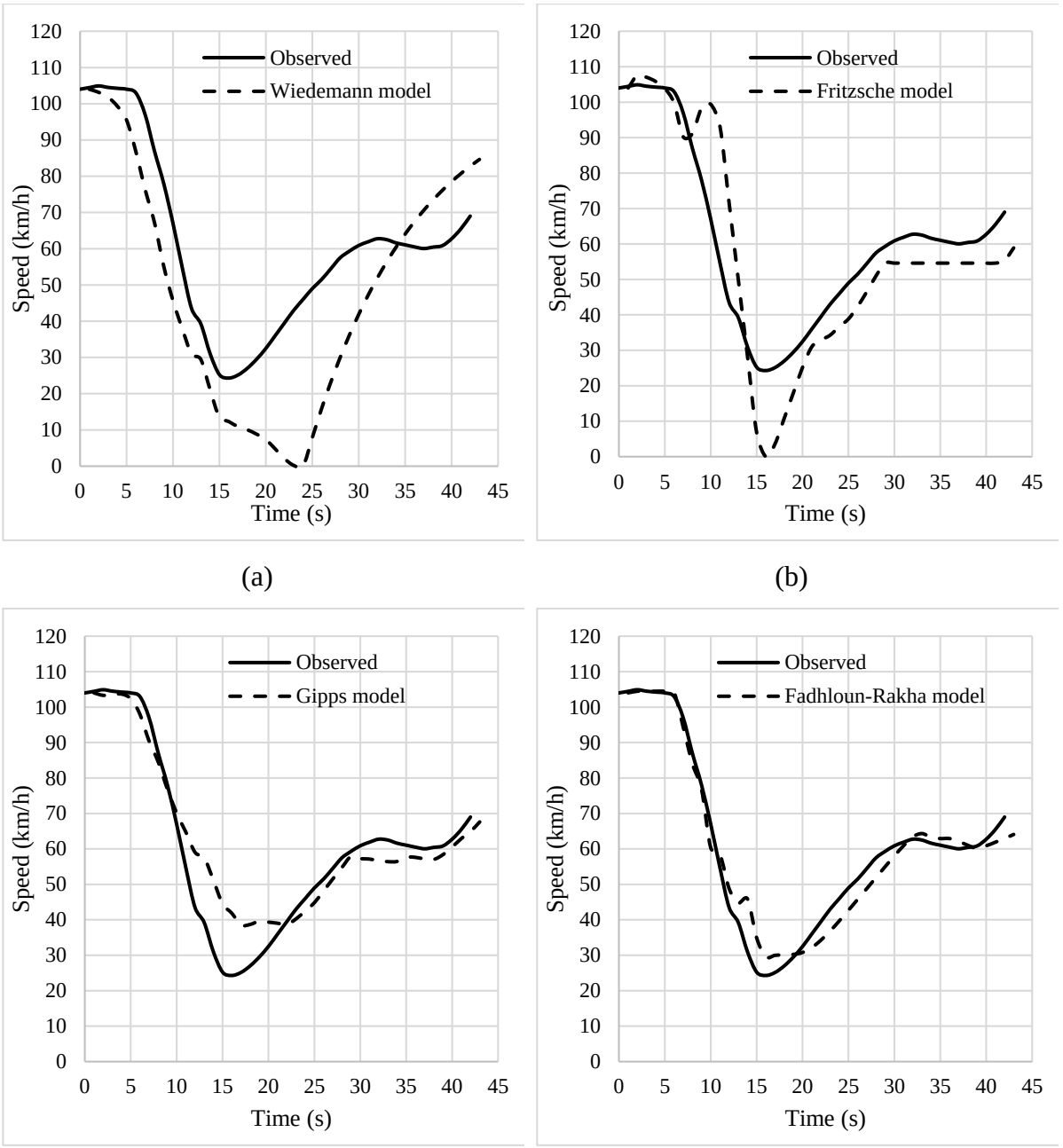


**Figure 24: Observed and predicted speed profile for Event 23: (a) Wiedemann model (b) Fritzsche model (c) Gipps model (d) FR model.**

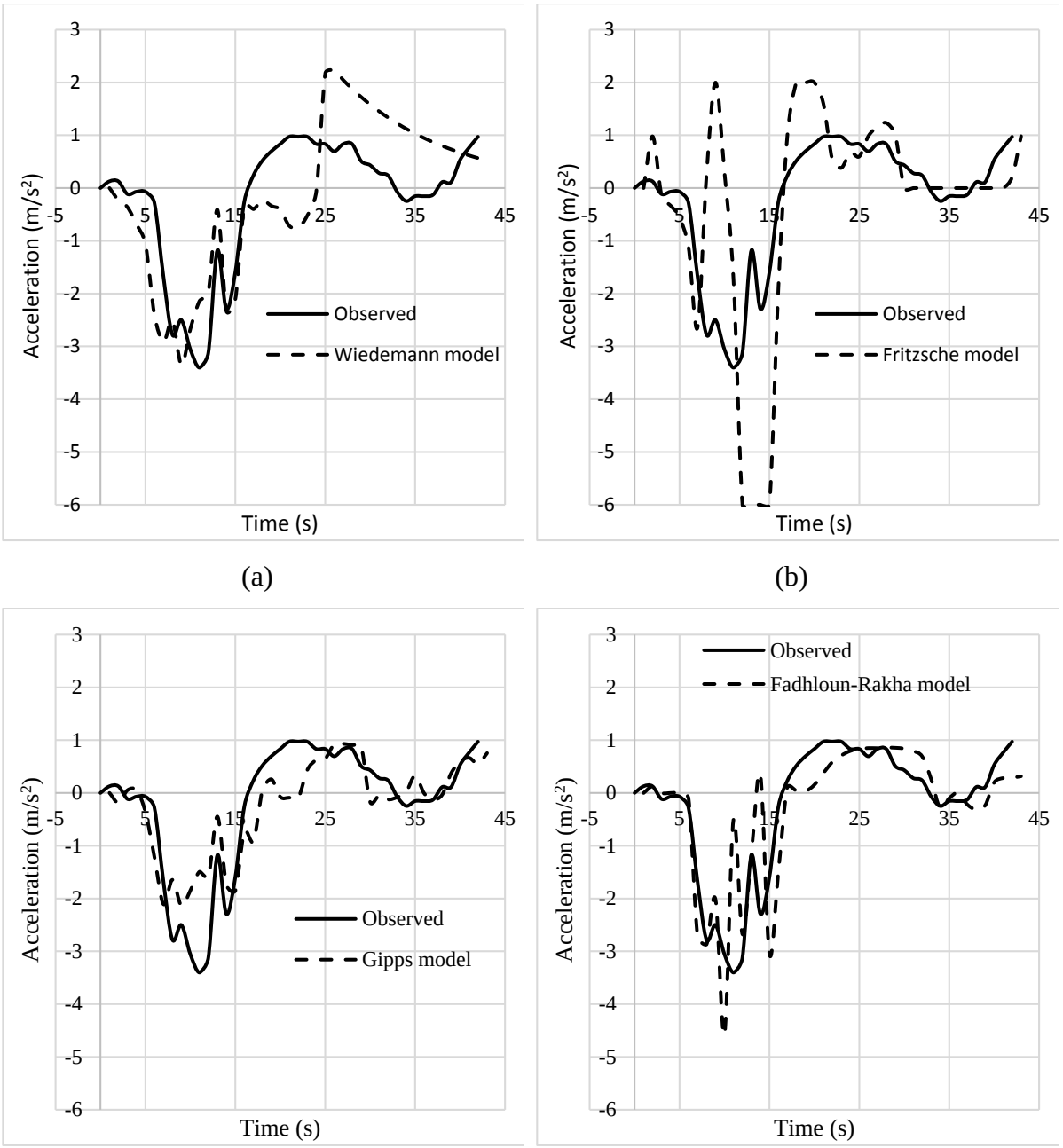


**Figure 25: Observed and predicted acceleration profile for Event 23: (a) Wiedemann model (b) Fritzsche model (c) Gipps model (d) FR model.**

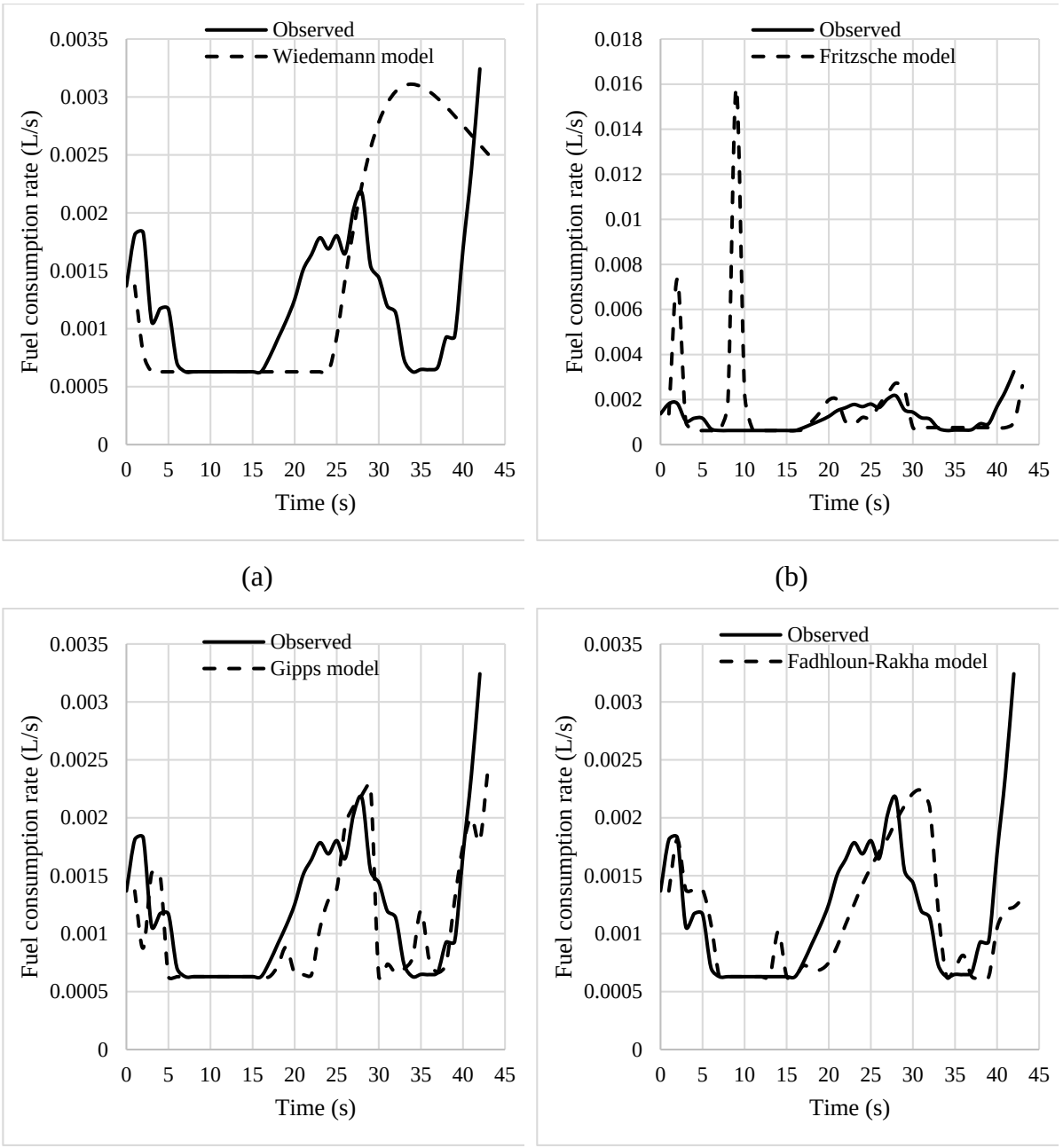


**Figure 26: Observed and predicted fuel consumption rate for Event 23: (a) Wiedemann model (b) Fritzsche model (c) Gipps model (d) FR model.**

Figure 27 shows the calculated consumed fuel for event 23 using the Toyota Camry as the follower vehicle. This fuel quantity is obtained using Equation VII.4 and the fuel consumption rate data shown in Figure 26. For this particular event and vehicle, the observed consumed fuel was found to be equal to 0.05 L. Using the Wiedemann and Fritzsche predicted speed and acceleration profiles resulted in overestimating the consumed fuel for this particular event and car by 27.8% and 35.8%. On the other hand, the Gipps and FR models

underestimated the consumed fuel for this particular event and car by 12.1% and 6.3%, respectively.

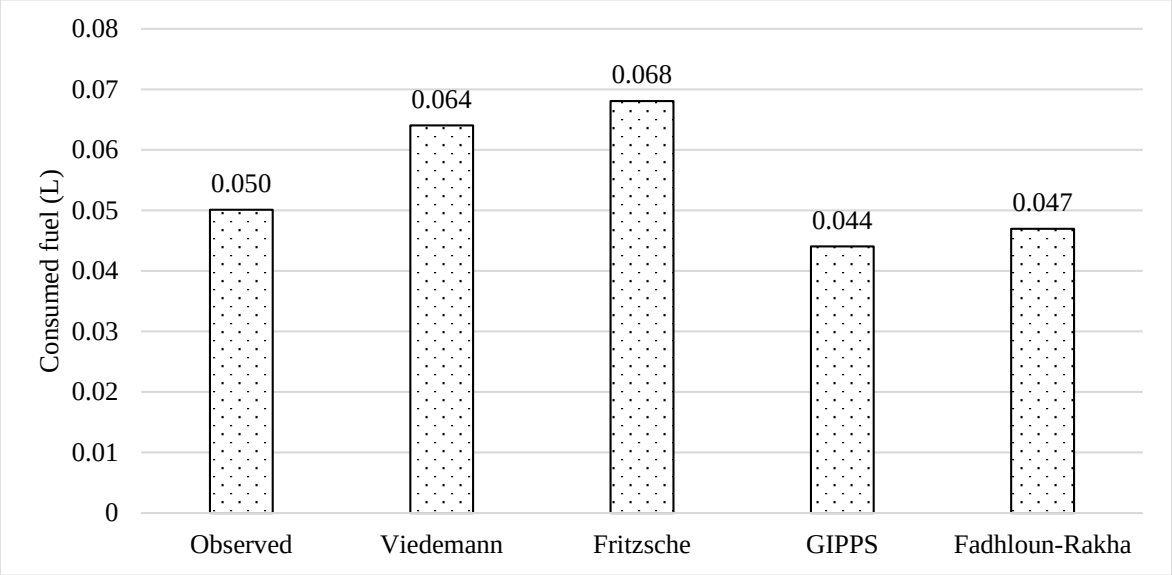


**Figure 27: Observed and predicted consumed fuel for Event 23**

The analysis presented earlier for Event 23 and the Toyota Camry was performed for all the events and all other nine studied cars. In order to quantify the difference in consumed fuel between the observed and predicted models, the variable %_*error* as defined by Equation VII.8 was used. In this equation $FQ_0$ and $FQ_p$ are the observed and predicted fuel quantity, respectively. Using all 1180 events, a distribution of the %_*error* is achieved. The descriptive statistics of this distribution indicate quantitatively the differences between car-following models in predicting consumed fuel. For example, Figure 28 shows the obtained distribution for this variable when using the Toyota Camry. Figure 28.a shows that for the Wiedemann model, *%_error* values as high as 40% were calculated for more than quarter of the events. This model was successful in predicting the consumed fuel within 24% for half of the studied events. The Fritzsche model (Figure 28.b) had a *%_error* smaller than 8% for about 20% of the events, however *%_error* as high as 72% were calculated for some events. The Gipps and FR models (Figure 28.c and Figure 28.d, respectively) had better distributions as proved by their maximum *%_error* values of 28 and 21%, respectively. Descriptive statistics for this variable distribution for all studied cars are shown in Table 19. Using all the cars, the median values for the %_error were 25.2, 22.1, 9.0, and 6.2 for Wiedemann, Frietzsche, Gipps, and FR models, respectively.

$$\%\_error = \left| \frac{FQ_0 - FQ_p}{FQ_0} \right| \times 100\% \qquad \text{(VII.8)}$$

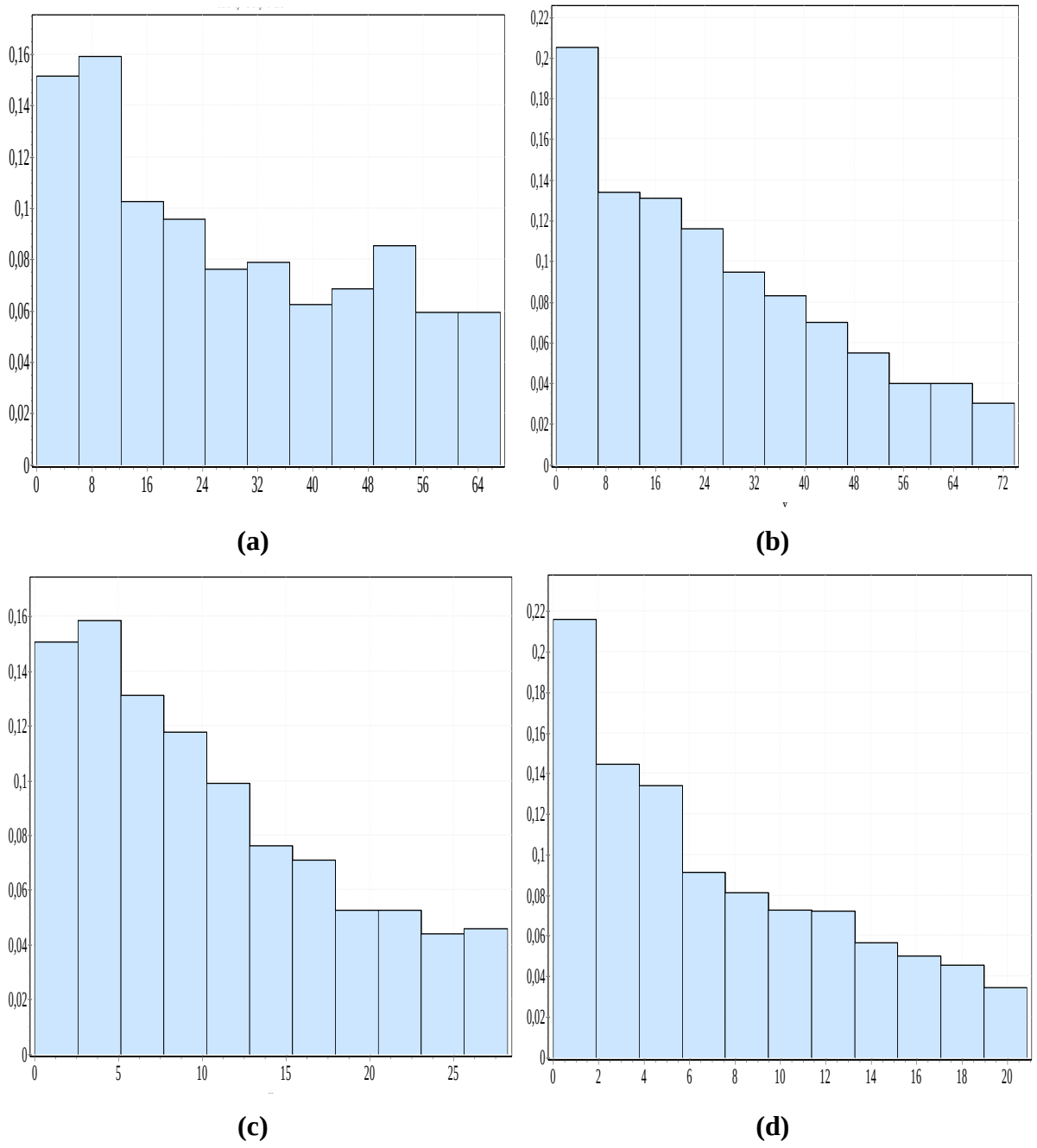


**Figure 28: Distribution of the %_error using the Toyota Camry: (a) Wiedemann model (b) Fritzsche model (c) Gipps model (d) FR model.**

**Table 19: Descriptive statistics for the *%_error* variable for all studied car-following models and gasoline cars**

| | | Min. | Max. | Average | Median | 75% | 95% |
|---|---|---|---|---|---|---|---|
| Toyota Camry | Wiedemann | 0 | 67.1 | 27.4 | 23.6 | 44.6 | 62.7 |
| | Fritzsche | 0 | 73.8 | 25.6 | 21.7 | 39.3 | 63.5 |
| | Gipps | 0 | 28.2 | 10.5 | 8.9 | 16.0 | 25.1 |
| | FR | 0 | 20.9 | 7.3 | 5.8 | 11.6 | 18.2 |
| Toyota Corolla | Wiedemann | 0 | 75.5 | 31.7 | 28.3 | 52.2 | 69.5 |
| | Fritzsche | 0 | 76.2 | 27.4 | 23.3 | 41.6 | 67.9 |
| | Gipps | 0 | 33.0 | 11.9 | 9.6 | 18.5 | 29.1 |
| | FR | 0 | 22.4 | 8.0 | 6.8 | 12.6 | 19.1 |
| Honda Accord | Wiedemann | 0 | 67.2 | 27.4 | 23.1 | 44.4 | 62.5 |
| | Fritzsche | 0 | 69.9 | 24.6 | 21.4 | 37.9 | 60.1 |
| | Gipps | 0 | 27.8 | 10.2 | 8.6 | 15.5 | 24.6 |
| | FR | 0 | 20.6 | 7.1 | 5.7 | 11.2 | 17.9 |
| Honda Civic | Wiedemann | 0 | 79.4 | 34.7 | 32.2 | 56.2 | 74.2 |
| | Fritzsche | 0 | 80.0 | 29.1 | 24.5 | 44.4 | 70.3 |
| | Gipps | 0 | 36.3 | 13.1 | 10.5 | 20.5 | 32.5 |
| | FR | 0 | 24.1 | 9.0 | 7.5 | 14.0 | 21.4 |
| Nissan Altima | Wiedemann | 0 | 59.9 | 23.8 | 19.9 | 39.1 | 55.3 |
| | Fritzsche | 0 | 67.0 | 22.5 | 19.3 | 35.2 | 56.0 |
| | Gipps | 0 | 24.4 | 9.0 | 7.7 | 13.6 | 21.8 |
| | FR | 0 | 18.7 | 6.3 | 4.9 | 10.2 | 16.1 |
| Ford Fusion | Wiedemann | 0 | 68.2 | 27.9 | 24.0 | 45.3 | 63.4 |
| | Fritzsche | 0 | 74.8 | 26.0 | 22.1 | 39.9 | 64.2 |
| | Gipps | 0 | 28.7 | 10.7 | 9.1 | 16.3 | 25.6 |
| | FR | 0 | 21.1 | 7.4 | 5.9 | 11.7 | 18.4 |
| Hyundai Elantra | Wiedemann | 0 | 75.5 | 31.8 | 28.4 | 52.2 | 69.3 |
| | Fritzsche | 0 | 76.5 | 27.5 | 23.2 | 41.8 | 67.6 |
| | Gipps | 0 | 33.2 | 12.0 | 9.7 | 18.6 | 29.3 |
| | FR | 0 | 22.8 | 8.2 | 6.9 | 12.9 | 19.8 |
| Chevrolet Cruze | Wiedemann | 0 | 78.0 | 33.5 | 29.5 | 55.0 | 72.9 |
| | Fritzsche | 0 | 84.6 | 29.8 | 25.2 | 45.9 | 74.7 |
| | Gipps | 0 | 35.3 | 12.8 | 10.4 | 20.0 | 31.4 |
| | FR | 0 | 23.9 | 8.7 | 7.4 | 13.7 | 20.8 |
| Hyundai Sonata | Wiedemann | 0 | 58.1 | 23.0 | 19.3 | 37.8 | 53.3 |
| | Fritzsche | 0 | 67.1 | 22.1 | 19.0 | 34.7 | 55.9 |
| | Gipps | 0 | 23.6 | 8.8 | 7.4 | 13.4 | 21.0 |
| | FR | 0 | 18.3 | 6.2 | 4.8 | 9.7 | 15.9 |
| Nissan Sentra | Wiedemann | 0 | 75.6 | 31.9 | 28.4 | 52.3 | 69.8 |
| | Fritzsche | 0 | 75.0 | 27.2 | 23.0 | 41.0 | 66.5 |
| | Gipps | 0 | 33.0 | 11.9 | 9.6 | 18.4 | 29.2 |
| | FR | 0 | 22.2 | 8.0 | 6.9 | 12.5 | 19.2 |

Finally, to highlight the vehicle effect on consumed fuel, Event 408 was chosen for illustration purposes, but the shown trend in similar for all other events. Figure 29.a, shows the speed profile for this event, which is about 7-minute long. During this event, the driver decelerated and accelerated many times, which is known to lead to an increase in consumed fuel. Figure 29.b shows the consumed fuel for the 10 cars if they would have encountered this speed profile. As much as 17% difference is found between the highest and least values. Therefore, it is essential that micro-simulation tools select the right fleet of cars when simulating a given network.

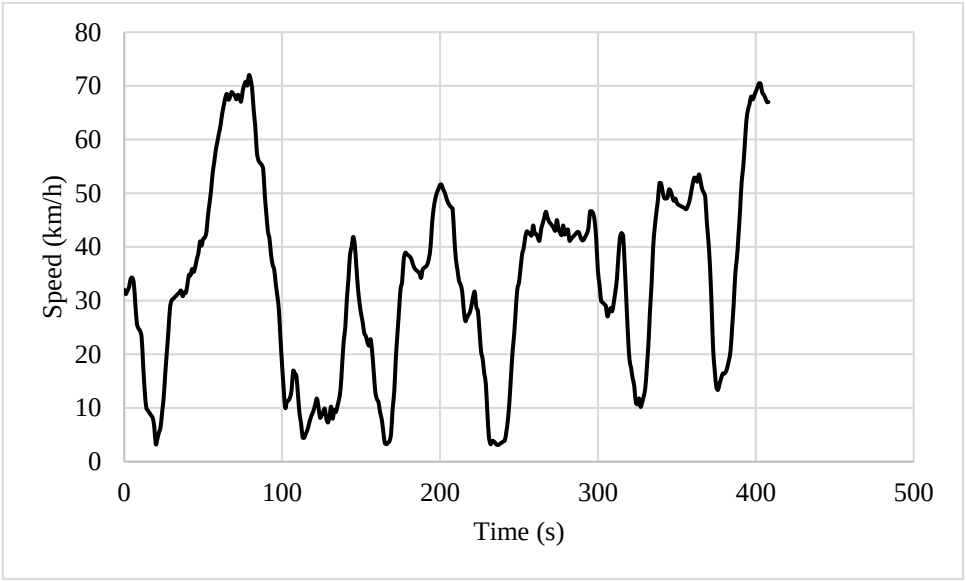


(a)

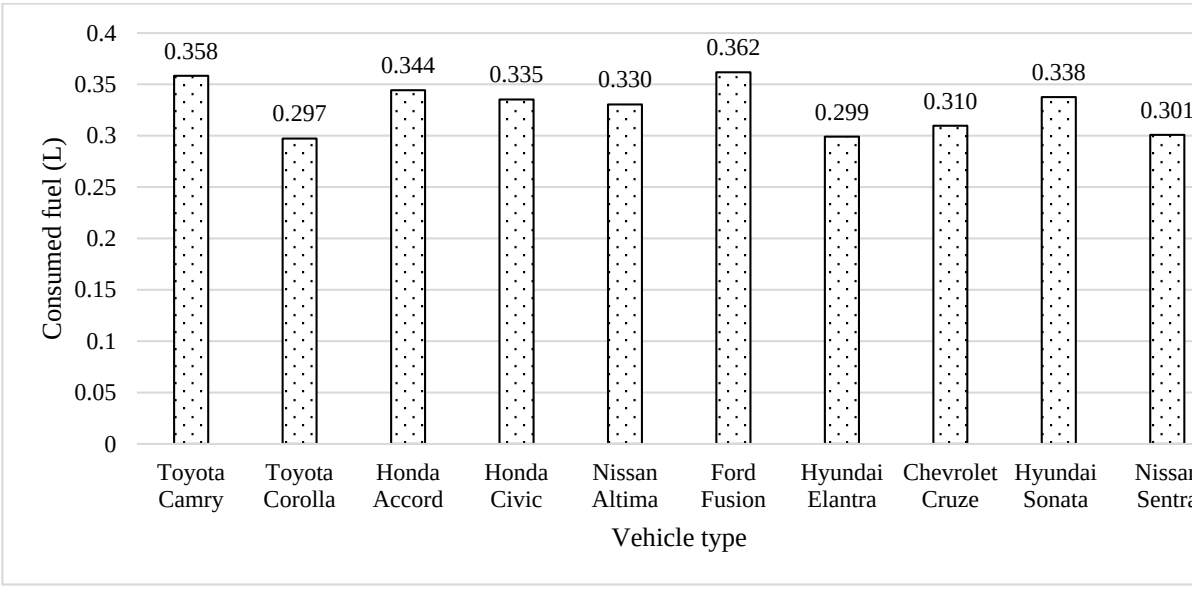


(b)

**Figure 29: a) Event 408 speed profile – b) Effect of vehicle type on observed consumed fuel for Event 408**

## 7.7 CONCLUSIONS

In the context of sustainable development, good estimates of fuel consumption as provided by traffic micro-simulation software is essential. For that reason, the effect of car-following models, which constitute the heart of micro-simulation tools, on estimated fuel consumption of gasoline cars was analyzed and quantified. The findings of this research led to the following conclusions:

1. For the same data (speed of following and leader vehicles and spacing between them), different car-following models produce different speed profiles of the following vehicle depending on the logic used in their formulation.
2. Differences in the predicted speed profile leads to a considerable difference in the predicted acceleration, which itself significantly affects the estimated fuel consumption level.
3. Differences between observed and predicted fuel consumption was found to depend on the used car-following model.
4. The newly developed FR car-following model showed very promising results in terms of predicting fuel consumption. Specifically, the $95^{th}$ percentile of its *%_error* distribution was found not to exceed 22% for all studied gasoline cars and all 1180 events.
5. Even though, micro-simulation tools are mostly used to compare between alternatives and therefore it is always argued that a relative difference is all that is needed in this case, it is always better to estimate reasonable absolute fuel consumption levels for each alternative. For that reason, using a good representative sample of the vehicles used in the network is essential since different cars were found to consume different quantities of fuel for a given event.

## 7.8 ACKNOWLEDGEMENTS

The authors acknowledge the financial support provided by the University Mobility and Equity Center (UMEC) and the Department of Energy through the Office of Energy Efficiency and Renewable Energy (EERE), Vehicle Technologies Office, Energy Efficient Mobility Systems Program under award number DE-EE0008209.

# Chapter 8 Cooperative Platooning Algorithms for Connected Vehicles

**Authors:**

Karim Fadhloun

Youssef Bichiou, Ph.D

Hesham Rakha, Ph.D, P.Eng.

*Submitted for presentation at the 2020 TRB Annual Meeting*

## 8.1 ABSTRACT

Congestion is one of the major problems facing modern urban cities worldwide. This is the result of the ever-increasing number of commuters and vehicles. It results in inefficient infrastructure use as well as increased fuel consumption and vehicle emission levels. Road users waste precious hours on the road, which in turn reduces productivity. Solutions have been developed and continue to be developed to lessen traffic congestion. Vehicle platooning through cooperative adaptive cruise control (CACC) systems offers a way to increase the road capacity while maintaining existing infrastructure. The fundamental concepts and the theories behind vehicle platooning were researched as early as the 1960s. Only recently with the advances in wireless communication technology, implementation is feasible. This paper delivers two platooning strategies that aim at maintaining a desired time gap between vehicles within the platoon. The two controllers offer acceleration/deceleration values that satisfy dynamic vehicle motion models and constraints. A validation was performed through investigating the responses and performance of the two strategies for real traffic situations. The results show that the two controllers perform as expected with one of them requiring very little effort to tune.

## 8.2 INTRODUCTION

Over the last decade, the interest in vehicle cooperation as a means of mitigating congestion and increasing traffic flow has grown exponentially among traffic engineers and researchers. While the fundamental concepts and the theories behind vehicle platooning were investigated as early as the 1960s, it is only quite recently that the vehicle cooperation concept was explored from an implementation and experimentation perspective. The main factor that contributed to

the transition of vehicle platooning from a theoretical concept to a feasible functional system is the advancement in wireless communication technology. It is noteworthy to mention that the affordability and reliability of wireless communication technology is complemented by the diverse and advanced driver assistance and navigation systems.

To illustrate how this traffic concept is rapidly converging towards becoming a reality, there is no better argument than noticing the number of recent studies funded by the legislator preparing the technical and legal ground to vehicle cooperation and other intelligent transportation systems (ITSs). Two projects of the Federal Highway Administration (FHWA) can serve as examples for the latter statement. The first study [37] relates, among others, to investigating the human factors involved in the cooperative adaptive cruise control (CACC) concept, identifying the necessary equipment and resources, and assisting researchers in the design process of test scenarios. The main contribution of the study is the development of a framework that can be used to evaluate the human-factors, safety, and implementation issues associated with CACC. The second FHWA project [38] is oriented towards the case in which the CACC concept is applied to heavy trucks. Aiming to evaluate the commercial feasibility of Driver Assistive Truck Platooning (DATP), the study performed the necessary technical work, evaluation, and industry engagement to identify the key questions that must be answered prior to market introduction of heavy truck platooning.

Technically speaking, intelligent vehicle cooperation can be cast as an extension or an upgrade to the commercially available adaptive cruise control systems (ACC). Through transmitting information about the speeds and positions of the vehicles in the platoon using centralized and/or decentralized wireless communication, a controller automatically adjusts the speeds of the vehicles in the platoon resulting in a higher traffic flow as vehicles operate at a much closer spacing. A successful cooperative adaptive cruise control system would be one that is implementable in a fast and cost-effective manner without resulting in any disruptions and instabilities to the flow of vehicles or giving rise to any safety concerns and accidents. In that context, several CACC strategies and controllers have been developed during the last decade [39-47]. Most of these CACC systems focused primarily on improving fuel efficiency assuming or using simplified vehicle operational concepts and simple fuel consumption models. However, a few studies both designed and experimentally evaluated the controller performance on a platoon of vehicles in a cooperative setting.

The research presented in this paper proposes two platooning strategies that intelligently modulate the longitudinal motion of vehicles within a cooperative platoon. The

proposed controllers aim to maintain a desired time-headway between the vehicles through the minimization of the spacing error between the current conditions and the desired following policy in different traffic situations. In addition to presenting the design of the controllers, the paper describes the development process of the models controlling the vehicles' behavior in the acceleration and deceleration regimes.

Besides providing a comprehensive overview of the literature, the objectives and contributions of this paper are two-fold: 1) Formulate and develop novel platooning algorithms for acceleration and deceleration maneuvers along with presenting the methodologies and procedures that led to their development; 2) Validate the developed controllers through investigating their responses and evaluating their performance for real traffic situations. A dataset comprised of two driving cycles characterizing different typical traffic scenarios was used for the validation work. It is also important to note here that to our knowledge we are the first to formulate a comprehensive dynamic models of the vehicle motion with the various constraints associated: acceleration constraints and collision avoidance. The developed logic ensures also string stability (i.e. platoon stability) with minimal communication between the vehicles and minimal controller tuning.

Concerning the layout, this paper is organized as follows. First, an overview of the most relevant CACC strategies and controllers developed in the last decade is provided. While reviewing the literature, a special focus is dedicated to the platooning algorithms used in these systems. After that, the architecture of the proposed platooning controllers is presented along with an explanation of the different steps that led to their development. Next, results illustrating the response and performance of the new controllers are presented. Finally, the conclusions of the paper are drawn and insights for future work are provided.

## 8.3 BACKGROUND

In this section, the most recent literature that involved developing and investigating cooperative vehicle platooning strategies in an experimental setting is outlined. For instance, one can start by mentioning the research conducted by Naus et. al [39] in which a CACC system was designed and tested using two vehicles for scenarios involving both constant and speed-dependent inter-vehicle spacing. The objective of the study was oriented towards investigating the feasibility and the stability of the proposed control system. It was demonstrated that a speed-dependent gap between vehicles is necessary in order to ensure the overall string stability. In this study, a feedback controller, composed of a standard Proportional-Derivative

(PD) controller and a first-order low-pass filter, was used to regulate the longitudinal motion of the following vehicle. Another practical CACC system was proposed by Milanes et. al [40]. In a similar fashion to [39], a set of feedback PD controllers were used to control the following vehicles. The underlying controller was examined by implementing it in four production passenger vehicles and testing it in several experimental settings. Among the experimental trials that were carried out, the paper distinguishes between situations that aim to emulate cut-in and cut-out maneuvers as well as the case in which the time gap setting is changed by the driver. The system performance was then evaluated by comparing its resulting traffic behavior against that generated by the original ACC system of the vehicles.

In relation to heavy duty vehicles (HDVs), platooning and cooperative systems have been extensively investigated. The intense interest in developing and designing control strategies that specifically target HDVs is due to the significant reduction in fuel consumption and emissions that could be achieved through vehicle platooning. In fact, through minimizing the inter-vehicle gap, fuel efficiency and emission reduction are achieved through lowering the aerodynamic resistance to which the truck is exposed. Aside from the environmental impact and financial benefit to transportation companies, it is worth mentioning that truck platooning is conceptually different than when passenger vehicles are involved. The latter is explained by the huge impact that the heavy mass, the air drag and the road grade has on the system dynamics.

Motivated by the significant savings in fuel costs resulting from truck platooning, Alam [41] developed a framework for the design, implementation, and evaluation of energy efficient HDV platooning. Using game theory, HDV platooning was investigated as an optimization problem that aims to minimize the inter-vehicular gap between trucks while ensuring that the platoon is string-stable and collision-free. In that regard, a decentralized feedback controller was developed. In a first stage, the control system adjusted the behavior of the following truck as a function of just its immediate predecessor. However, the controller was modified later on to account for several preceding vehicles. The main contribution of this research resides in the fact that it proceeded to validate the developed control strategy both through computer simulation and experimental testing using real HDVs. The experiments demonstrate that fuel savings of at least 4% and up to 20% could be achieved depending on the tested scenario.

All of the aforementioned studies share in common the fact that a prototype was created and implemented in real vehicles allowing for experimental testing of the system ensuring both its functionality and safety to a certain degree. In other words, it was verified that they were

incorporative of the different transmission and response delays along with any non-linear dynamics involved. The latter is not the case for several studies about vehicle platooning that are usually based on simplified theoretical models and assumptions. Research that fall under the latter category include the study of Stanger and Del Re [42]. Noticing the achievability of a lower fuel consumption using CACC, the study developed a linear model predictive control approach that aims to directly optimize the fuel efficiency of the vehicles in the platoon rather than trying to minimize the acceleration variability or the inter-vehicular gap. For that purpose, the authors assumed a simplified linear car-following model along with a piecewise quadratic approximation of the non-linear static fuel consumption map of the internal combustion engine. Using numerical simulation, the proposed control approach was validated by observing that the CACC scenario results in around 20% fuel efficiency when compared to the standard non-cooperative case. With a similar stated objective of attaining an optimal fuel efficiency, Deng and Ma [43] derived a speed planning algorithm that is based on the Pontryagin Minimum Principle (PMP) for the case of HDVs. First, the study investigated the case of a single vehicle before extending it, in a second stage, to a platoon of two trucks. The Oguchi fuel consumption model was used in order to evaluate the potential energy savings due to the control strategy. Through numerical investigation, the developed controller was demonstrated to result in a 30% reduction in fuel consumption when decelerating and a 3.5% reduction when accelerating.

Another control approach was proposed by Schmied et al. [44]. The paper opted for a Nonlinear Model Predictive Control (NMPC) approach to develop a CACC system that ensures efficiency at the level of fuel consumption and emissions. The use of a NMPC has many advantages when compared to a basic linear model predictive control. For instance, NMPCs would allow to achieve several goals and objectives even if they contradict each other while ensuring the respect of several constraints. Despite the latter, linear model predictive controls remain the ones implemented in vehicles due to the fact that NMPCs are computationally burdensome compared to linear controls. That could possibly explain why the proposed NMPC for cooperative adaptive cruise control [44] was tested in a Hardware In the Loop (HIL) configuration on a dynamic engine test bench rather than implemented directly in a real vehicle. A scenario involving two consecutive vehicles with infrastructure-to-vehicle (I2V) communication was tested using the HIL configuration. The outcome of the conducted experiments demonstrates the potential for a 13% reduction in the fuel consumption level and a decrease of NOx and PM emissions by 24% and 28% respectively. A very similar experimental setting was used in another research effort [45] in which a controller was

integrated to a HIL configuration. The main difference between the two studies relates to using a heuristic controller for vehicle cooperation rather than a NMPC. In a different study, Diaby and Sorkati [46] investigated the case in which a platoon of heavy trucks is traveling in a hilly region and presented a method that results in a minimal fuel consumption with respect to both the topography of the area and the air drag. The proposed algorithm formulates the problem as a convex quadratic programming problem that optimizes the speeds of the different trucks in the platoon.

## 8.4 METHODOLOGY AND FORMULATION

In this section, the methodologies leading to the development of the proposed platooning strategies are presented. From a control perspective, the formulation of the first model is closely related to that of several models proposed in the literature. In fact, the implementation of the model is based on linear feedback control theory through the use of Proportional-Derivative controllers. With regards, to the second model, the controller is derived from feedback linearization. A change of variable is introduced to achieve a simple and easy to implement control structure. At the design level, the proposed systems share most of the characteristics of a typical cruise control system in that controllers are used to adjust the throttle and apply the brakes in such a way that the vehicle motion respects a desired following policy.

However, rather than trying to keep a constant desired speed, the models aim to maintain a desired longitudinal time gap in a platoon of connected vehicles. Mathematically speaking, the latter objective translates to trying to minimize the error function presented in Equation VIII.1. The equation computes the instantaneous gap error as the difference between the actual distance gap (the spacing between vehicle *n-1* and *n* from which the spacing at jam density $s_j$ is extracted) and the desired distance gap that is estimated through the multiplication of a constant desired time headway $h_{des}$ by the speed of the following vehicle $v_n$.

$$e_n(t) = \left[x_{n-1}(t) - x_n(t) - s_j\right] - h_{des} \times v_n(t) \qquad \text{(VIII.1)}$$

The car-following strategy of Equation VIII.1 is similar to that used in standard commercial Adaptive Cruise Control systems. However, given the cooperative and connected environment in which the vehicles are located, desired time gaps that are significantly shorter will be achievable and sustainable in a multi-vehicle platoon. To ensure the continuous sustainability of small time gaps between vehicles, the proposed controllers need to be stable

and inclusive of smooth and flexible collision avoidance strategies so that the safety and the comfort level of passengers are both respected.

Before going any further, it is worth mentioning that the research team opted to use the vehicle dynamics model of the RPA car-following model [12] as the descriptive model for the acceleration behavior while developing both platooning strategies. The latter model was developed by Rakha *et al*. [16, 34] and was proven to provide a good approximation for maximum acceleration behavior. The model computes the maximum acceleration of a vehicle $a_{max}$ as the ratio of the resultant tractive force to the vehicle mass. The resultant force is computed as the difference between the tractive force $F$ acting on the following vehicle and the sum of the resistive forces; namely the aerodynamics resistance $R_a$, the rolling resistance $R_r$ and the grade resistance $R_g$. The different equations of the model are presented in Equation VIII.2 through Equation VIII.6.

$$a_{max}(t) = \frac{F(t) - \left(R_a(t) + R_r(t) + R_g(t)\right)}{m} \tag{VIII.2}$$

With

$$F = \min\left(\frac{3600\eta_d P}{v}, m_{ta} g \mu\right) \tag{VIII.3}$$

$$R_a = \frac{\rho C_d C_h A_f g v^2}{2} \tag{VIII.4}$$

$$R_r = mgC_{r0}(C_{r1}v + C_{r2}) \tag{VIII.5}$$

$$R_g = mgG \tag{VIII.6}$$

The different parameter definitions are as follows: $\eta_d$ is the driveline efficiency (unitless); $P$ is the vehicle power (kW); $m_{ta}$ is the mass of the vehicle on the tractive axle (kg); $g$ is the gravitational acceleration (9.8067 m/s$^2$) and $\mu$ is the coefficient of road adhesion or the coefficient of friction (unitless).; $\rho$ is the air density at sea level and a temperature of 15◦C (1.2256 kg/m$^3$); $C_d$ is the vehicle drag coefficient (unitless), typically 0.30; $C_h$ is the altitude correction factor equal to 1-0.000085$h$ where $h$ is the altitude in meters (unitless); $A_f$ is the vehicle frontal area (m$^2$), typically 0.85 multiplied by the height and width of the vehicle; $C_{r0}$ is a rolling resistance constant that varies as a function of the pavement type and condition (unitless); $C_{r1}$ is the second rolling resistance constant (h/km); $C_{r2}$ is the third rolling resistance constant (unitless); $m$ is the total vehicle mass (kg); and $G$ is the roadway grade (unitless).

### 8.4.1 First Control Approach: Proportional Derivative Controller

The proposed architecture for the first control strategy consists of three core modules that are connected using a feedback loop. The first component is the car-following policy module which receives information about the speeds and positions of the two vehicles and uses it to determine the difference between the current conditions and the desired policy. That information is then transmitted to the controller module (based on Proportional-Derivative feedback control) which acts upon the current gap error to generate an output signal $u$. The controller output serves one of two purposes: it either controls the engine output regulating the tractive force responsible for the motion of the vehicle; or it actuates the vehicle brakes when the situation dictates that a deceleration is needed. The final component is the vehicle dynamics module which emulates how the vehicle would respond to the actuation of the gas and brake pedals during the acceleration and deceleration phases as a response to changes in the target speed.

#### *8.4.1.1 Acceleration Behavior Modeling*

The model used as the descriptor of the vehicle dynamics in the acceleration regime was presented in Equation VIII.2. Taking into account the latter model, the dynamical system of the car could be modeled as presented in Equation VIII.7.

$$m\frac{dv_n}{dt} = u.\left(F - R_a - R_r - R_g\right) \tag{VIII.7}$$

The model presented in Equation VIII.7 is a non-linear dynamical system of the first order in which the controller output $u$ aims to model the engine output and varies between 0 and 1. The non-linearity of the system is a direct result of the expressions of the aerodynamic resistance and the maximal tractive force.

In Equation VIII.7, the controller output can be cast as an acceleration coefficient. The application of the output signal to the expression of the net tractive force is made possible given that the vehicles are operating in a cooperative adaptive environment. In fact, the different resistive forces could be estimated given that the road characteristics and topography are assumed to be known beforehand.

#### *8.4.1.2 Deceleration Behavior Modeling*

The proposed architecture for the deceleration controller is almost the same as the one responsible for regulating the platoon during the acceleration maneuvers. In fact, there are only two key differences worth mentioning between the acceleration and deceleration controllers. The first difference concerns the dynamical system equation (Equation VIII.7) in which the tractive force $F$ is replaced by the maximum braking Force $F_{b\ max}$ (Equation VIII.8). The dynamical system governing the motion of the vehicles while decelerating is presented in Equation VIII.9. Again, the output signal is delimited by 0 and 1.

$$F_{b\ max} = mn_b g \tag{VIII.8}$$

$$m\frac{dv_n}{dt} = -u.\left(F_{b\ max} + R_a + R_r + R_g\right) \tag{VIII.9}$$

Here $n_b$ is the braking efficiency of the vehicle.

An additional requirement that needs to be satisfied by the deceleration controller is the inclusion of a collision avoidance strategy. That aims to ensure that the system is able to smoothly and adequately actuate the vehicle's braking system whenever the following vehicle is closing in on the vehicle ahead of it. From a physical perspective, the collision avoidance model attempts to ensure that the following vehicle is able to decrease its speed to that of the leading vehicle in a distance that is equal to the current gap between them through the application of an appropriate deceleration level. That is achieved through the implementation of an upper bound that delimits the deceleration level to be applied; thus guaranteeing that no collisions occur.

The strategy that is implemented at the level of the deceleration controller in order to ensure that the traffic remains collision-free is presented in Equation VIII.10. The logic behind the chosen collision avoidance strategy is straightforward from a physical perspective. In fact, assuming that the following vehicle is approaching the leading vehicle, the algorithm makes use of $b_{kinematics}$ (Equation VIII.11), which denotes the deceleration level that is needed in order for the following vehicle to decrease its speed to the speed of the leading vehicle with the stopping distance being equal to the distance gap separating them, to compute the deceleration level to be applied by the following vehicle. To maintain a collision-free traffic, the following vehicle needs to decelerate at a level that is at least equal to $b_{kinematics}$ whenever its speed exceeds that of the leading vehicle.

Furthermore, the chosen functional form allows capturing different braking patterns. That is due to the fact that the adopted braking strategy uses a desired deceleration level $b_{desired}$ (i.e. on a plain road, varies with the road grade) that is set by the user in addition to $b_{kinematics}$. The collision avoidance function, presented in Equation VIII.10, computes the needed deceleration to apply as the ratio of the square of the kinematics deceleration $b_{kinematics}$ needed to decelerate from the current speed to the leading vehicle speed and the desired deceleration level $b_{desired}$. The adopted strategy ensures that collisions do not occur between vehicles. In fact, one can notice that in the case that $b_{desired}$ is smaller than $b_{kinematics}$, the applied deceleration is greater than the desired deceleration level. In the opposite case in which $b_{desired}$ is greater than $b_{kinematics}$, it would be converging smoothly towards it.

$$a_{collision} = \frac{b_{kinematics}^2}{(b_{desired} + g\ Gr)} \quad \text{(VIII.10)}$$

$$b_{kinematics} = \frac{\left(v_n^2 - v_{n-1}^2 + \sqrt{(v_n^2 - v_{n-1}^2)^2}\right)}{4\left(x_{n-1} - x_n - s_j\right)} \quad \text{(VIII.11)}$$

#### *8.4.1.3 Controller Design Modeling*

As mentioned earlier, the proposed design for the system involves a PD controller that is implemented in a feedback loop. Subsequently, the expression of the output signal *u* has the form presented in Equation VIII.12.

$$u(t) = K_p e(t) + K_d \frac{de(t)}{dt} \quad \text{(VIII.12)}$$

As shown in Equation VIII.12, the computation of the controller output *u* requires the calibration and tuning of its two parameters $K_p$ and $K_d$ which represent the proportional and derivative gains respectively. Assigning appropriate values to the latter parameters is of an utmost importance to the performance of the overall system. In fact, even a small change in one of the controller gain variables might cause a stable system with good performance and regulation of the longitudinal motion in the platoon to become unstable and chaotic.

First, the research team started by investigating the performance of the system for a platoon of vehicles through casting the platoon as a succession of two vehicles at a time. In that regard, a platoon of 10 homogenous vehicles was used to explore and test the system response to different changes in the platoon leader speed. For illustrative purposes, the speed of the

leading vehicle of a platoon that is cruising under steady state conditions is abruptly changed and the response of each of the following vehicles is determined and investigated. The results of a case scenario are presented at the level of Figure 30. The four subfigures illustrate the resulting acceleration and speed profiles for each following vehicle (Figure 30.a and Figure 30.b respectively) along with the evolution of both the instantaneous time headway (Figure 30.c) and the error (Figure 30.d).

Two main conclusions can be drawn from the results plotted in Figure 30. The first one concerns relatively short platoons. When the total number of following vehicles is relatively small such as three vehicles, a linear Proportional-Derivative controller can control the longitudinal motion of vehicles in a stable and efficient manner. However, stability issues will ultimately arise as the platoon size increases. In fact, the applied deceleration levels continue to amplify and increase as we move up in the platoon, as shown in Figure 30.a, resulting in an unavoidable collision if the platoon size exceeds a certain critical threshold. In addition, even though Figure 30.b confirms that the steady state is eventually achieved, it illustrates at the same time that the maximum speeds attained by the following vehicle is increasing which constitutes a problem. Furthermore, the following strategy adopted by the controller would not be comfortable to the travelers due to the high levels of variability in the acceleration profiles. Finally, Figure 30.c and Figure 30.d further confirm the unsuitability of the controller to be integrated in the platooning system given its failure in terms of decaying the rate of growth of the error term over time.

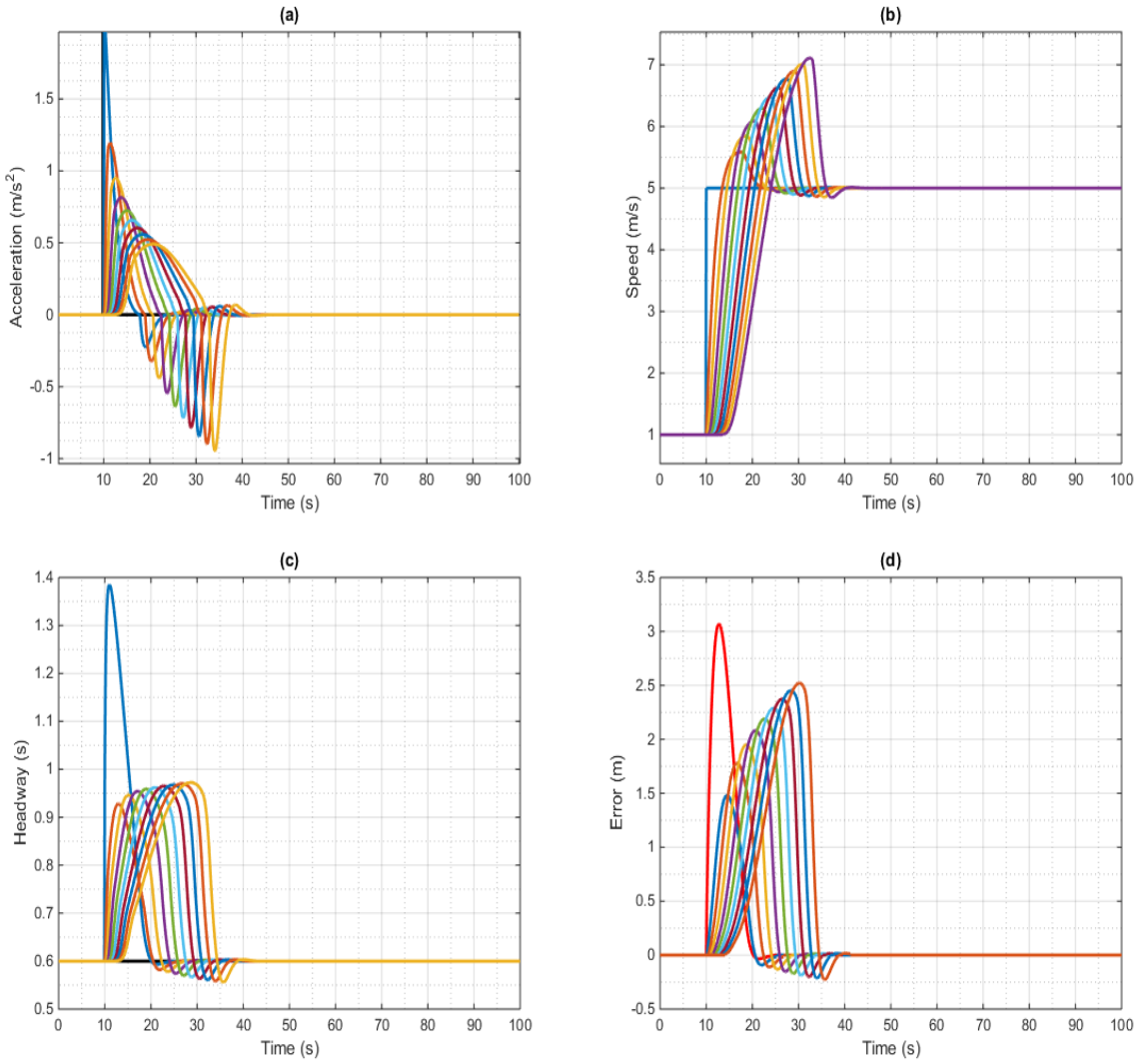


**Figure 30: Response of the different vehicles in the platoon: a. Acceleration; b. Speed; c. Time Headway; d. Error**

In order to mitigate the observed instabilities in the deceleration regime, a certain degree of cooperation should be incorporated into the system. In other words, the controller needs to make adjustments to the speeds of the following vehicles based upon information that looks further ahead in the platoon beyond the corresponding immediate leader. In that context, a cooperative control strategy was developed by the research team. Through making the controller output sensitive to the speed and position of the platoon's leader ($n=1$), a following vehicle $n$ is able to pre-detect the future behavior of vehicle $n-1$. Subsequently, the proposed controller will act in such a way that the speed of vehicle $n$ (with $n \geq 3$) is pre-adjusted. As it will be demonstrated later, adopting such an approach will result in a stable platoon in which the deceleration levels are gradually absorbed in the upstream direction.

Mathematically speaking, the proposed design for the system attempts to minimize two error functions. The first one captures the instantaneous error with regards to the preceding vehicle. The corresponding error (Equation VIII.13) is computed as the difference between the actual distance gap and the desired distance gap that is estimated through the multiplication of the desired time headway $h_{des}$ by the speed of the vehicle $v_n$. In a similar manner, the second error function (Equation VIII.14) calculates the difference between the actual and the desired conditions with regards to the vehicle leading platoon.

$$e_{n1}(t) = \left(x_{n-1}(t) - x_n(t) - s_j\right) - h_{desired}.\, v_n(t) \quad \text{(VIII.13)}$$

$$e_{n2}(t) = \left(x_1(t) - x_n(t) - s_j\right) - \left[(n-1).\, h_{desired}.\, v_n(t) + (n-2)s_j\right] \quad \text{(VIII.14)}$$

In the next step, the control output (Equation VIII.15) is estimated as the cumulative sum of the outputs of two standard PD controllers that are respectively applied to $e_{n1}(t)$ and $e_{n2}(t)$ as presented in Equation VIII.16 and Equation VIII.17. Here, special attention should be dedicated to the fact that the second control output $u_{2n}$ is not of the same order of magnitude for all the vehicles in the platoon because the distance gap to the first vehicle keeps growing as we move upstream the platoon. Subsequently, the related control gains should be different for each vehicle. Rather than assigning a set of values for each vehicle which will drastically increase the number of parameters required, the research team opted to make use of a decreasing series that is sensitive to the position of the vehicle in order to estimate $K_{pn}$ and $K_{dn}$ from the respective values of $K_p$ and $K_d$ (Equation VIII.18 and Equation VIII.19). By doing so, the platooning controller would only require the input of only two parameters rather than a number that is sensitive to twice the platoon size.

$$u_n(t) = u_{1n}(t) + u_{2n}(t) \quad \text{(VIII.15)}$$

$$u_{1n}(t) = K_p e_{n1}(t) + K_d\left(v_{n-1} - v_n\right) \quad \text{(VIII.16)}$$

$$u_{2n}(t) = K_{pn} e_{n2}(t) + K_{dn}\left(v_1 - v_n\right) \quad \text{(VIII.17)}$$

$$K_{pn} = K_p / n \quad \text{(VIII.18)}$$

$$K_{dn} = K_d / n \quad \text{(VIII.19)}$$

The above control approach is evaluated using the same case scenario illustrated in Figure 30. A homogeneous platoon of 10 vehicles is modeled for the case in which $K_p$ and $K_d$ are respectively equal to 0.30 and 0.35. The different results are plotted in Figure 31. From the figures, one can confirm the success of the proposed platooning strategy in addressing the stability issues in the deceleration regime. Specifically, Figure 31.a and Figure 31.b illustrate the latter statement clearly as it is shown that the maximum applied deceleration level continues to decrease as we move from upstream within the platoon. Furthermore, Figure 31.c and Figure 31.d allow for a better understanding of how the stability and observed efficiency of the platooning strategy is achieved. In fact, the controller applies a small acceleration level as the speed of the platoon's leader is changed. That acceleration results in a smaller time headway and distance gap than the desired policy for a short period of time. Through the pre-adjustment of the following vehicles' speeds, the controller is able to converge back to the desired steady state conditions while preserving the stability of the platoon.

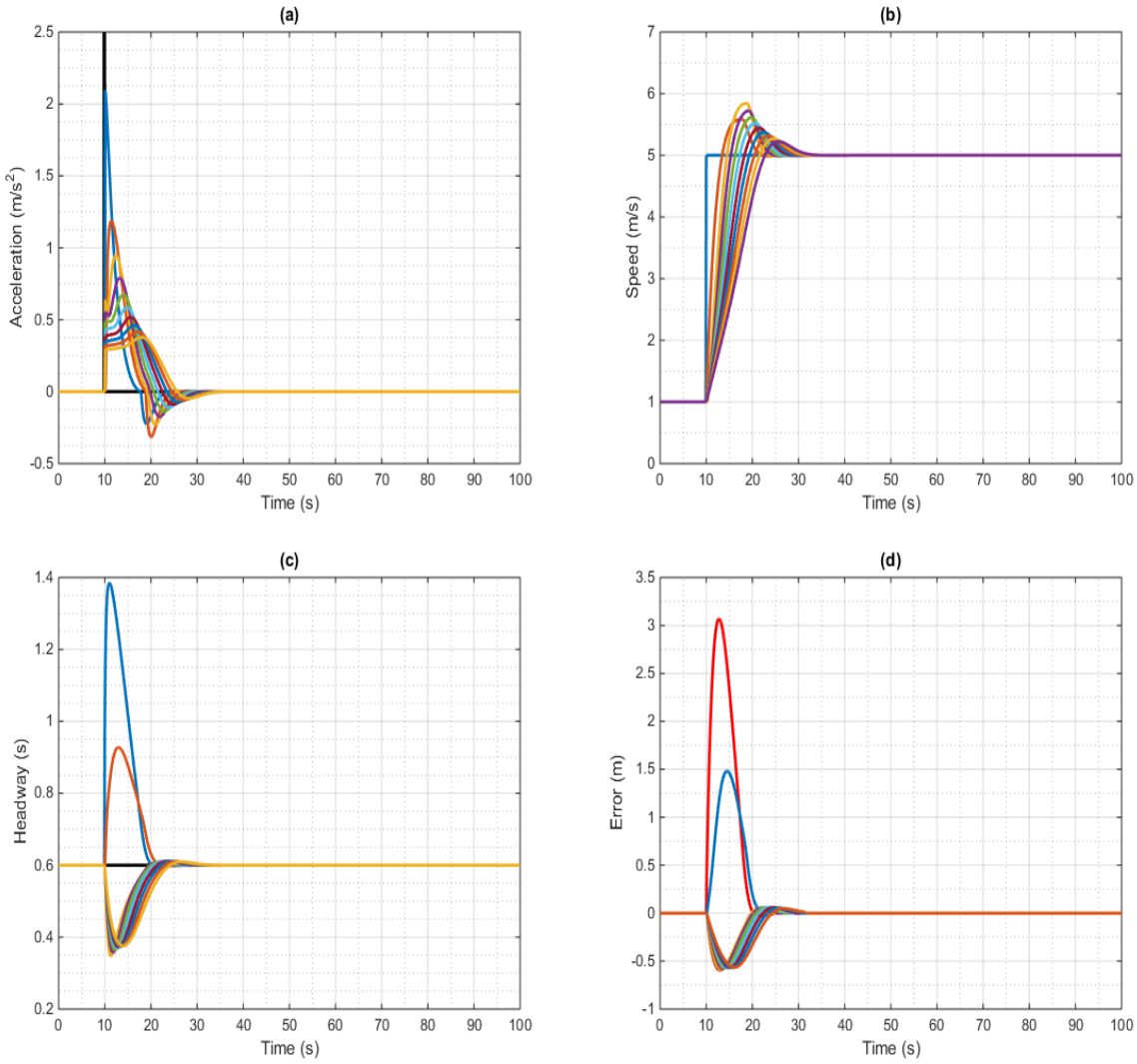


**Figure 31: Response of the different vehicles in the platoon: a. Acceleration; b. Speed; c. Time Headway; d. Error**

### 8.4.2 Second Control Approach: Change of variables

This section uses most of the models presented in the previous section. We consider two consecutive vehicles. The objective remains to drive the error defined by Equation VIII.1 to zero by letting the following vehicle apply successive and corrective acceleration/deceleration inputs. One way of achieving this result is by enforcing that the time rate of change of the error $e_n(t)$ (i.e. $\frac{d}{dt}\left(e_n(t)\right)$ ) satisfies Equation (VIII.20)

$$\frac{d}{dt}\left(e_n(t)\right) = -\lambda\, e_n(t) \qquad \text{(VIII.20)}$$

Where $\lambda$ is a strictly positive real number. The solution to Equation (VIII.20) is given by

$$e_n(t) = e_n(0)\, Exp[-\lambda\, t]$$

And guarantees that $e_n(t)$ converges to zero as time increases provided $\lambda$ strictly positive.

Substituting Equation VIII.1 into Equation VIII.20 leads to

$$a_n = \frac{-\lambda\, e_n(t) + v_{n-1} - v_n}{h_{res}} \tag{VIII.21}$$

Namely,

$$a_n(t) = \frac{1}{h_{res}}[-\lambda\,(x_{n-1}(t) - x_n(t) - Sj) + v_{n-1}(t) + (\lambda\, h_{res} - 1)v_n(t)] \tag{VIII.22}$$

Equation VIII.22 requires knowledge of the difference in position between two consecutive vehicles as well as their respective velocities. The presented controller has one hyper-parameter and is one order of magnitude less complex than the one presented in the previous section. The amount of data that needs to be transferred between the vehicles is minimum (i.e. velocity of the vehicle ahead). It is also possible to avoid this transfer of information by estimating the position and velocity of the vehicle in front via radar.

It is also important to note that the computed value for the acceleration $a_n(t)$ need to satisfy the conditions presented in Equations VIII.23 and VIII.24.

$$a_n(t) \leq\ a_{max}(t) \qquad \text{if } a_n\ > 0 \tag{VIII.23}$$

$$a_{min}(t) \leq\ a_n(t) \leq\ a_{collision}(t) \qquad \text{if } a_n \leq 0 \tag{VIII.24}$$

where $a_{max}(t)$ is defined in Equation VIII.2, $a_{collision}(t)$ is defined in Equation VIII.10 and $a_{min}(t)$ is defined in Equation VIII.25

$$a_{min}\ =\ -(G+1)g\ \mu\ b_e \tag{VIII.25}$$

If the value of $a_n(t)$ computed using Equation VIII.22 violates the mentioned constraints, $a_n(t)$ will be taken equal to value of the bound it is violating.

## 8.5 PRELIMINARY TESTING AND RESULTS

The next step of this research effort consists on testing the two platooning strategies for different real traffic scenarios in order to evaluate their performance and stability. For that purpose, a dataset comprising a total of sixteen driving cycles was used. The driving cycles are composed of vehicle trajectories that are characteristic of typical traffic phenomena and scenarios such as traffic on highways and arterial roads and stop-and-go-waves. A platoon of 5 homogenous vehicles was used to explore and test the system response to different changes in the leader's speed for each of the evaluated scenarios.

The following inputs were used for the testing procedure:

- Five homogeneous vehicles were used with a power-to-mass ratio equal to 0.15 kW/kg and an engine power of 285 kW,
- For the acceleration controller, the proportional and derivative gains were set equal to 2.5 and 0.5, respectively,
- In a similar manner, the proportional and derivative gains for the deceleration controller were set to 1.5 and 0.15, respectively,
- The desired following policy consists on maintaining a constant time headway of 0.6 seconds between the vehicles.
- The parameter $\lambda$ is taken equal to 10.

The results corresponding to two of the driving cycles are presented at the level of Figure 32 and Figure 33 for the linear platooning strategy using Proportional-Derivative controllers, and Figure 34 and Figure 35 for the alternative platooning strategy using the $\lambda$ factor. Each of the latter figures consists of four subfigures. Subfigures a plot the desired time gap of 0.6 s against the actual time gap separating each vehicle in the platoon with its immediate predecessor. Next, the error between the desired following policy and the current conditions is shown in Figure 32.b, Figure 33.b, Figure 34.b, and Figure 35.b. Finally, the resulting acceleration and speed profiles for each following vehicle in the platoon are presented at the level of subfigures c and subfigures d respectively.

The different figures demonstrate the success of the two control approaches in achieving the main objective of applying the desired constant time headway policy between the different vehicles of the platoon. The results show that the actual time headway fluctuates between a minimum of 0.56 s and a maximum of 0.66 s for all of the presented driving cycles. Even more, the small peaks observed at the level of the time headways is mostly related to the very low speeds of the vehicles that are approaching a complete stop rather than a problem with the controller itself. The performance of the controller is further demonstrated through looking at the results of driving cycle 2, which corresponds to highway traffic in which the speeds of the vehicles is between 24 m/s and 33 m/s. In that scenario, the time gap is almost maintained at the desired gap of 0.6 s and the fluctuations are very minor and unnoticeable (Figure 33.b and Figure 35.b). The graphs of the error functions further support the performance of the proposed design of the controller as they show that the error always remain within a range of 0.1 m of the desired policy. Finally, it is worth mentioning that the acceleration profiles demonstrate that the maximum deceleration levels applied by the vehicles

decrease towards the upstream of the platoon which is a proof of the ability of the controller to limit the propagation and to absorb any instabilities in the deceleration regime.

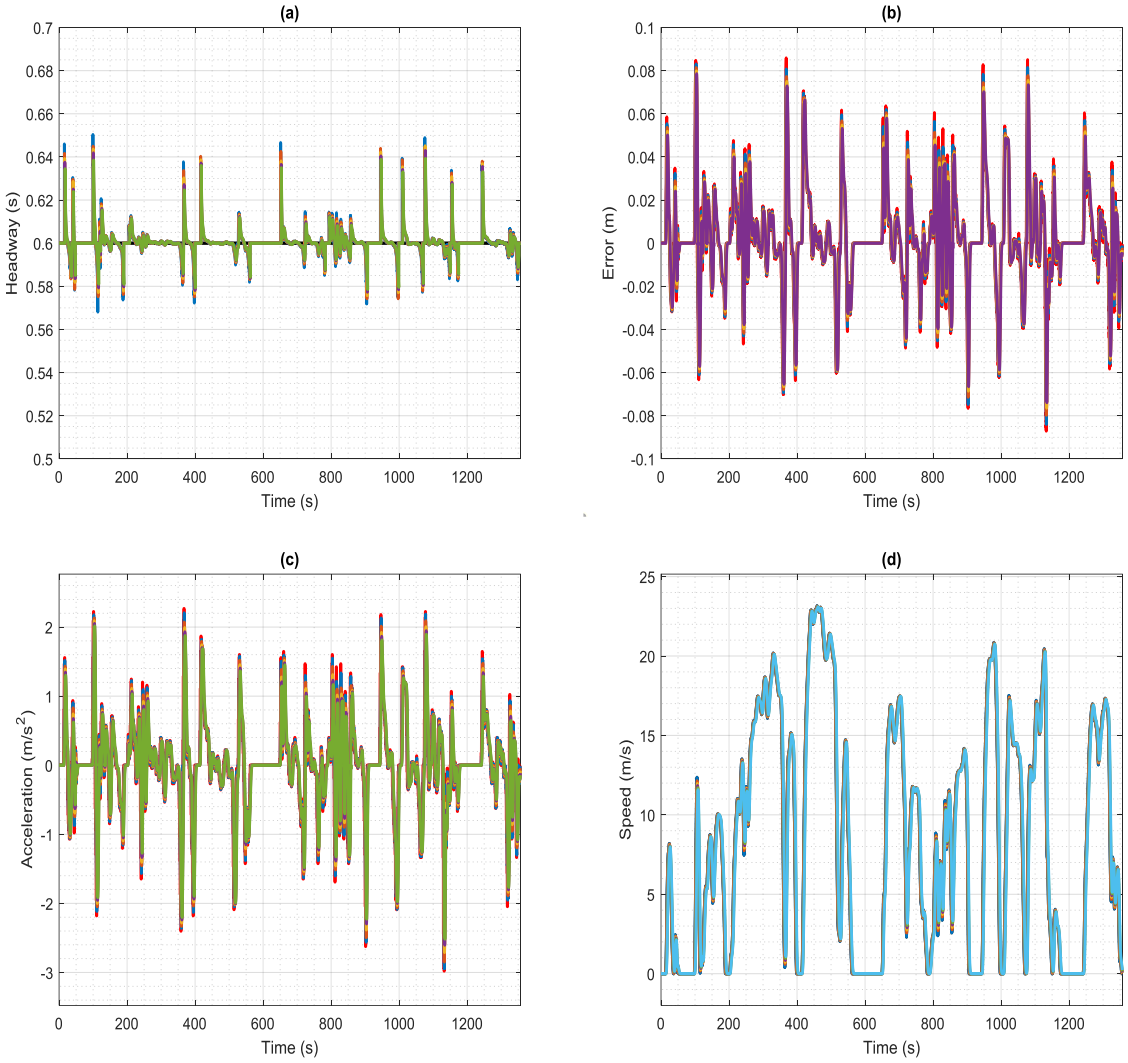


**Figure 32: Response of the following vehicles in the platoon for driving cycle 1 using linear control strategy: a. Time headway; b. Error; c. Acceleration; d. Speed**

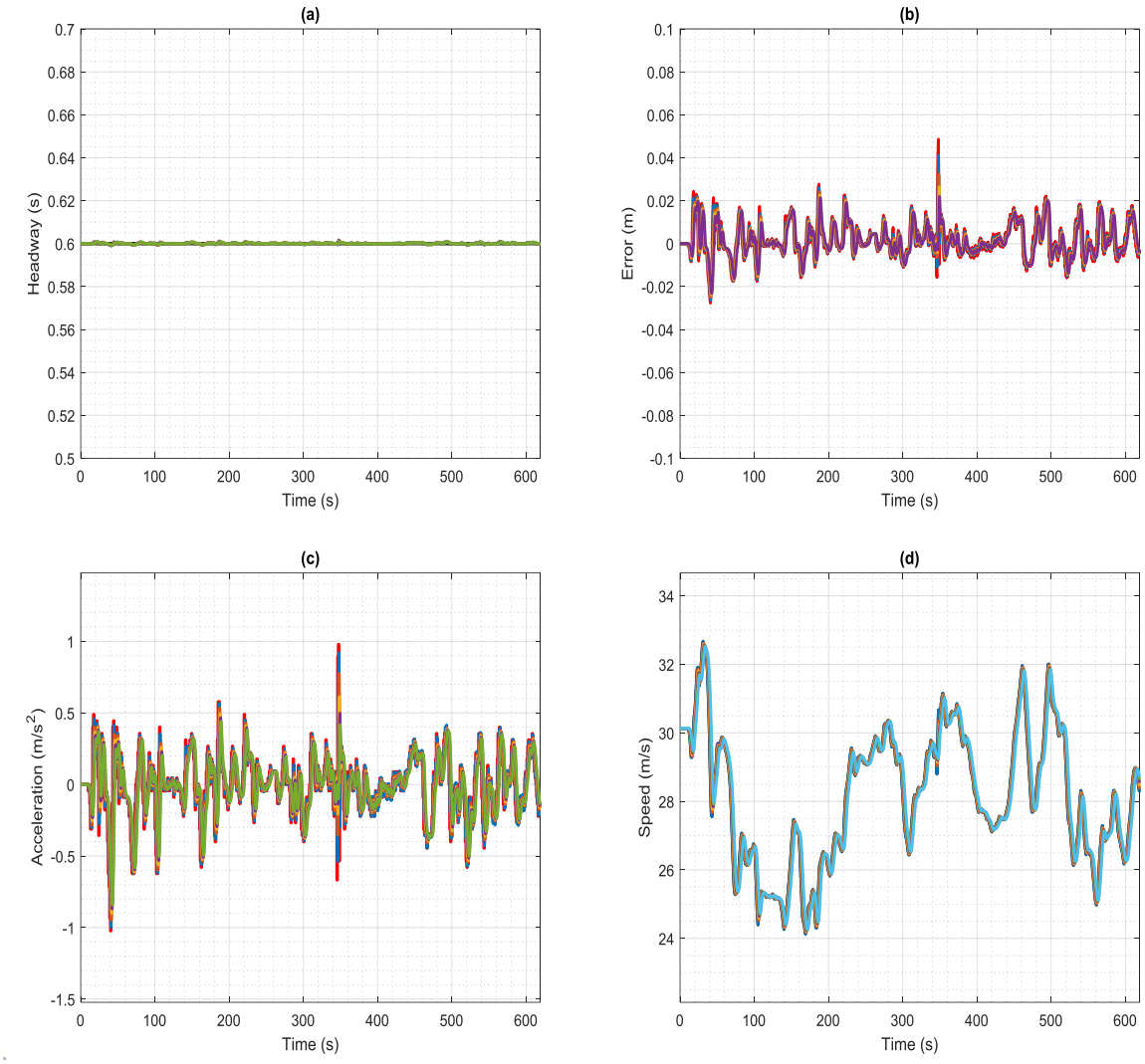


**Figure 33: Response of the following vehicles in the platoon for driving cycle 2 using linear control strategy: a. Time headway; b. Error; c. Acceleration; d. Speed**

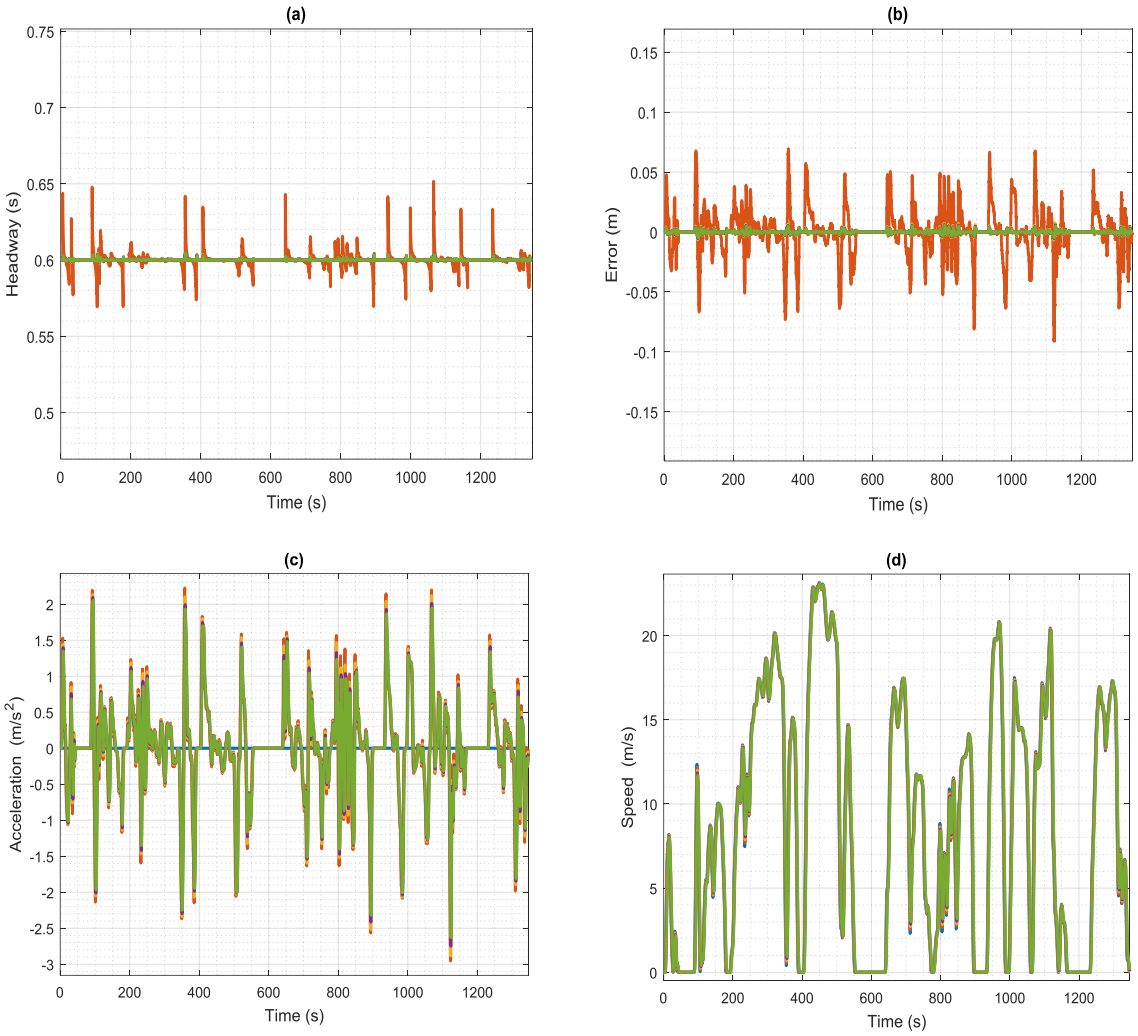


**Figure 34: Response of the following vehicles in the platoon for driving cycle 1 using alternative control strategy: a. Time headway; b. Error; c. Acceleration; d. Speed**

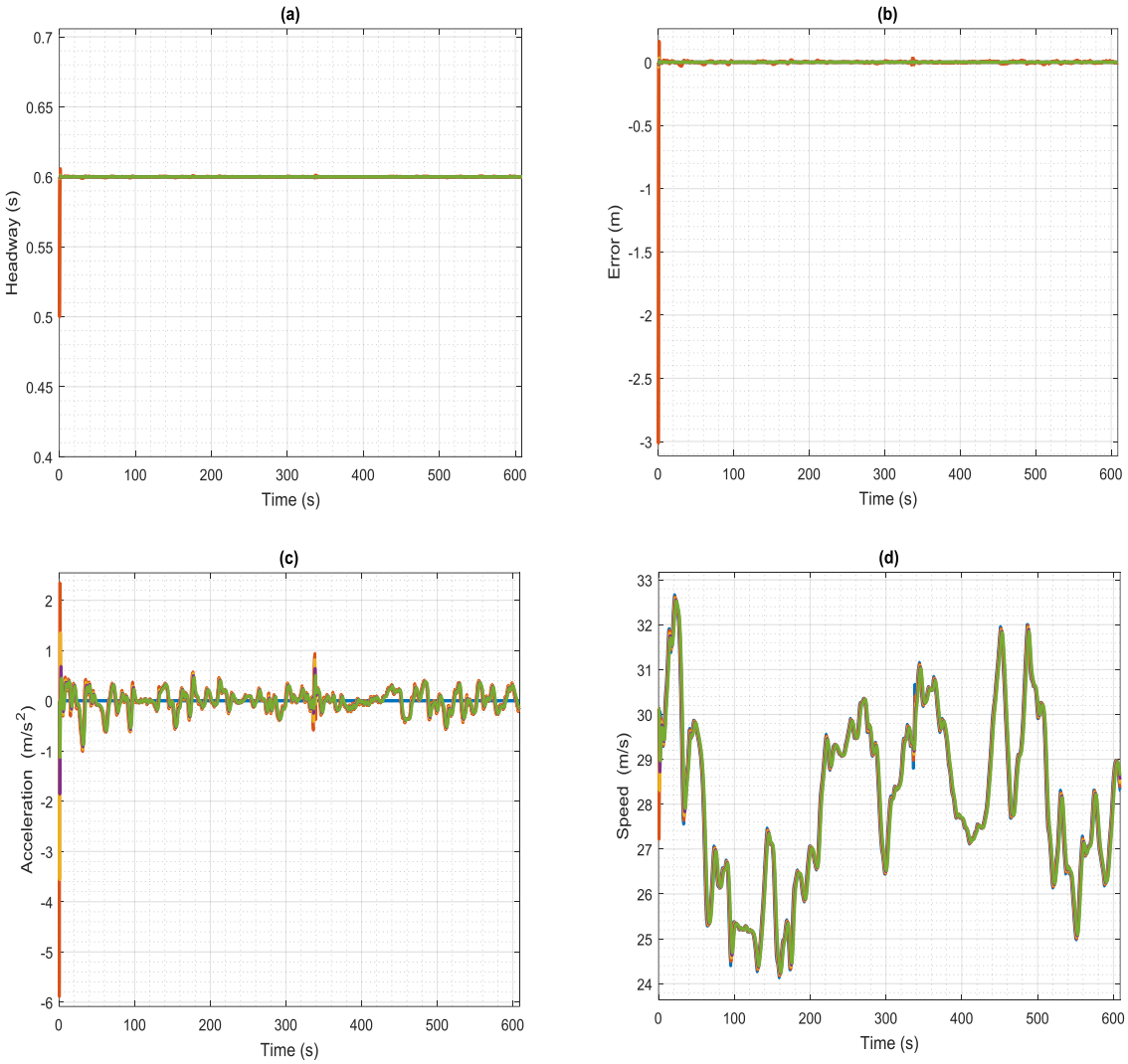


**Figure 35: Response of the following vehicles in the platoon for driving cycle 2 using alternative control strategy: a. Time headway; b. Error; c. Acceleration; d. Speed**

## 8.6 CONCLUSIONS

In this paper, two platooning logics were presented in order to alleviate congestion in urban cities. One controller is a PI controller the other is simple feedback controller obtained through a change of variables. The PI controller requires tuning in order to determine the appropriate gains for best performance. The second controller features one-hyper parameter the user chooses and governs how fast the systems converges to the desired state (i.e. how long it takes to form and maintain the platoon). Both logics do satisfy the required dynamic constraints and perform as expected on the tested driving cycles. It is also noteworthy the second controller is less complex, requiring no tuning and has the possibility to avoid the transfer of information

between vehicles altogether through the use of vehicle radar. This renders it very attractive for field implementation.

## 8.7 ACKNOWLEDGMENTS

The authors acknowledge the financial support provided by the University Mobility and Equity Center (UMEC) and the Department of Energy through the Office of Energy Efficiency and Renewable Energy (EERE), Vehicle Technologies Office, Energy Efficient Mobility Systems Program under award number DE-EE0008209.

# Chapter 9 Conclusions and Recommendations for Future Research

The research presented in this thesis provides a comprehensive investigation of the human-in-the-loop component in car-following theory leading to a better understanding of the human-vehicle interaction. This study was initiated due to the noticeable overlooking of driver behavior in the existing literature which, as a result, fails to capture the effect of human error. Ironically, that makes the current car-following models more representative of newer technologies that did not exist when they were developed — i.e., connected and autonomous vehicles.

To overcome the latter, this study attempted to explicitly model and integrate the human-in-the-loop aspect in car-following theory. The completion of each of the dissertation tasks marks the beginning of success of car-following models in terms of reflecting the transition from human driven vehicles to connected and self-driving vehicles. In fact, having an explicit term that captures the effect of the human-in-the-loop allows for the modeling of different levels of human control.

That is especially true for the case of the developed FR model which can increase and decrease the level of autonomy through the interaction of its different parameters. In addition, the FR model is demonstrated to capture human driving variability in its acceleration function and to emulate the effects of human estimation errors and driving imperfections. Furthermore, the FR model is proved to outperform several state-of-the-practice car-following models in terms of statistically matching naturalistic driving data.

Similarly, the modification of the RPA model to account for the driver resulted in a better representation of traffic as it captured the heterogeneity of human behavior, in terms of driving patterns and styles. While it is true that the calibration procedure is more complicated than the original model given the addition of three model parameters, the importance of the subject makes the proposed model noteworthy to traffic flow theory. As a matter of fact, both the proposed variant of the RPA model and the new FR model can be used in traffic simulation to directly model the variation and the randomness between the different drivers rather than using a speed coefficient of variation.

Finally, the final chapter of this dissertation investigated a case in which the driver is excluded and the vehicles are operating autonomously in a connected environment. Besides

showcasing a scenario in which the human-in-the-loop is deactivated, Chapter 8 presented some techniques that can be used to control the motion of connected cooperative multi-vehicle platoons.

While the research presented in this dissertation is comprehensive, it is far from complete. Several research areas should be addressed in order to expand on the results of the current study such as:

- In order to enhance the capabilities of the proposed variant of the RPA model and of the FR model, further naturalistic data should be considered with different vehicle types and for a larger group of drivers. That would result in a better understanding of the correlations that might exist between the model parameters. In an optimistic outlook, that would lead to the reduction of the number of needed parameters and/or the range of these parameters.
- This study only considered light-duty vehicles. A similar methodology could be adopted in order to investigate the human-in-the-loop component in to the case of heavy-duty vehicles. The outcome will be of significant importance for the case of cooperative platooning.

# REFERENCES


1. Chandler, R.E., R. Herman, and E.W. Montroll, *Traffic dynamics: studies in car following.* Operations research, 1958. **6**(2): p. 165-184.
2. Drew, D.R., *Traffic flow theory and control*. 1968.
3. Gazis, D.C., R. Herman, and R.W. Rothery, *Nonlinear follow-the-leader models of traffic flow*. Operations research, 1961. **9**(4): p. 545-567.
4. Jiang, R., Q. Wu, and Z. Zhu, *Full velocity difference model for a car-following theory.* Physical Review E, 2001. **64**(1): p. 017101.
5. Newell, G.F., *A simplified car-following theory: a lower order model.* Transportation Research Part B: Methodological, 2002. **36**(3): p. 195-205.
6. Olstam, J.J. and A. Tapani, *Comparison of Car-following models*. 2004.
7. Gipps, P.G., *A behavioural car-following model for computer simulation.* Transportation Research Part B: Methodological, 1981. **15**(2): p. 105-111.
8. Treiber, M., A. Hennecke, and D. Helbing, *Congested traffic states in empirical observations and microscopic simulations.* Physical review E, 2000. **62**(2): p. 1805.
9. Fritzsche, H.-T., *A model for traffic simulation.* Traffic Engineering+ Control, 1994. **35**(5): p. 317-21.
10. Wiedemann, R., *Simulation des Strassenverkehrsflusses*. 1974, Schriftenreihe des Instituts für Verkehrswesen der Universität Karlsruhe: Karlsruhe, Germany.
11. Wiedemann, R., Reiter, U., *Microscopic traffic simulation: The simulation system MISSION, background and actual state*, in *CEC Project ICARUS (V1052), Final Report*. 1992: Brussels. p. 1-53 in Appendix A.
12. Rakha, H., Pasumarthy, P., and Adjerid, S. , *A Simplified Behavioral Vehicle Longitudinal Motion Model.* Transportation Letters: The International Journal of Transportation Research, Vol. 1(2), pp. 95-110., 2009.
13. Searle, J., *Equations for Speed, Time and Distance for Vehicles Under Maximum Acceleration.* Advances in Safety Technology, Society of Automotive Engineers Special Publications, 1999. **1433**.
14. M. Van Aerde and H. Rakha." INTEGRATION © Release 2.30 for Windows: User's Guide – Volume I: Fundamental Model Features, *M. Van Aerde & Assoc., Ltd.* (Blacksburg2007).
15. M. Van Aerde and H. Rakha. "INTEGRATION © Release 2.30 for Windows: User's Guide – Volume II: Advanced Model Features, *M. Van Aerde & Assoc., Ltd.* (Blacksburg2007).
16. Rakha, H., M. Snare, and F. Dion, *Vehicle Dynamics Model for Estimating Maximum Light-Duty Vehicle Acceleration Levels.* Transportation Research Record: Journal of the Transportation Research Board, 2004. **1883**(-1): p. 40-49.
17. Rakha, H., M. Snare, and H. Yue, *Characterization of Typical Driver Acceleration and Deceleration Behavior for Traffic and Environmental Modeling.* 14th CRC On-Road Vehicle Emissions Workshop, San Diego, CD-ROM, March, 2004.
18. Fadhloun, K. and H. Rakha, *A novel vehicle dynamics and human behavior car-following model: Model development and preliminary testing.* International Journal of Transportation Science and Technology, ISSN 2046-0430, 2019.
19. Drew, D., *Traffic Flow Theory and Control*. 1968: McGraw-Hill.

20. Bham, G. and R. Benekohal, *Development, Evaluation, and Comparison of Acceleration Models.* 81st Annual Meeting of the Transportation Research Board, Washington, D.C, 2002.
21. Long, G., *Acceleration Characteristics of Starting Vehicles.* Transportation Research Record: Journal of the Transportation Research Board, 2000. **1737**(-1): p. 58-70.
22. Lee, C. and T. Rioux, *The TEXAS Model for Intersection Traffic – Development Research Report.* University of Texas at Austin, 1977.
23. Akcelik, R. and D.C. Biggs, *Acceleration Profile Models for Vehicles in Road Traffic.* Transportation Science, 1987. **21**(1): p. 36-54.
24. Varat, M. and S. Husher, *Vehicle Impact Response Analysis Through the Use of Accelerometer Data.* Accident Reconstruction: Analysis, Simulation, and Visualization. Society of Automotive Engineers, Inc, 2000(SP-1491).
25. Barceló, J. *GETRAM/AIMSUN: A software environment for microscopic traffic analysis*. in *Proc. of the Workshop on Next Generation Models for Traffic Analysis, Monitoring and Management*. 2001.
26. PTV-AG, *VISSIM 5.40–01 User Manual*. 2012: Karlsruhe, Germany.
27. Smith, M., G. Duncan, and S. Druitt, *PARAMICS: microscopic traffic simulation for congestion management.* 1995.
28. Chandler, R.E., R. Herman, and E. Montroll, *Traffic Dynamics: Studies in Car Following.* Operations Research, 1958. **6**(2): p. 165-184.
29. Greenshields, B.d., et al., *A study of traffic capacity*. Highway research board proceedings, 1935. **1935**.
30. Pipes, L.A., *An Operational Analysis of Traffic Dynamics.* 1953. **24**(3): p. 274-281.
31. Rakha, H. and W. Wang, *Procedure for Calibrating Gipps Car-Following Model.* 2009. **2124**(1): p. 113-124.
32. Rakha, H., C.C. Pecker, and H.B.B. Cybis, *Calibration Procedure for Gipps Car-Following Model.* 2007. **1999**(1): p. 115-127.
33. Van Aerde, M. and H. Rakha. *Multivariate calibration of single regime speed-flow-density relationships [road traffic management]*. in *Vehicle Navigation and Information Systems Conference, 1995. Proceedings. In conjunction with the Pacific Rim TransTech Conference. 6th International VNIS. 'A Ride into the Future'*. 1995.
34. Rakha, H., et al., *Vehicle Dynamics Model for Predicting Maximum Truck Acceleration Levels.* Journal of Transportation Engineering, 2001. **127**(5): p. 418-425.
35. van Winsum, W., *The human element in car following models.* Transportation Research Part F: Traffic Psychology and Behaviour, 1999. **2**(4): p. 207-211.
36. Helly, W., *Simulation of bottlenecks in single-lane traffic flow*. 1959.
37. Jones, S., *Cooperative adaptive cruise control: Human factors analysis*. 2013, No. FHWA-HRT-13-045.
38. Bevly, D., et al., *Heavy Truck Cooperative Adaptive Cruise Control: Evaluation, Testing, and Stakeholder Engagement for Near Term Deployment: Phase Two Final Report*. 2017, FHWA EAR study report.
39. Naus, G., et al. *Cooperative adaptive cruise control, design and experiments*. in *Proceedings of the 2010 American Control Conference*. 2010.
40. Milanés, V., et al., *Cooperative adaptive cruise control in real traffic situations.* IEEE Transactions on Intelligent Transportation Systems, 2014. **15**(1): p. 296-305.
41. Alam, A., *Fuel-efficient heavy-duty vehicle platooning*. 2014, KTH Royal Institute of Technology.
42. Stanger, T. and L. del Re. *A model predictive cooperative adaptive cruise control approach*. in *American Control Conference (ACC), 2013*. 2013. IEEE.

43. Deng, Q. and X. Ma, *A fast algorithm for planning optimal platoon speeds on highway.* IFAC Proceedings Volumes, 2014. **47**(3): p. 8073-8078.
44. Schmied, R., et al., *Nonlinear mpc for emission efficient cooperative adaptive cruise control.* IFAC-PapersOnLine, 2015. **48**(23): p. 160-165.
45. Mukherjee, P., *Investigation of Cooperative Adaptive Cruise Control with Experimental Validation*. 2016, University of Minnesota.
46. DIABY, M. and A. SORKATI, *Optimization for Energy Efficient Cooperative Adaptive Cruise Control.*
47. Bayar, B., *An Extended Cooperative Adaptive Cruise Control Algorithm to Increase Energy Efficiency and Traffic Flow Rate.*
48. Rakha, H. and I. Lucic, *Variable Power Vehicle Dynamics Model for Estimating Truck Accelerations.* Journal of Transportation Engineering, 2002. **128**(5): p. 412-419.
49. Dingus, T., S. Klauer, and V. Neale, *The 100-car Naturalistic Driving Study: Phase II–Results of the 100-Car Field Experiment. Washington, DC: National Highway Traffic Safety Administration; 2006. Report no.* Contract No. DTNH22-00-C-07007.
50. Brackstone, M. and M. McDonald, *Car-following: a historical review.* Transportation Research Part F: Traffic Psychology and Behaviour, 1999. **2**(4): p. 181-196.
51. Sangster, J., H. Rakha, and J. Du, *Application of Naturalistic Driving Data to Modeling of Driver Car-Following Behavior.* Transportation Research Record: Journal of the Transportation Research Board, 2013. **2390**: p. 20-33.
52. Fadhloun, K., et al., *Vehicle Dynamics Model for Estimating Typical Vehicle Accelerations.* Transportation Research Record: Journal of the Transportation Research Board, 2015. **2491**: p. 61-71.
53. Park, S., et al., *Empirical Study of Impact of Icy Roadway Surface Condition on Driver Car-Following Behavior.* Transportation Research Record: Journal of the Transportation Research Board, 2011. **2260**: p. 140-151.
54. Rakha, H. and M. Arafeh, *Calibrating steady-state traffic stream and car-following models using loop detector data.* Transportation Science, 2010. **44**(2): p. 151-168.
55. Van Aerde, M. and H. Rakha, *" INTEGRATION © Release 2.30 for Windows: User's Guide – Volume I: Fundamental Model Features, " M. Van Aerde & Assoc., Ltd.* 2007(Blacksburg).
56. Van Aerde, M. and H. Rakha, *"INTEGRATION © Release 2.30 for Windows: User's Guide - Volume II: Advanced Model Features, " M. Van Aerde & Assoc., Ltd.* 2007(Blacksburg).
57. Rakha, H., *Validation of Van Aerde's simplified steadystate car-following and traffic stream model.* Transportation letters, 2009. **1**(3): p. 227.
58. Rakha, H., et al., *Vehicle dynamics model for predicting maximum truck acceleration levels.* Journal of Transportation Engineering, 2001. **127**(5): p. 418-425.
59. Rakha, H., M. Snare, and F. Dion, *Vehicle dynamics model for estimating maximum light-duty vehicle acceleration levels.* Transportation Research Record: Journal of the Transportation Research Board, 2004. **1883**(1): p. 40-49.
60. Wang, J., H.A. Rakha, and K. Fadhloun, *Validation of the Rakha-Pasumarthy-Adjerid car-following model for vehicle fuel consumption and emission estimation applications.* Transportation Research Part D: Transport and Environment, 2017. **55**: p. 246-261.
61. Gazis, D., R. Herman, and R. Rothery, *Nonlinear follow-the-lead models of traffic flow.* Operations Research, 1961. **9(4)**: p. 545-567.
62. Pipes, L.A., *Car-following models and the fundamental diagram of road traffic.* Transportation Research, 1967. **1**: p. 21-29.
63. Pipes, L.A., *An operational analysis of traffic dynamics.* Journal of Applied Physics, 1953. **24**: p. 274-287.

64. Van Aerde, M. *Single regime speed-flow-density relationship for congested and uncongested highways*. in *74th TRB Annual Conference*. 1995. Washington DC.
65. Van Aerde, M. and H. Rakha. *Multivariate calibration of single regime speed-flow-density relationships*. in *Proceedings of the 6th 1995 Vehicle Navigation and Information Systems Conference*. 1995. Seattle, WA, USA: Vehicle Navigation and Information Systems Conference (VNIS) 1995. IEEE, Piscataway, NJ, USA,95CH35776..
66. Wu, N. and H. Rakha, *Derivation of Van Aerde Traffic Stream Model from Tandem-Queuing Theory.* Transportation Research Record: Journal of the Transportation Research Board, 2009. **2124**(1): p. 18-27.
67. Rakha, H., P. Pasumarthy, and S. Adjerid, *A simplified behavioral vehicle longitudinal motion model.* Transportation Letters: The International Journal of Transportation Research, 2009. **1**(2): p. 95-110.
68. Dingus, T.A., et al., *The 100-car naturalistic driving study, Phase II-results of the 100-car field experiment*. 2006.
69. Treiber, M., A. Hennecke, and D. Helbing, *Congested traffic states in empirical observations and microscopic simulations.* Physical Review E, 2000. **62**(2): p. 1805-1824.
70. Soria, I., L. Elefteriadou, and A. Kondyli, *Assessment of car-following models by driver type and under different traffic, weather conditions using data from an instrumented vehicle.* Simulation Modelling Practice and Theory, 2014. **40**: p. 208-220.